MODIFIERS IN RHODIUM CATALYSTS FOR CARBON MONOXIDE HYDROGENATION: STRUCTURE-ACTIVITY RELATIONSHIPS

DELAWARE UNIV., NEWARK. DEPT. OF CHEMICAL ENGINEERING

MAY 1989

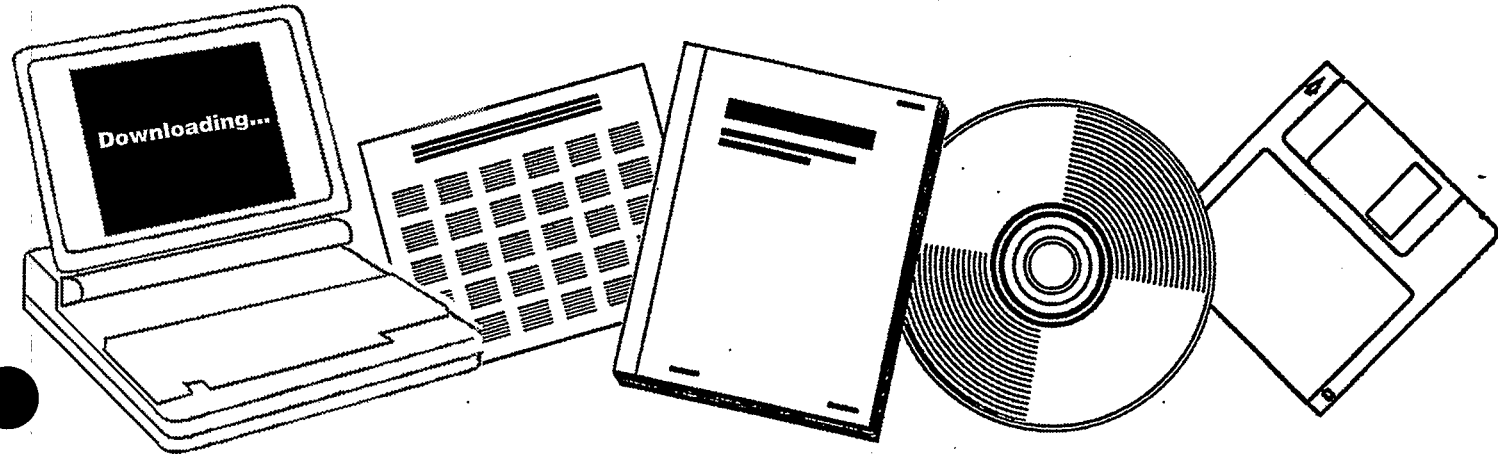

One Source. One Search. One Solution.

NTIS

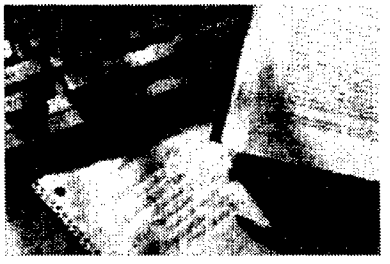

Providing Permanent, Easy Access to U.S. Government Information

National Technical Information Service is the nation's largest repository and disseminator of government-initiated scientific, technical, engineering, and related business information. The NTIS collection includes almost 3,000,000 information products in a variety of formats: electronic download, online access, CD-ROM, magnetic tape, diskette, multimedia, microfiche and paper.

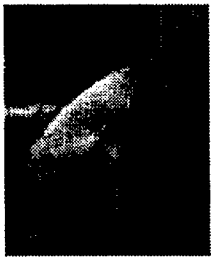

Search the NTIS Database from 1990 forward

NTIS has upgraded its bibliographic database system and has made all entries since 1990 searchable on **www.ntis.gov.** You now have access to information on more than 600,000 government research information products from this web site.

Link to Full Text Documents at Government Web Sites

Because many Government agencies have their most recent reports available on their own web site, we have added links directly to these reports. When available, you will see a link on the right side of the bibliographic screen.

Download Publications (1997 - Present)

NTIS can now provides the full text of reports as downloadable PDF files. This means that when an agency stops maintaining a report on the web, NTIS will offer a downloadable version. There is a nominal fee for each download for most publications.

For more information visit our website:

www.ntis.gov

U.S. DEPARTMENT OF COMMERCE
Technology Administration
National Technical Information Service
Springfield, VA 22161

DOE/PC/70780--T10
DE89 013802

DOE/PC/70780--T1

MODIFIERS IN RHODIUM CATALYSTS FOR CARBON MONOXIDE HYDROGENATION: STRUCTURE-ACTIVITY RELATIONSHIPS

by

Nazeer Ahmed Bhore

A dissertation submitted to the Faculty of the University of Delaware in partial fulfillment of the requirements for the degree of Doctor of Philosophy in Chemical Engineering

May 1989

DISCLAIMER

ABSTRACT

More efficient manufacture of oxygenates from syngas can fulfill a vital need for additives to transportation fuels. To achieve this, a much better understanding of the factors that control catalytic syngas reactions is needed, especially those that produce oxygenates rather than hydrocarbons. Some of the multi-functional systems used here are not only a better catalyst for oxygenates, but also provide an excellent system to investigate the effect of modifiers on the reaction pathways.

Catalytic hydrogenation of carbon monoxide on supported rhodium catalysts gives rise to a variety of products such as hydrocarbons, alcohols, aldehydes, acids, esters and ethers. The effect of metal precursor, the support, and the nature and the amount of modifier on the rates and selectivity to these products is studied. Sodium and molybdenum modified Rh/Al_2O_3 catalysts are investigated in detail.

Also a new method of kinetic analysis, the delplot method, was developed and used. The delplot method sorts products according to their rank, finds the number and location of slow steps in a reaction network and separates regimes of conversion where product rank changes. Quantitative foundations of this method for general kinetics and higher rank products were developed.

Incorporation of large amounts of molybdenum into Rh/Al_2O_3 catalysts was found to increase the rate of carbon monoxide hydrogenation greater than ten-fold. The selectivity to oxygenates particularly methanol and dimethylether was increased significantly and the shift reaction was also accelerated. Application of the delplot method to the data from $Rh\text{-}Mo/Al_2O_3$ catalysts of this study shows that almost all the products are primary products and that the slow step in the

entire reaction network is the formation of CH_x precursor on the surface. Kinetics and test reaction results indicate that the hydrogenation activity of Rh-Mo/Al_2O_3 unlike Rh/Al_2O_3 is less inhibited by presence of carbon monoxide.

Catalysts were also investigated using a battery of characterization techniques such as chemisorption, FTIR, XRD, XPS, TEM/EDX, TPD, ISS, ESR and solid-state NMR. Results from kinetics, characterization and test reaction studies are consistent with a dual-site mechanism where carbon monoxide is activated by Rh and hydrogen is activated by MoO_{3-x}. Increased activity and selectivity is attributed to a more effective hydrogenation capability provided by partially reduced molybdena. The physical and chemical state of molybdenum, its proximity to the metal crystallite and its relevance to the dual-site mechanism was investigated.

Addition of sodium to Rh/Al_2O_3 decreases the rate of carbon monoxide hydrogenation substantially. The selectivity to oxygenates is increased slightly. Investigation of the chemical and physical state of rhodium and sodium after various catalysts treatments shows that sodium blocks the rhodium surface and decreases the number of ensembles available for carbon monoxide activation. Addition of sodium also hinders the formation of gem-dicarbonyl species because of the removal of surface -OH groups.

TABLE OF CONTENTS

LIST OF FIGURES

LIST OF TABLES

CHAPTER 1
INTRODUCTION, SCOPE AND APPROACH

1.1 Synthesis Gas Reactions

Synthesis gas consists of hydrogen, carbon monoxide and may also contain carbon dioxide. Syngas can be made from coal, natural gas or naphtha. Thus a wide range of feed stocks can be employed to utilize syngas technology. About 7.5 trillion standard cubic feet of syngas is consumed each year[1]. According to Hirsch[2], the projected high level ($\sim$ 50%) of dependence of U.S. markets on foreign oil, the resultant crippling of the U.S. petroleum industry, the continued existence of the Organization of Petroleum Exporting Countries (OPEC) cartel, the instabilities in the Middle East, the huge cost and the long periods of time required to change the energy infrastructure and the short-term orientation of the U.S. public, government and industry suggests a strong likelihood of a new U.S. energy crisis in the early to middle 1990s. Currently, with a few exceptions such as SASOL, syngas is used for manufacture of chemicals and not liquid fuels.

Carbon monoxide is an extremely reactive and versatile molecule and can be catalytically converted to a variety of chemicals, see figure 1.1. Syngas also constitutes an important source for manufacture of hydrogen, which is used in manufacture of ammonia, nitric acid and fertilizers. Also, acetic acid, methyl acetate, acetic anhydride, ethylene glycol and many other products can be produced by a series of reactions involving syngas. Furthermore, syngas can be used to make liquid fuels such as gasoline, diesel and mixtures of higher oxygenates. Figure 1.2 shows the commercial or near commercial processes for production of liquid fuels

from syngas. As seen from this figure a wide variety of fuels such as gasoline, diesel oil, fuel cells, turbine fuel, MTBE and C1-C6 alcohols.

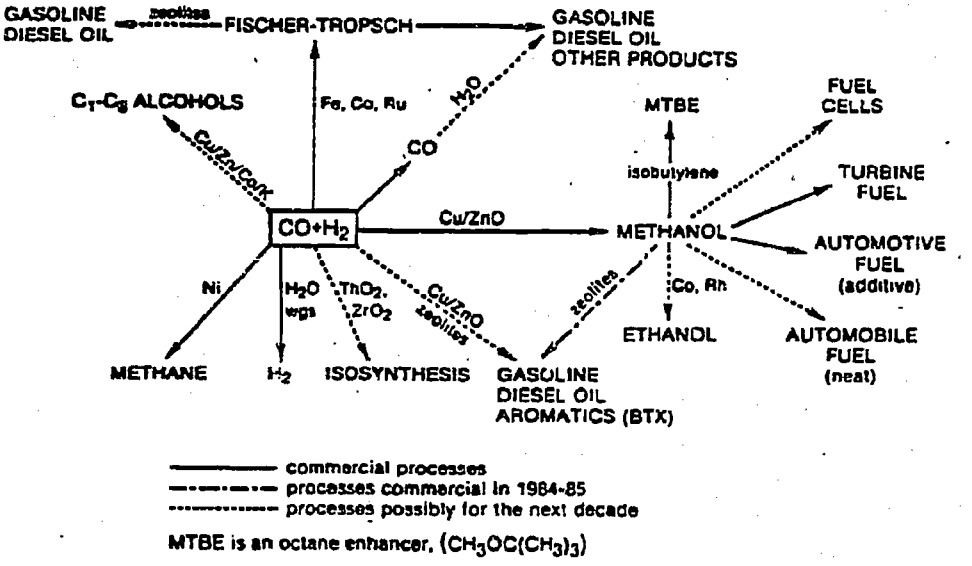

Figure 1.1: Commercial of near commercial processes for the production of fuels from synthesis gas[1]

The Hydrogen/CO ratio of the syngas from the gasifier depends on the feedstock. e.g., for a coal based syngas, the hydrogen/CO is 0.5-1. If the process requires a different hydrogen/CO, then the water gas shift reaction is to be used to get the required optimum ratio required for the process. This substantially increases the cost of the syngas. For a coal based synthesis gas the cost of raw material is as follows:

$$Methanol > Ethylene > 2:1 Syngas > Propylene > CO > 1:1 Syngas$$

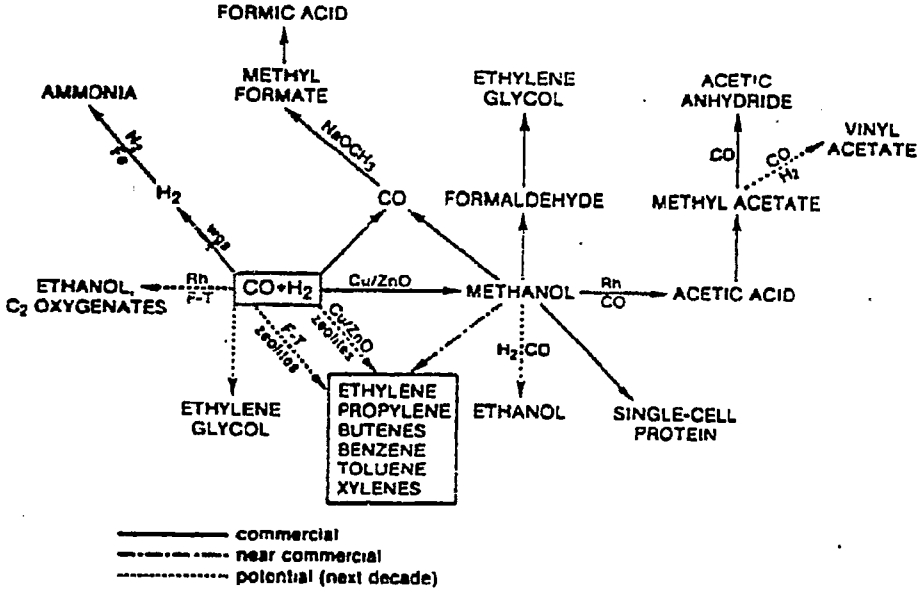

Figure 1.2: Commercial of near commercial processes for the production of potential chemicals from synthesis gas[1]

As the fraction of hydrogen in the synthesis gas increases, the cost of the syngas also increases. Thus new coal based processes should preferably use a 1:1 syngas.

Reactions of syngas on supported transition metal catalysts can give rise to a gamut of products[3]. For example, on supported nickel catalysts methane is formed , and on supported Fe and Ru catalysts methane and higher hydrocarbons are formed. In contrast, supported Cu and Pd catalysts gives exclusively methanol. Reactions of syngas on supported Rh catalysts, not only gives hydrocarbons and methanol but also produces higher oxygenates. This is particularly important because higher oxygenates are high-value added products. At present with a few exceptions, Rh is the only transition metal known to produce higher oxygenates from syngas. This is because of the ability of Rh to insert CO ligands in the

metal-carbon bond. This property of rhodium is extensively used in homogeneous catalysis for the manufacture of acetic acid from methanol.

1.2 Oxygenates

Oxygenates are oxygen containing organic compounds such as methanol, ethanol, acetic acid, acetaldehyde, dimethyl ether, methyl acetate and others. The individual oxygenates are valuable chemicals and there exist many commercial methods for synthesis of each of these oxygenates from syngas. Due to the phase down of lead in gasoline, the more stringent environmental regulations, and the higher demand for high octane gasoline, the refiners are in search for alternative ways of enhancing the octane rating of the gasoline pool[3]. Addition of oxygenates such as MTBE or mixtures of alcohols is one economical method of solving this problem. The US gasoline consumption is nearly 250 million gallons per day and hence chemicals added even in minor percentages represent enormous consumption for the chemical industry[4].

Mixtures of oxygenates alone can be used as a fuel, but more often the oxygenates are blended with conventional gasoline. Thus, unlike the unblended oxygenate mixture, the blended gasoline can be used in the engines and in the gasoline distribution network without any change. This oxygenate gasoline blend increases the octane rating and also results in much better combustion characteristics[5]. Also, if the syngas is made from natural gas or coal, it decreases the dependence on imported crude oil. In contrast, MTBE and methanol have the potential of being used in pure form as octane enhancers. The only proven mixed oxygenate technology on an industrial scale is the MAS technology with a demonstrative industrial plant of 15000MTPY capacity[6]. A 70:30 methanol: higher oxygenates mixture is produced from the MAS technology. This mixture is

used at 4.3 volume % in gasoline and is being distributed in southern Italy since 1985[6].

It is estimated that in 1986, 50 million vehicles were running on motor fuels containing substantial amounts of alcohols or ethers. The number of vehicles running on oxygenates blends in the three major countries/areas are as follows: Western Europe 25 million, US 15 million and Brazil 11 million. Consumption of oxygenate as motor fuels in 1984 were EtOH 7.5Mt/yr, MeOH 1.3 Mt/yr, TBA 0.8 Mt/yr and MTBE 1.0 Mt/yr[7].

There are many methods of manufacture of higher oxygenates; some of then are listed in figure 1.3. The IFP process based on modified Cu/ZnO catalysts is also promising[8]. However there are serious thermodynamic limitations owing to the low activity of these catalysts. The molybdenum sulfide route has recently become popular due to the discovery of Dow[9]. The last category is the modified Fisher-Tropsch catalysts. After the initial discovery from Union Carbide[10], the modified rhodium based catalysts have been extensively investigated. Here again many different approaches have been used. Some of then include the use of different support or different modifier. In this dissertation, the scientific issues in the catalytic reaction of synthesis gas to form mixtures of higher oxygenates on modified rhodium catalysts are investigated.

It is important to recognize the technological issues related to the catalytic conversion of syngas to higher oxygenates. Figure 1.4 shows the problem and the solution with some of the technological issues with the higher oxygenates catalysts. Most of the higher oxygenates catalysts, especially the Cu/ZnO based catalysts have low activity and hence have to be used at higher temperatures. The use of higher temperature brings in the thermodynamic limitations on many products. The thermodynamic limitations can be partially overcome by higher pressures. Also, these catalysts are not selective for formation of oxygenates. Thus these

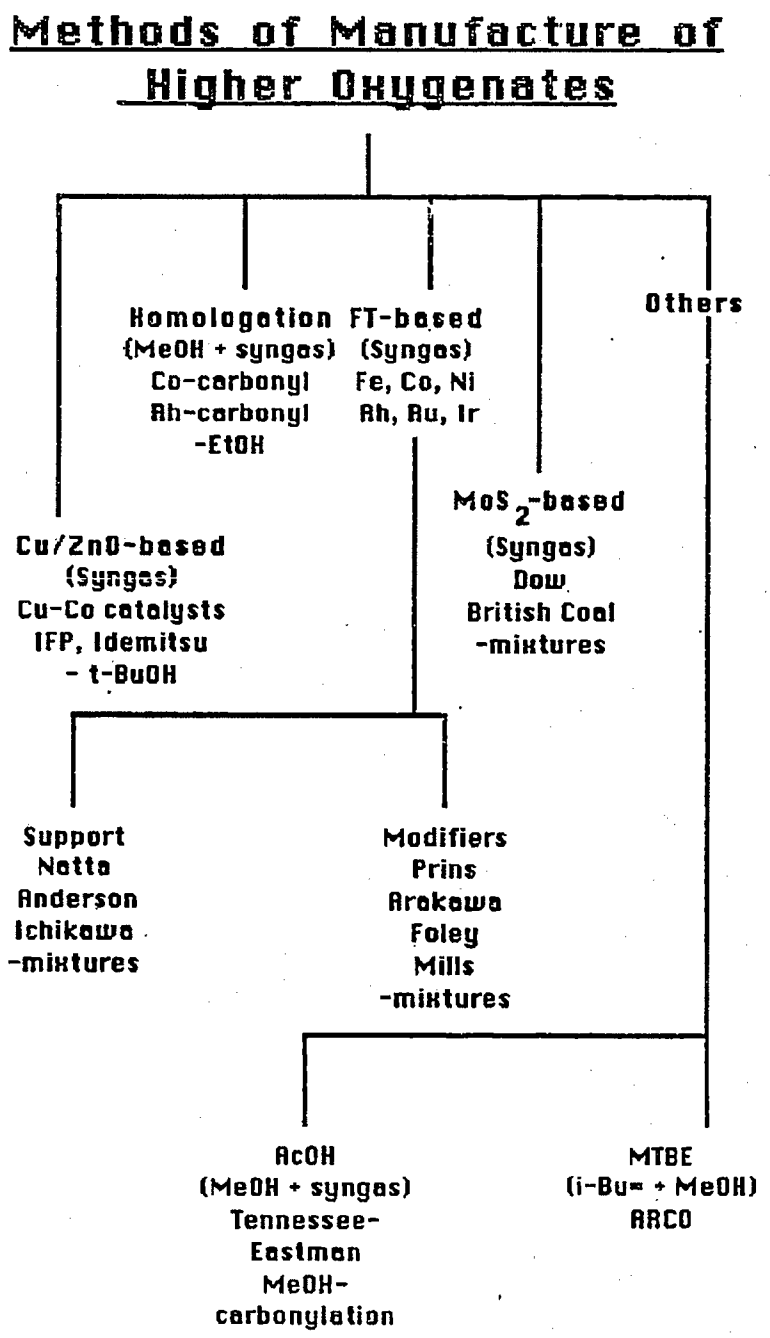

Figure 1.3: Methods of manufacture of higher oxygenates[3]

catalysts have to be modified, e.g., Rh/Al_2O_3 catalysts may be modified with molybdenum to increase the selectivity.

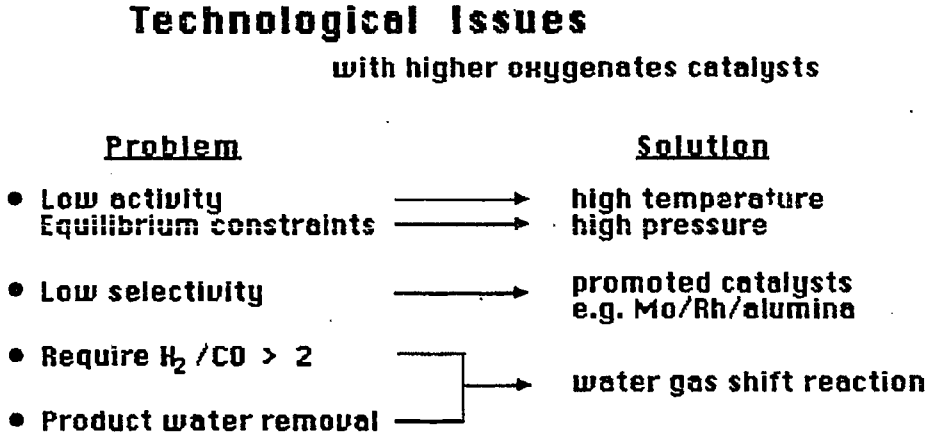

Figure 1.4: Technological issues with higher oxygenate catalysts

The third problem is the removal of product water. Water is formed as a by-product when hydrocarbons or higher oxygenates or secondary products such as esters or ethers are formed. The water severely affects the combustion characteristics of the gasoline oxygenates blend. Also water forms complex azeotropes with many mixtures of the oxygenates. Thus the formation of water is to be prevented as far as possible or should be removed in-situ. The water gas shift reaction, given in equation (1.1), provides an easy method of removal of water.

$$CO - H_2O = CO_2 - H_2 \qquad (1.1)$$

Thus the water can be removed by forming carbon dioxide through the water gas shift reaction. Hence a carbon atom is lost as carbon dioxide for each water molecule recovered. Thus it is important that the catalysts for production of higher oxygenates should also be good water gas shift reaction catalysts. The fourth problem is that most of the catalysts for higher oxygenate synthesis are not active for syngas with a hydrogen/CO < 2, i.e., they are active only for expensive syngas. For a coal based syngas the use of water gas shift reaction simultaneously solves the third and fourth problem since hydrogen is produced inside the reactor. Hence not only is the water removed from the products but also hydrogen is produced, thus increasing the hydrogen/CO ratio of the syngas. This solution is not attractive for natural gas based syngas since it is not hydrogen lean.

1.3 Scope

This dissertation is aimed at identifying interesting modified rhodium systems and elucidating structure-activity relationships in these systems with the overall goal of understanding the scientific issues in the catalytic conversion of syngas to oxygenates. Specific additives are selected based on the scoping experiments. The effect of the additives on supported rhodium catalysts is then investigated. Throughout the investigation, experiments and analysis were performed on real systems instead of ideal systems.

1.4 Approach and Structure-Activity Relationships

The approach of this dissertation towards elucidating structure-activity relationships is depicted in figure 1.5. The square box at the center of the figure shows the catalytic system that consists of the catalysts and the gas phase. The approach consists of probing the system at a certain level and then studying the response of the system. The problem is approached at two different levels, the macroscopic

level and the molecular level. At the macroscopic level, phenomenological models are used. This is shown as level 1 in the figure 1.5. At this level kinetics and performance testing is done. And the system is probed through the gas phase. The information obtained from the response of the system is shown in the box in the top right hand corner and consists of the catalysts activity for CO hydrogenation, the selectivity to various reaction pathways, the catalysts stability, and the results from test reactions. At the second level, shown as level II in figure 1.5, the problem is approached at the molecular level, and the catalysts are characterized by a battery of spectroscopic techniques. The probe at this level consists of electrons, photons such as x-rays, and IR rays, ions and magnetic field. The probes used are spectroscopic techniques such as X-Ray diffraction, X-Ray Fluorescence Spectroscopy, X-Ray Photoelectron Spectroscopy, Transmission Electron Microscopy, Energy Dispersive X-Ray Analysis, Infrared Spectroscopy, Ion-Scattering Spectroscopy, Electron Spin Resonance Spectroscopy and Solid-State Nuclear Magnetic Spectroscopy. The information obtained from these response consists of the types of phases present, the dispersion of various components, the oxidation state of different elements, the bonding of various species, the spatial distribution of species present and so on. At this level the focus is on the catalyst. As a rule, the investigation at the second level is not done under catalytic conditions. The final task in this approach is to combine the information obtained in Level I and Level II to give structure-activity relationships. Chapters 5, 6 and 8 elaborate the results obtained at level I of this approach. While, chapters 7 and 9, elaborate the results obtained at level II of this approach.

The investigation is started at the first level, where interesting trends in the performance of the catalysts are identified. Then the catalysts are characterized by different techniques. This rules out many but not all the possible hypotheses. Then, a series of test reactions at the first level are done to rule out some of the hypotheses. This is again confirmed by more characterization. Thus the approach

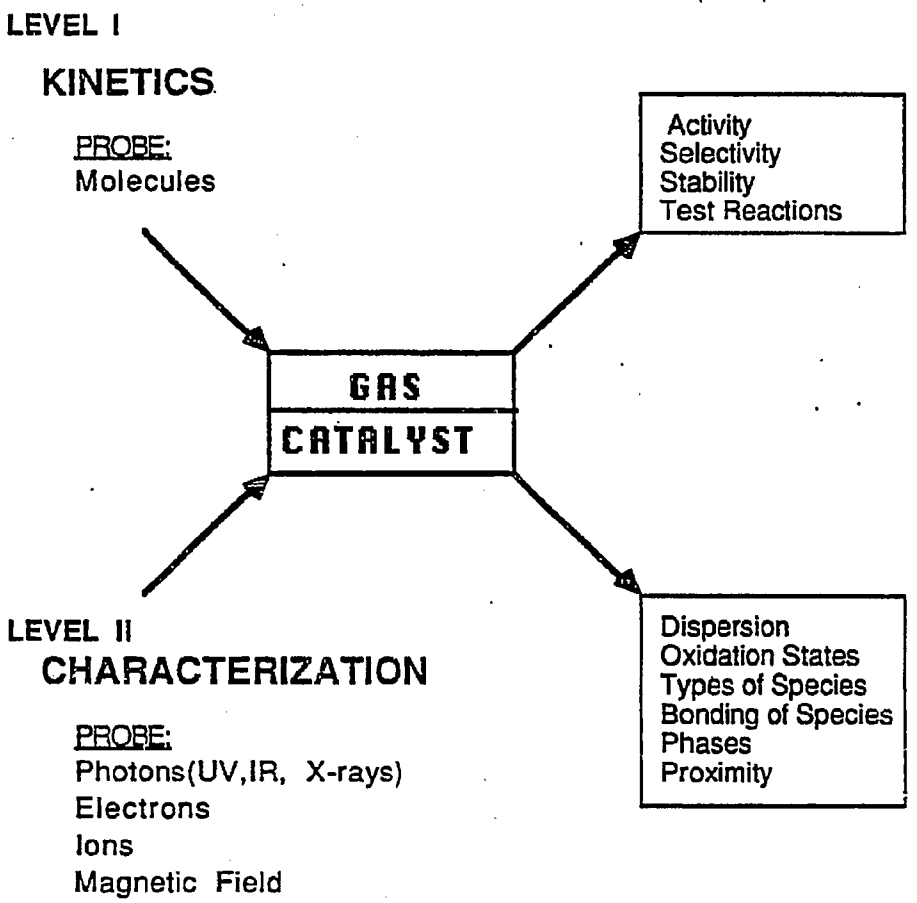

Figure 1.5: Approach to structure-activity relationships

is in the form of feedback loop where information in level I is used to design experiments at level II and vice versa. Of course, all the information from the two levels has to be internally consistent.

It is important to recognize the limitations of catalysts characterization techniques. The major disadvantage of the characterization techniques is that they seldom can be applied to catalysts under working conditions. This poses an open ended question: Is the state of the catalysts same under reaction conditions and characterization conditions? For example, XPS experiments are done under ultra-high vacuum environments and at room temperature, and the state of the catalysts is assumed not to change by this change in pressure. Solid-State NMR spectroscopy and ESR spectroscopy experiments are done at room temperature under a different gas environment. Also, XRD is done under ambient conditions. In contrast, IR spectroscopy can be used under reaction conditions.

The optimum characteristics of a sample needed for a characterization technique is not same as the optimum characteristics of a catalysts. Furthermore, the optimum characteristics of sample for two different characterization technique may not be same. In my opinion, because the main focus of this dissertation is on catalysis and not on characterization, the catalysts were not tailor made to suit a characterization technique. For example, it is well known that the performance of various alumina supported catalysts is different. CATAPAL alumina is a porous and a hard support. In contrast, the Degussa alumina is fluffy and non-porous. Because of the porosity of the CATAPAL alumina, good contrast between the support and metal particle cannot be achieved in TEM. Thus the distribution of metal particle on the support surface cannot be characterized by TEM. There are two ways of solving this problem: increasing the metal loading or using non-porous supports such as Degussa. However in doing this the problem is being modified, and the catalysts is being tailor made to suit a characterization technique.

Similarly, for solid-state NMR, the signal/noise ratio for ^{13}C NMR is low, this normally leads to 72-96 hours of data collection. This long data collection is not feasible for getting data for many samples. Thus many SS-NMR investigations use high metal loading about 15% to get good signal/noise. Because of the hardness of the CATAPAL alumina, pressing a self supporting IR transparent wafer is an arduous task. Also, the optimum loading of metal for CO adsorption studies for IR is low. Thus the ideal requirements of a sample for a characterization technique are often contradictory. In this investigation, no attempt was made to change the catalysts so that a particular characterization technique could be applied.

The third problem with the characterization techniques is the sensitivity and relevance to catalysis. For example, the extinction coefficients of carbonyl species on the surface are high compared to other carbonaceous species. Thus an IR spectrum shows only species with high extinction coefficient. Furthermore, the IR technique shows the species "parked" on the surface, which may or may not be of any significance to the catalytic activity. Also, many of the techniques are not surface sensitive and care should be taken in data interpretation. With these limitations in mind, a reactive molecule is still the best probe for the catalytic performance of the catalysts and hence the data from the reaction studies, kinetics and test reactions is combined with the characterization studies.

Another way of summarizing this approach, is to look at the hierarchy of models. Figure 1.6 shows the hierarchy of models at different levels. The x-axis is the relevant size scale of the problem and the y-axis is the relevant time scale of the problem. As we go away from the origin we look at the problem from a macroscopic view. In the work done in this dissertation, we are working in the middle three boxes that consists of continuum model, microstructural and phenomenological models and molecular models. For example, the kinetics and performance testing results give information on the macroscopic level and the analysis is done on a

phenomenological basis. In contrast, most of the spectroscopic techniques give details of the molecular model of the system. Here for instance, nuclear relaxation calculation shown in chapter 9 gives the average of the minimum distance between two species of interest. By working over a wide time scale and size scale, the information from the molecular level is integrated with the information at the macroscopic level to be of use in real catalysts.

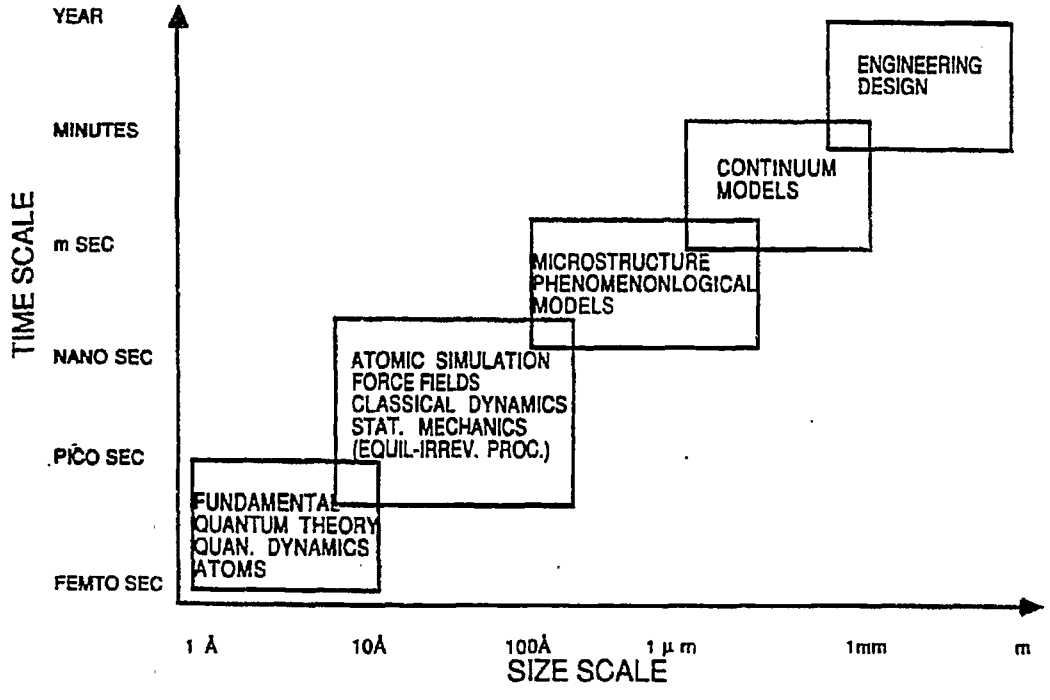

Figure 1.6: Hierarchy of models 11

The information obtained from various characterization techniques is summarized in table 1.1. For example, x-ray diffraction results give particle size of the

the crystalline phases present in the sample. However x-ray diffraction is usually done at room temperature under ambient atmosphere. X-ray fluorescence spectroscopy is used to find the elemental composition of a catalysts sample with atomic number $Z > 11$. Transmission electron microscopy is used to find particle size of the component that causes contrast. However for catalysts containing low loadings of metal supported on porous semi-crystalline support, the contrast is not good enough for visibility. Hence, the TEM results are used to rule out presence of large particles. Energy dispersive x-ray analysis is used to find the elemental composition of the sample probe area in a microscope. This probe area can be in thousands of angstroms for TEM mode and hundreds of angstroms for Scanning-TEM mode.

Chemisorption is frequently used to measure the number of metal atoms accessible to the gas phase. X-Ray photoelectron spectroscopy cna be used to find the chemical state of the elements within the top 10-30Å from the surface. The physical state of the phase containing a specific element can also be investigated. In contrast, ISS gives elemental composition of the top 1-2 layers of the sample. The magnetic resonance techniques such as ESR and SS-NMR spectroscopy give information about the local chemical environment around the paramagnetic center and the NMR-active center respectively. Finally, infrared spectroscopy provides an excellent, easy to use technique to investigate the bonding of reactants, products and various probe molecules on catalyst surfaces. Also, infrared spectroscopy can be used over a wide range of pressure and temperature.

1.5 Organization of Dissertation

The dissertation can be divided into two main group of chapters, the results chapters and the other chapters. Chapters 4 to chapter 9 are the results chapters. First an introduction to syngas and oxygenate technology is given in this chapter.

Table 1.1: Information obtained from characterization techniques

Technique	Information Obtained
X-Ray Diffraction	Particle size of crystalline phases
X-Ray Fluorescence	Elemental composition
Transmission Electron Microscopy(TEM)	Particle size and spatial distribution of components, nature of phases
Energy Dispersive X-ray Analysis	Elemental distribution from a given probe size
Chemisorption	Number of surface metal atoms
X-ray Photoelectron Spectroscopy	Chemical state of elements, physical state of elements(10-30Å) from surface
Ion-Scattering Spectroscopy	Elemental composition of top 1-2 layers
Electron Spin Resonance Spectroscopy	Local environment around the unpaired electron
Solid-State Nuclear Magnetic Resonance Spectroscopy	Local environment around the NMR-active center
Infrared Spectroscopy	Bonding of adsorbed species
TPD-TPR	Number and strength of sites and reduction states

Then the scope and approach is outlined. The second chapter discusses some of the background material. Because of the voluminous nature of topics such as infrared spectroscopy and mechanism of CO hydrogenation, and because of the availability of excellent texts and review articles, these topics are only briefly discussed and literature of immediate relevance is summarized. The theory of the spectroscopic techniques used is not discussed since it is available in many text. The only exception is the theory of relaxation of NMR-active nuclei by fixed paramagnetic species since it is seldom used in catalytic investigations. Even though a thorough understanding of this field needs a working knowledge of quantum mechanics, magnetism and nuclear dynamics, the background of this relaxation theory is not discussed. Instead the reader is referred to excellent texts and review articles in this field. The background chapter discusses the results of characterization studies on similar systems. For example, in the XPS section, the results of supported molybdenum catalysts and supported rhodium catalysts is discussed.

Chapter 3 develops a new kinetic method of analysis, the delplot method. This method is later used in chapters 6 and 8. Chapter 4 describes the experimental methods and related equipments. Here again, the experimental procedure for the traditional characterization techniques such as XRF, XRD, IR etc. is briefly described. The high pressure reactor is described in considerable detail since it was built exclusively for the experiments described in chapters 5, 6 and 8. Because the NMR sample preparation method is new, it is described in detail.

Chapter 5 describes the results of the scoping experiments described earlier. In this chapter, the effect of modifiers, support and various catalysts preparation parameters on the performance of these catalysts is discussed.

Chapters 6 discusses the effect of addition of sodium on rhodium/alumina catalysts. Various parameters such as the amount of addition of sodium, sodium salt precursor, sequence of addition is investigated. Also, the effect of various

process parameters such as temperature and pressure is investigated. The delplot method is applied to this system to separate the primary and non-primary products. Chapter 7 describes the results from characterization studies of the same catalysts. The physical and chemical state of rhodium and sodium is investigated after various treatments. The physical state of sodium and rhodium is investigated using XRD, TEM and hydrogen chemisorption while the chemical state of rhodium and sodium is investigated using XPS, IR and TPD/TPR. Also, the effect of silanization of the surface on the various adsorbed CO species is described.

Chapter 8 shows the dramatic effect of addition of molybdena to Rh/alumina on the activity and the selectivity for CO hydrogenation reactions. The effect of temperature, amount of molybdena added and pressure is investigated. The activation energies are also measured. The delplot method is applied to discern products according to their rank. Furthermore, the slowest step in the reaction network is also identified using delplot analysis.

Chapter 9 describes the results of the extensive characterization of Rh/Mo/alumina catalysts. The characterization of the physical and the chemical state of rhodium and molybdenum is important to identify features of catalytic importance in these systems. First, the physical state of rhodium is investigated using CO chemisorption, TEM and XRD. Then, the bonding of carbon monoxide is investigated using infrared spectroscopy. The effect of addition of molybdena and various catalysts pretreatments on the chemical state of rhodium is investigated using XPS. The chemical and physical state of molybdena is investigated using XPS and ISS. Furthermore, the local environment around rhodium and molybdenum is investigated using ESR and SS-NMR spectroscopy. Finally, the results from various spectroscopic techniques, reaction kinetics and test reaction results are integrated to yield structure-activity relationships.

Chapter 10 summarizes the role of sodium and molybdenum in rhodium/alumina catalysts. Also, recommendations for future work are listed.

REFERENCES

1. W.O. Haag, J.C. Kuo and I. Wender, in "Coal Gasification: Direct Applications and Synthesis of Chemicals and Fuels", ed. S.S. Penner, U.S. Dept. of Energy, Washington D.C., 1987.

2. R.L. Hirsch, Science. 1987, 235, 1467.

3. G.A. Mills, "Catalysts for Fuels from Syngas: New Research Directions" IEA Coal Research, London, 1988.

4. H. Witcoff, J. Chem. Educ. 1987, 64; 773.

5. G.A. Mills and E.E. Eckland, Ann. Rev. Energy. 1987, 12, 47.

6. F. Morandi, R. Trotta, G. Pecci and M. Sposini, Energy Progress 1988, 8, 1.

7. "Alcohols and Alcohols Blends as Motor Fuels", Swedish Motor Fuel Technology Co., International Energy Agency, Stockholm, 1986.

8. Ph. Courty, J.P. Arlie, A. Convers, P. Mikitenko and A. Sugier, Hydrocarbon Proc. 1984, 104.

9. Chemical Week. November. 1984, p28.

10. P.C. Ellgen and M.M. Bhasin, U.S. Patent 4, 014, 913. March 29, 1977

11. D.L. Cocke, in "Design of New Materials", ed. D.L. Cocke and A. Clearfield, Plenum Press. 1987. New York.

CHAPTER 2
BACKGROUND

2.1 Oxygenates

2.1.1 Manufacture

There are many excellent reviews on the technological aspects of the manufacture of oxygenates[1-3]. Therefore, only a brief summary of different methods of manufacture of oxygenates will be given here. The interplay between the environmental issues, technological issues, legal aspects, the engine characteristics and the distribution network is very well illustrated by Mills and Eckland[4]. Higher oxygenates can be formed using syngas by the following methods.

2.1.1.1 Modified Fisher Tropsch

Alcohols can be produced by using alkali-promoted or nitrided Fisher Tropsch synthesis catalysts. In this method the selectivity to oxygenates is less than 50%. Many alcohols are produced in the SASOL plant in South Africa.

2.1.1.2 Iso-Synthesis

In iso-synthesis, syngas is reacted at lower temperatures to yield alcohols predominantly methanol and isobutanol. The disadvantages of iso-synthesis are its low selectivity and formation of large amounts of methane. The iso-synthesis reaction has never been used commercially.

2.1.1.3 Homologation

In homologation reaction, methanol is reacted with syngas in the presence of catalysts such as cobalt octacarbonyl to give ethanol. The selectivities to ethanol are not high and the process is still in the development stage.

2.1.1.4 Co-Production with MeOH

It has been long known that addition of alkali to methanol synthesis catalysts and the use of high temperature leads to an increased share of C2-C5 alcohols. Addition of cobalt increases the yields of straight chain alcohols.

Historically, in the 1930's and 1940's 'isobutyl oil' was commercially produced in Germany by alkali promoted zinc-chromium catalysts in the old-high pressure methanol synthesis processes. The product 'isobutyl oil' contained 30% higher alcohols out of which $\approx$ 15% was isobutanol. Also in England, ICI has produced higher alcohols according to high pressure technology under modified process conditions. The recent developments in the co-production technology are enumerated below.

1. Dow Chemical

Dow Chemical has introduced a higher alcohol process based on molybdenum sulfide based catalysts to convert CO rich syngas to mostly straight chain C1-C5 alcohols. The water content in the product stream is low (1-2%) and the process can be tuned to give a wide variation of methanol to higher alcohols. This process is in its advanced developmental stage.

2. IFP

The typical product stream from the IFP process is given in table 2.1. Note that hydrocarbons are not included in the reported analysis. A specially prepared

Co promoted Cu/ZnO catalyst is used. The synthesis is divided into two stages. In the first stage higher alcohols are produced with a special catalyst at high temperature. In the second stage a conventional methanol synthesis catalysts is used. The selectivity to methanol and higher alcohols is poor (70-75%), and the amounts of C1-C5 hydrocarbons formed is large.

The product stream contains 35 wt% water. The separation of water from these streams is complex because EtOH and higher alcohols form azeotropes. In such cases extractive distillation with diethyeneglycol is done. The process is natural gas based.

Table 2.1: Product distribution of oxygenates of various processes

% Product	IFP	Snamprogetti	Lurgi
MeOH	70-50	70	53.5
EtOH	16-23	1.5-2	3.0
PrOH	8-14	3.5	3.1
> C3 alcohols	6-13		
BuOH		15.5	6.2
Pentanol			3.8
Hexanol			14.8
C5− alcohols		9.5-9	
water		20	0.3
other oxyg.			16.1
C5− hydro			4.3

3. Snamprogetti

The Snamprogetti process uses Zn-Cr catalysts at 80-150 bar and at 360-420 C. The advantage of this process is that it does not require large amount of carbon dioxide in the feed stream. Approximately 15% of the products are hydrocarbons. The typical product stream is given in table 2.1. Multi column distillation is used to separate water. The process is natural gas based and a feasibility analysis for a 2000 tpd plant was carried out.

4. Lurgi

The Lurgi process uses modified copper catalyst with a syngas with hydrogen to carbon monoxide ratio of 1:1. It does not require syngas with high amounts of carbon dioxide. The selectivity to higher alcohols is > 40 % and the amount of hydrocarbons formed is 4-5 %. The main advantage of this process is the very low amount of water formed (0.3-0.4 wt %). Molecular sieves are used to lower water content to less than 0.15 wt %. The typical product distribution from this process is given in table 2.1. Some other methods not discussed here are the Vulcan-Cincinnati process and the Chem Systems process.

2.1.1.5 Modified Rh Catalysts-Based Processes

At present, except for oxoalcohols, almost all the processes based on rhodium catalysts for manufacture of oxygenates have not been commercialized, primarily because of the high cost of rhodium. However Rh catalysts have higher activity. Because of their higher activity they can be used at lower temperatures. Cu/ZnO based catalysts are not very active. Hence they are used at higher temperatures. The use of higher temperature leads to equilibrium constraints on the process. Use of higher pressure overcomes most of the equilibrium constraints. Because of the above mentioned reasons Rh based catalysts can be used at lower pressure, that may lead to lower operating costs and plant investment.

2.1.2 Uses

Oxygenates in pure form can be used as chemicals. However, mixture of oxygenates can be used as a fuel or as a fuel additive. The addition of fuel oxygenates can decrease the pollution from exhaust and increase the octane rating. However other factors such as volatility, optimum air/fuel ratio, compression ratio, cold start-up, compatibility with materials and compatibility with the existing distribution network should be considered. A summary of the approved low oxygenate blends in the United States is given in table 2.2.

2.2 CO Hydrogenation

2.2.1 Reaction Pathway

CO hydrogenation on supported transition metals catalysts is reviewed in many excellent articles[5-13]. In this section, the state of current understanding of CO hydrogenation specially with special reference to the synthesis of oxygenates will be briefly summarized. CO hydrogenation on supported transition metal catalysts proceeds through the dissociative mechanism, or the "carbidic" mechanism. CO monoxide can adsorb dissociatively and non-dissociatively. The carbon on the surface is then hydrogenated to form partially hydrogenated carbonaceous species. These higher partially hydrogenated carbonaceous species can then be hydrogenated to form methane or a CH_x species that can be inserted into the metal-carbon bond to give rise to higher carbon containing species. The two carbon atom containing partially hydrogenated species can again be hydrogenated to give ethylene or ethane or a CH_x species can be inserted into the metal-carbon bond. Thus this process can go on producing the higher carbon containing chains. The rates of each insertion and chain hydrogenation step are independent of chain length. This gives rise to the well-known Anderson-Schulz-Flory distribution given

Table 2.2: Approved low level blends in USA

Oxygenates	Description	Approved content
Ethanol		Up to 10 vol. %
Arconol (GTBA)	Gasoline-grade TBA (small amounts of water acetone, butane, etc.)	Up to 3.5 wt. % O (16 vol. %)
Oxinol	1:1(vol) max ratio MeOH and GTBA	Up to 3.5 wt. % O (9.5 vol. %)
MTBE		Up to 11 vol. % (2 wt. % O)
Petrocoal	Methanol/C4 alcohols (6.5:1 max)	Up to 12 vol. % MeOH and 6 vol. % butanol
DuPont	Methanol/cosolvents (EtOH, PrOH, BuOH)	Up to 3.7 wt. % O (max 5 vol. % MeOH min 2.5 vol. % co-solvents)
General rule	Any except methanol	Up to 2 wt. % O

in equation (2.1).

$$log X_n = log\frac{(1-\alpha)}{\alpha} - nlog\alpha \qquad (2.1)$$

The SF distribution limits the amount of higher oxygenates formed. Molecular sieving effects and mass transfer effects have been successfully used to overcome the SF distribution.

The best to-date mechanism for CO hydrogenation on supported rhodium catalysts to hydrocarbon and oxygenates is by van den Berg[14]. His mechanism, shown in figure 2.1 combines the now accepted FT mechanism and CO insertion pathway to oxygenates. According to van den Berg, the CO ligand on the surface can insert into the metal-carbon bond of the M-C_xH_y species. This is shown as step 4 in figure 2.1. This gives rise to oxygen containing species on the surface, that can produce oxygenates such as ethanol, acetaldehyde and acetic acid. It is important to recognize that the formation of methanol proceeds through a separate reaction pathway. There are important implications of the reaction pathway shown in figure 2.1. They are:

1. Since methanol is formed in a separate reaction pathway, it is theoretically possible that of the oxygenates all could be C2 oxygenates and none C1 oxygenates. This should be compared with Fisher-Tropsch products, where only 100% methane can be formed. Thus according to this reaction network, the catalysts functions needed for higher oxygenate synthesis are CO dissociation, hydrogenation and CO insertion.

2. Assuming that the rate constant for the CO insertion step does not depend upon the chain length, the oxygenates should also follow the SF distribution. However, now the C1 analog of the SF distribution is the C2 oxygenates since methanol is formed from a separate reaction pathway.

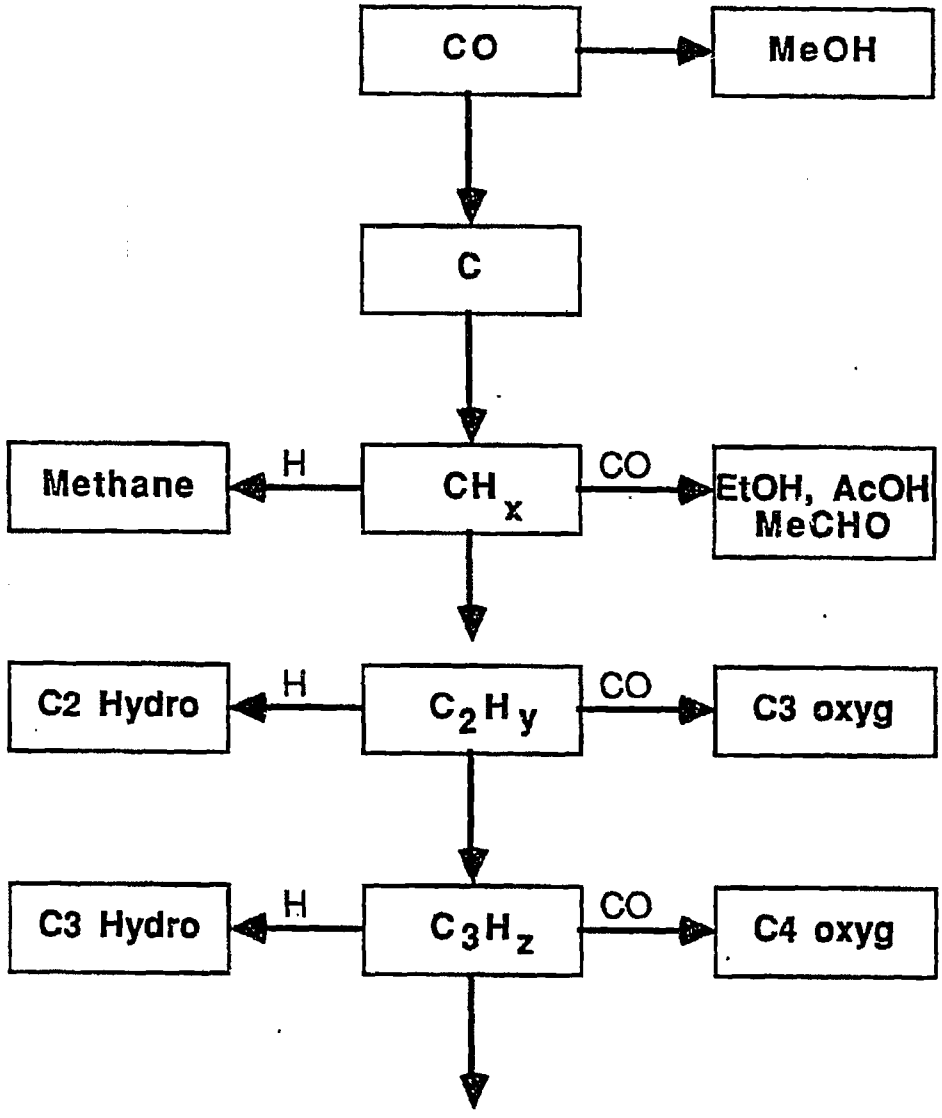

Figure 2.1: Mechanism for CO hydrogenation on supported Rh catalysts[14]

2.2.2 Effect of Support and Modifiers

There are many reviews on the effect of support and modifiers on CO hydrogenation on supported transition metal catalysts[1,5-9, 15]. The results of previous investigations of rhodium-based catalysts are summarized in tables 2.3 and 2.4. The patent literature is not considered here, but an excellent summary of patent literature upto 1982 can be obtained elsewhere[16].

It is clear from the table 2.3 and 2.4 that the addition of modifier can change the activity and selectivity characteristics of the catalysts considerably. Table 2.3 shows that the role of support has been intensively investigated. However, as seen from table 2.4 most of the investigations of the effect of modifier have been on silica supported system. Because of the good mechanical strength and the framework strength of alumina and because of the wide range of surface properties of alumina, supported alumina catalysts are preferred. Hence alumina supported catalysts will be the primary focus of this thesis. Furthermore. other supports such as titania and florisil were also investigated.

The most detailed investigation of the role of additives to supported rhodium catalysts is by Arakawa et al.[34]. Figure 2.2 shows a summary of their results. They find that Mn, Sc, Ti. V and La increase th CO dissociation, Mn, Sc, Ti, Fe and Ir increase the chain propagation in the FT chain, K and Li increase the hydroxylation, and Fe and Ir increase the secondary hydrogenation.

2.2.3 Effect of Metal Precursor

There have been very few investigations on the effect of metal precursor on the performance of supported rhodium catalysts and again most of the previous investigations have been on silica supported catalysts[35-39]. Jackson et al.[35] found that there was a decreased in the amount of ethanol formed when going

Table 2.3: Summary of the effect of support on CO hydrogenation of supported rhodium catalysts

Support	Effect on CO hydrogenation	Ref.
ZnO, MgO	produces mainly methanol	17, 18
ZrO_2 , TiO_2 , La_2O_3	produces mainly C2 oxygenates.	17, 18
MgO, SiO_2 , Al_2O_3	methanol is formed on basic	19
TiO_2 , CeO_2	support	
La_2O_3	high selectivity to oxygenates	20
SiO_2 , Nd_2O_3 , Sm_2O_3		
SiO_2 , Al_2O_3 , TiO_2	Act.: Nb_2O_5 >Al_2O_3 >SiO_2 >MgO	21
Nb_2O_5 , MgO		
SiO_2 , Al_2O_3	Act.: TiO_2 >Al_2O_3 > SiO_2 > MgO	22
MgO, TiO_2	small amount of oxyg.	
Al_2O_3 , TiO_2 , MgO	Act.: TiO_2 >Al_2O_3 >MgO	23
SiO_2 , TiO_2	Act., Sel.: TiO_2 ≫SiO_2	24
WO_3 , MoO_3	increase in reactivity	25

Table 2.4: Summary of the effect of modifier on CO hydrogenation of supported rhodium catalysts

Support	Modifier	Effect on CO hydrogenation	Ref.
SiO_2	V, Ti, Ta, Th, Zr	EtOH activity V,Ti,Ta,Zr,Th	26
	Hf, Mo, W, Cr	$\gg$ Ce,La,Cr,Mo,W	
SiO_2	V, Th, Mo	high activity	27
	Mo, Fe, La	high methanol activity	
	V, Th, Ce, Mn, Ti	high C2 oxygenates	
SiO_2	Mn-Mo	activity increases	14
		C2 oxygenate selectivity increases	
SiO_2	Ti-Fe-Ir, Mn-Li	C2 oxyg. sel. high	28
TiO_2	Li, K, Cs	C2 oxyg sel. high	29
ZrO_2	Mo	good CO insertion	30
SiO_2	Mn, Mo, W, Fe	increase sel.	31
SiO_2	Na	Increases sel.	32, 33

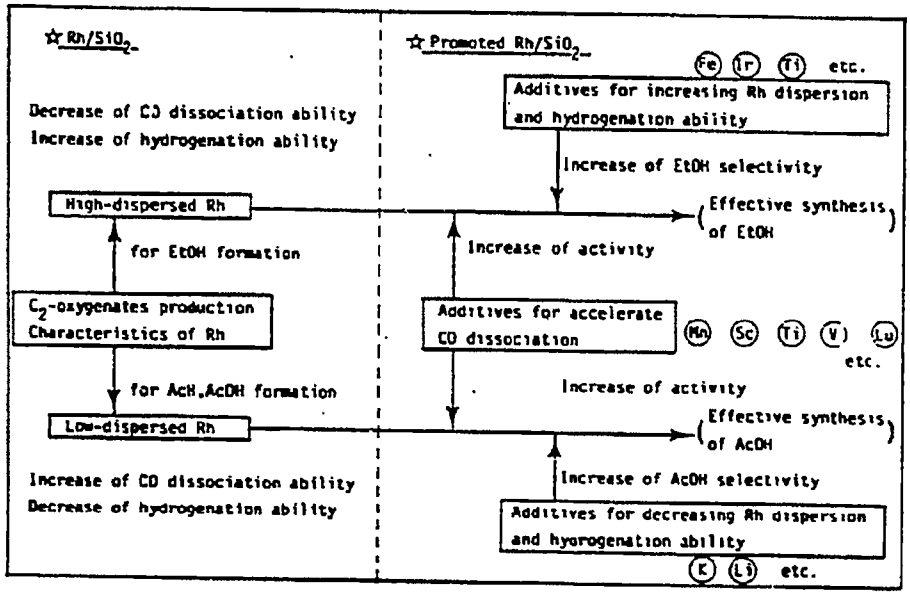

Figure 2.2: The effect of additives on Rh/SiO_2 [34]

from chlorine based Rh/SiO_2 to nitrate-based or acetate based Rh/SiO_2. . A kinetic compensation effect was observed on these catalyts. Jackson et al.[35] have found that the activity of the Rh/SiO_2 catalysts vary as follows

$$(NH_4)_3RhCl_6 > Rh(acac)_3 > RhCl_3 > (Rh(CO)_2Cl)_2$$

$$> Rh(NO_3)_3 > Rh(CO)_2acac > Rh_2O_3$$

Also they find that the catalyst obtained from Na_3RhCl_6 is much more active than Rh-Na (derived from $RhCl_3$ and NaCl) catalysts. The results are very surprising because. unlike the results of Wilson[33], they find that the sodium

modified catalysts are more active than the non-modified catalysts. The amount of hydrocarbonaceous residue on these catalyst varies in the same order as the activity. They postulated that this hydrocarbonaceous residue acts as a hydrogen-transfer agent. Worley et al.[40] have found changes in the IR spectra of CO adsorbed on Rh/Al_2O_3 derived from different metal preucrsors. Specifically, very little CO was adsorbed on the catalysts prepared from rhodium acetate dimer. This was attributed to the residual acetate ligands poisoning the surface. Reduction of the catalysts showed that the acetonylacetate ligands left a residue that blocked the surface.

Kip et al.[41] have observed that the TOF for CO hydrogenation on Rh/SiO_2 was constant with increasing rhodium content and particle size when prepared prepared from rhodium nitrate. In contrast, the turnover frequency increased with increasing particle size when the catalysts is prepared from rhodium chloride. These differences were attibuted to the morphology of the particle.

2.2.4 Role of Additives in CO Hydrogenation

Kip[27] has presented an excellent exposition on the role of additives of the in synthesis of oxygenate products from syngas. A summary of different roles of additives is given in table 2.5. As seen from the table the additives can either dilute the metal, stabilize the metal ions, neutrilize the acid centers, be responsible for CO dissociation, CO insertion or hydrogen activation.

2.2.5 Effect of Alkali Modifier

Mross[62] has reviewed the effects of alkali doping in heterogeneous catalysts. Specifically for carbon monoxide hydrogenation in Fisher-Tropsch Synthesis, alkali can act by

Table 2.5: The role of additives in CO hydrogenation[27]

Role	System example	Ref.
Decrease in active metal surface area	Rh/Cu, Ru/Cu	42-44
Stabilization of metal ions	Pd/SiO_2	45-47
Neutralization of support acid centers	Alkali	48-50
SMSI	TiO_2 supported	51
CO dissociation	$Rh\text{-}Na/Al_2O_3$	52-54
CO insertion		55, 56
Hydrogen activation	$Ni\text{-}Mo/Al_2O_3$	35,40,57-59
Additive as catalytic center	$Fe\text{-}Ir/SiO_2$	60, 61

(i) Increasing selectivity

In the case of FTS it is possible increase the olefin and alcohol content by doping the iron or cobalt catalyst with alkali[63,64]. The activity of FTS was reported to pass through a maximum when the ratio of K:Fe was $\approx$ 0.75:100.

(ii) Increasing the effective lifetime of the catalysts

The effective working life of Ni/Al_2O_3 catalysts for methanation can be prolonged by addition of small amount of alkali metal[65]. The alkali suppressed the deposition of "kinetic" coke on the catalyst. On the other hand it is also observed that the alkali accelerates the recrystallization of Al_2O_3 support. This reduces the effective lifetime of the catalysts by decreasing the effective surface area.

(iii) Change in the electronic environment of the transition element

The activity enhancing effect of alkali on metallic catalysts is frequently attributed to the electronic factor[66,67]. Very often conflicting trends are observed on

different transition metal catalysts. The adsorption of alkali metal ions onto the metal surface facilitates an electron-donor effect by the neighboring metal atoms. Martin et al.[68] have observed an increase in the electron density of the metallic nickel on addition of potassium on Ni/SiO_2 . Also patches or islands of Ni-O-K surface complex concentrated on the nickel surface were found. Mori et al.[69] have observed that the rate of C-O dissociation as observed by Pulse Surface Reaction Rate Analysis is decreased on addition of alkali carbonates such as sodium carbonates, potassium carbonates and lithium carbonates. They find a linear relationship between the logarithm of the rate constant against the CO-shift as observed in IRS.

Bartley[70] has used substituted pervoskite material such as $[La_{1-x}P_x]$-$[Rh_{1-y}Q_y]O_3$, where examples of P and Q are

P: Na, K, Rb, Cs and others

and Q: Fe, Ru, Ni, Co, Cu, and others

CO hydrogenation on these pervoskite material gave substantial amount of MeOH, methane and C2 oxygenates. Chuang et al.[29] have reported an increase in selectivity to oxygenates on alkali addition to Rh/titania. The activity of the alkali-modified catalysts varies as

$$Un - promoted < Li < K = Cs$$

while the overall selectivity decreased in the order

$$Un - promoted > Li > K > Cs$$

They observe a strong hydrogenation suppression ability that leads to decreases in hydrocarbon activity and selectivity.

Campbell and Goodman[71,72] have reported a marked increase in the rate of carbon monoxide dissociation on potassium addition on Ni(100) surface. Unlike the supported catalyst. the overall rate of higher hydrocarbon production was faster on the potassium covered surface. This increase in higher hydrocarbon production is attributed to the increase in the steady state active carbon level during the reaction.

Gonzalez et al.[73,74] have observed that the addition of alkali metal to Ru/silica did not change the hydrocarbon product distribution compared at same conversion or methane turnover frequency. Dry et al.[75] have reported an increase in methanation activity of Fe/Al_2O_3 . These results show the opposite trend to the results of various other investigations of alkali metal addition on transition metal surfaces.

Bartley et al.[76] have reported in increases in oxygenate formation on addition of alkali metal to Rh/silica and Rh-Mn/silica. Methane formation was suppressed on addition of alkali metal. The product consisted of 2-carbon hydrocarbons and oxygenates mainly containing acetic acid.

Wilson et al.[33] have investigated the effects of adding lithium and sodium salts to Rh-Mn silica. They show that the addition of alkali metals reduces the activity of the catalyst for conversion of synthesis gas and increase the selectivity to oxygenates. predominantly acetaldehyde and acetic acid. For example, the addition of 0.23% of sodium per gram of 2.5%Rh-0.1%Mn/silica catalyst led to 20 carbon % hydrocarbons . 33% acetic acid, 38%acetaldehyde and 5% ethanol. Surprisingly. the alkali metals first concentrates itself on the rhodium metal crys-

tallite surfaces instead of the support and hence lead to an increase in the heats of chemisorption of carbon monoxide instead of hydrogen.

Tamaru et al.[77] found that acetaldehyde and ethanol can be selectively formed from carbon monoxide and hydrogen by addition of alkali metal to rhodium catalysts. The activity for formation of methane and other higher hydrocarbons was similar on non-doped and sodium-doped catalysts, but the activity for formation of oxygenated compounds was one order of magnitude higher on addition of alkali metal.

Table 2.6 shows the summary of the effect of alkali addition on carbon monoxide hydrogenation on supported transition metal catalysts. There is a general consensus, except the work by Tamaru et al.[77,78] that addition of alkali modifier decreases the overall activity, however greater amount of higher hydrocarbons are formed and the selectivity to oxygenates is increased.

2.2.6 Role of Alkali Modifier

It is well-known that the chemisorption of carbon monoxide places an increased demand on the electrons from the 3d band and leads to strengthing of Fe-C bond and weakening of the C-O bond. When hydrogen is chemisorbed, it transfers electron to the iron and thus electron donating alkali weakens the Fe-H bond. Dry[66] has observed that the heat of chemisorption of carbon monoxide falls by 50%, while the heat of chemisorption of hydrogen falls only slightly. He attributes this to the electronic factor. The addition of alkali carbonate to Ru/Al_2O_3 increases the electron density . This in turn leads to the donation of electron to the antibonding π^* orbital of adsorbed carbon monoxide to the decrease of the bond strength. Mori et al.[69] surprisingly find that the rate of carbon monoxide dissociation decreases instead of increasing with addition of alkali metal. This conclusion was different from that for the simple dissociation of CO(a) to C(a)

Table 2.6: Summary of observed effects on alkali addition

System	Effect on alkali addition	Ref.
K-Fe/Al_2O_3	Increase in selectivity to olefins and alcohols	63, 64
Na-Ni/Al_2O_3	Increase in life-time of the catalysts decrease in coking	65
K-Ni/SiO_2	Increase in Ni electronic density	68
K-Fe/Al_2O_3	Chain growth in FTS accelerated hydrogenation suppressed	67
Na-Ru/Al_2O_3	Decrease in CO dissociation	69
Alkali-Rh/TiO_2	Increase in selectivity to oxygenates decrease in activity	29
K-Ni(100)	Increase in CO dissociation	71,72
Alkali-Ru/SiO_2	No change in hydrocarbon distribution at the same turnover frequency	73, 74
Alkali-Fe/Al_2O_3	Increase in methanation activity	75
Alkali-Rh(Mn)/SiO_2	Increase in oxygenate selectivity	33, 76
Na-Rh/SiO_2	No change in methanation rate; oxyg. rate increased substantially	77,78

and O(a) in the absence of hydrogen. Their results contradict the many experimental and theoretical investigations of the effect of alkali metal additives where an increase in the electron density of the metal and an increase in the simple dissociative process is either predicted or observed.

Campbell and Goodman[71,72], based on their carbon formation studies on K-promoted Ni(100) surface, found that potassium caused a significant increase in the carbon monoxide dissociation rate and a decrease in the activation energy for carbon formation due to electronic effect.

Ertl et al.[79] have performed a detailed study on the role of potassium in the catalytic synthesis of ammonia over supported Fe catalysts. They find that potassium segregates to the surface forming a submonolayer of adsorbed potassium and oxygen. Crowell et al.[80] have observed enormous downshifts in carbon monoxide stretching frequencies on Pt and Rh single crystals. Even though large down shifts were observed for Pt and Rh single crystals, carbon monoxide dissociation was observed only on Rh single crystals.

Gonzalez et al.[73,74] from their TPD and IR studies observed that the binding states of carbon monoxide are not greatly changed on addition of alkali metal. They proposed that the red shifts observed in the C-O stretch region on alkali metal addition is due to the decoupling of CO dipole-dipole interactions by virtue of the disruption in the periodicity of adsorbed layer induced by the presence of alkali metal. They further proposed that the increase in carbon overlayer is not caused by a significant increase in the rate of Boudouard reaction on account of an electronic effect but by the presence of alkali metal in which the hydrogenation of surface carbon species occurs. Their results point out to the two possibilities

1. The effect of alkali is to reduce the availability of hydrogen on the surface.

2. The role of alkali metal is to modify the rate at which hydrogen adds to the carbon atom on the surface, as a result of an ensemble effect.

The exact role of the alkali metal in decreasing the hydrogenation of species is not clear. They believe that the electronic effect in carbon monoxide hydrogenation, unlike that in ammonia synthesis is secondary to a geometric effect brought about by site blocking of the ruthenium ensemble by adatoms. It is important to realize that methanation and FT reactions are sensitive to metal dispersion and hence are very sensitive to site blockage effects.

Because Tamaru et al.[77] observed that addition of sodium to Rh/Al_2O_3 only increased the rate of oxygenate but did not affect the rate of hydrocarbons, they suggested that the active sites for formation of oxygenated compounds are different from those for methane and higher hydrocarbons. The lower alkane/alkene and alcohol/aldehyde ratios of reaction products was observed on addition of potassium , causing a decrease in the hydrogenation of carbon monoxide.

Tamaru et al.[77] further deposited ^{13}C on fresh reduced sodium-doped catalysts. They find that the hydrocarbons produced initially contained considerable amount of ^{13}C indicating that the incorporation of dissociative carbon in the formation of hydrocarbons. However, the role of the dissociative carbon in the formation of C2 oxygenates was not clear owing to the induction period in the formation of the products. Addition of $^{13}CH_3OH$ to the reactants produced products with ^{13}C atom in it except for ethanol. Their conclusion was that the active sites for the formation oxygenated compounds are different from those for methane and other hydrocarbon formation.

Tamaru et al.[78] find that the addition of alkali metal increased the rates and the selectivity of C2 oxygenated compounds considerably and decreased those of the hydrocarbons. The rate of formation of ethanol was more influenced by

the addition of alkali metal cations than that of acetaldehyde. The ethanol selectivity decreased with decreasing ionization potential of the alkali metal, i.e. Li>Na>K>Cs. The role of the alkali metal was to increase the number of active sites of C2 oxygenates and to depress the rate of hydrocarbon formation.

Inui et al.[81] observed a high activity for carbon monoxide hydrogenation on Ru-Mo-Na/Al_2O_3 . But more than 70% of the product was methanol. Furthermore, they find that the catalysts prepared from ruthenium chloride precursor gave a higher selectivity to higher oxygenates.

Table 2.7 summarizes the various explanations put forward to explain the role of alkali modifiers in changing the reactivity of alkali modified rhodium/Al_2O_3 catalysts. As seen from the table, the role of alkali modifier on supported transition metal catalysts has been controversial. Basically, there are two schools of thought. The first set of investigations point out that the predominant role of sodium is to decrease the number of ensembles. Hence, these investigations show that the bonding of CO is not greatly affected on alkali modified catalysts. The second school of thought believes in the electronic effect. This group of investigators believe that the electron density on the metal particle increases on addition of alkali modifier. The synthesis of oxygenates concomitantly produces hydrocarbons and carbon dioxide. Furthermore, the role of alkali modifier on each of these separate reaction pathways has not been investigated. Thus a more detailed investigation of the changes in the activity and selectivity of alkali modified rhodium/ alumina catalysts and simultaneous detailed characterization is warranted.

2.2.7 Effect of Mo Modifier

In the first part of this section the patent literature on Rh-Mo/Al_2O_3 and related catalysts will be summarized. The patent literature is discussed only in this

Table 2.7: Summary of explanations for changes in the performance of catalysts on alkali modifier addition

System	Role of alkali modifier	Ref.
Na-Ni/Al_2O_3	Decrease in coke leads to long life-time	65
K-Fe/Al_2O_3	Weakening of CO bond - more electron donation more CO dissociation	66-68
K-Ni(100)	increase in CO dissociation - increase in steady state carbon- electronic effects	71,72
Alkali-Ru/SiO_2	alkali does not affect CO binding states but hydrogen binding states geometric effect predominant	73,74
Na(Li)-Rh-Mn/SiO_2	Electron rich Rh crystallite causes more CO dissociation	33
Na-Rh/SiO_2	Different sites for oxygenates and formation	77,78

section because there are very few reported investigations on molybdena modified Rh/Al_2O_3 catalysts. In the second part, other relevant literature will be reviewed.

The first reported investigation of supported Rh-Mo catalysts was by Ellgen and Bhasin[16, 82]. This was one of the large series of patents from Union Carbide on the use of modified supported rhodium catalysts for converting syngas to C2 oxygenates. Ellgen and Bhasin found that it was possible to form C2 oxygenates in substantial amount on a catalysts containing $Rh\text{-}Mo/SiO_2$. The support used was silica, and nearly equimolar amounts of molybdenum to rhodium was used. Even though a large range of Mo/Rh ratio was specified, the advantage of using large Mo/Rh ratio was not shown. Reaction conditions were: Temperature, 250C to 350C, pressures 300 to 5000psig, mol ratios of hydrogen to CO range from 5:1 to 1:5 and space velocities of 10^4 to 10^6 GHSV. The amount of C2 oxygenates such as ethanol, acetic acid and acetaldehyde was between 50-75wt.%.

The earliest detailed investigation of the reactivity of $Rh\text{-}Mo/Al_2O_3$ catalysts, particularly the effect of addition of large amounts of molybdena, was investigated by Huang of Ethyl Corporation[83]. Huang found a process for selectively preparing dimethyl ether and methanol by contacting syngas with rhodium-molybdena catalysts. The catalyst consisted of Rh, Mo, and sometimes Fe on a high surface area support. $\gamma\text{-}Al_2O_3$ was found to be the highly preferred support even though no data was presented comparing $\gamma\text{-}Al_2O_3$ to other claimed support such as silica, silica-alumina, magnesia, carbon and zeolite. The catalysts were prepared either by co-impregnation or by sequential impregnation. There are some differences in the details of catalysts preparation from the method used in this investigation, for example, the catalysts were air calcined at 500-600C, for 12-16 hours. Also the catalyst was reduced at 300C for 2 to 3 hours. He found that the reaction temperature had profound impact on the activity and the selectivity of the catalyst. The selectivity to carbon dioxide increased with increase in temperature. Table 2.8 on page 43 shows typical data from the patent. Surprisingly,

they find that addition large amounts of molybdena did not have the dramatic increases in the activity of the catalysts reported here. This may be because of the lower reduction temperature or 600C precalcination used.

Jackson[84] has shown that group VIII metals, particularly supported on WO_3 and MoO_3 , gave higher activity for CO hydrogenation and higher selectivity to oxygenates as compared to group VIII metals on SiO_2 and Al_2O_3 . Particularly Rh gave very dramatic results, the activity increased by orders of magnitude, and the catalyst could be used at temperatures as low as 100C. A typical set of data is shown in table 2.9, in which the differences in the activity between Rh/SiO_2 and Rh/MoO_3 is illustrated. The turnover number for methanol formation on Rh/MoO_3 is 15 times the turnover number for methanol formation on Rh/SiO_2 , compared at two different temperatures(150C and 250C). Also, the role of temperature in changing the selectivity and activity was emphasized. The key feature of Jackson's work was the use of higher activity to use lower reaction temperature, which in turn leads to higher selectivities.

Table 2.9: Comparison of Rh/SiO_2 and Rh/MoO_3

Catalysts	Temp(C)	Methane		Methanol		Ethanol	
		TOF	S	TOF	S	TOF	S
Rh/SiO_2	250	2.002	52	0.081	2	0.135	7
Rh/MoO_3	150	2.29	32	1.509	21	0.554	16

TOF=sec^{-1} $\times 10^3$ S=selectivity, % Pressure=10atm

According to Jackson et al.[25], the crucial issue is the balance between rate of hydrogenation and the rate of spillover. If the rate of spillover is slower than

Table 2.8: Reaction data on Rh-Mo/Al_2O_3 catalysts. as reported by Huang[83]

	3%Rh 6.5%Mo/Al_2O_3			3%Rh 14%Mo/Al_2O_3	
Temp	218	245	277	247	276
Hydrogen/CO	2.2	2.1	2.2	2.2	2.1
GHSV	1440	1480	1570	1600	1570
Press(psig)	230	231	231	231	231
% CO conv.	3.9	20.1	35.4	13.2	27.8
Product Distribution					
CO_2	17.5	30.7	32.0	29.7	34.4
CH_4	23.4	15.8	26.2	11.7	17.9
C_2-C_4 HC's		3.9	8.4	2.7	9.1
MeOH	10.6	5.1	3.7	4.6	3.4
EtOH	1.6	1.1	1.1	0.4	0.2
MeOMe	46.7	37.8	23.4	47.9	33.3
MeOEt		5.5	5.3	3.2	1.7

the rate of hydrogenation then there is no rate enhancement. They have observed presence of molybdena bronzes in these systems corresponding to $H_{0.7}MoO_3$. Also, adsorption of ^1H followed by ^2H and CO gave methane with different isotopic composition. The isotopic distribution of methane showed that ^1H and ^2H exchanges fast, giving credence to the reverse spillover theory. According to Jackson et al.[25], the reduction in support is caused by the spillover, but no comparisons are made with the reduction of only support. The decrease in the CO chemisorption on Rh/MoO_3 as compared to Rh/SiO_2 was attributed to SMSI effect.

Foley and O'Toole[85] have prepared Rh(Ru)-Mo(W) catalysts by depositing metal oxides or sub-oxides on the surface of alumina by chemisorption from solution and subsequent oxidation of molybdenum and tungsten carbonyls. Then, carbonyls of rhodium and ruthenium were deposited followed by an air calcination treatment. The temperature was between 250-350C, with a GSHV of 240 to 2400, pressure between 1 and 4 atm. Typical conversions were between 1 to 10%. A second related invention by Foley and O'Toole[7] was on the use of wide-pore carbon with Rh and Mo components. A summary of relevant patent literature is given in table 2.10.

Turning now to the scientific literature, Inoue et al. have recently reported an extensive investigation of $Ru\text{-}Mo/Al_2O_3$ catalysts[87,88]. Addition of molybdena increased the oxygenate selectivity, however large amounts of hydrocarbons are formed, e.g., the carbon selectivity to oxygenates is 0.8% of the 1.6% CO conversion. The catalysts were prepared by two different methods. In the first method, Ru was impregnated using $RuCl_3$ precursor, followed by Mo impregnation from ammonium molybdate solution. The details of catalysts preparation such as the pH of the solution, calcination after ruthenium impregnation are not reported. Also, it is not clear on how the authors impregnated 10 wt. % Mo, taking into account the solubility limitations of molybdenum oxyanions in aque-

Table 2.10: Review of literature

Authors	Summary of Results	Ref.	System Details
Patent Literature			
Ellgen and Bhasin	Increase in select.	82	Rh-Mo/SiO_2 (Al_2O_3) small amt. of Mo
Huang	Incr. act. & select.	83	Rh-Mo/Al_2O_3 large Mo
Jackson et al.	Increase in activity and selectivity	84	Rh(Group VIII)/MoO_3 (WO_3) very high activity
Foley and O'Toole	Increase in activity and selectivity	85	Rh-Mo/carbon or Al_2O_3 from $Mo(CO)_6$ & $Rh(CO)_2(acac)$
Scientific Literature			
Kip	Incr. rate & select.	27	Rh-Mo/Al_2O_3
Walther et al.	Increase in rate.	91	$RhMo_2cp_3(CO)_6/Al_2O_3$
This Work	Incr. rate & select.	86	Rh-Mo/Al_2O_3 large Mo
Carimati et al.	Incr. rate & select.	30	Rh-Mo/ZrO_2

ous solutions. They found that catalyst prepared from sequential impregnation technique was more active than the catalysts prepared from co-impregnation. The reaction temperature was around 250C and pressures were around 75atm. They also found that the selectivity versus conversion curve was flat, and the selectivity drops by 30% when conversion is increased from 3% to 75%. The carbon monoxide uptake decreased on Mo addition and Na addition. The decrease in CO uptake on Ru-Mo-Na was the sum of decrease in CO uptake on Ru-Mo and Ru-Na catalysts. Also. the addition of sodium ions to Ru-Mo catalyst, decreased CO uptake by one-fourth while the activity decreased by one-half. The ruthenium wt. loading used was 5 wt. %. the Mo loading was varied from 5 wt.% to 10 wt.%. XRD pattern of all catalysts showed Ru peaks. indicating a particle size of greater than 30Å. Addition of sodium to Ru-Mo/Al_2O_3 catalysts made Ru XRD peaks sharper indicating that addition of sodium sintered the catalysts. The reduction conditions consisted of passing hydrogen at 400C for 10 minutes. Because of this short reduction time Mo was found in oxidation state VI.

XPS results showed surface segregation of Mo and Ru in all samples, i.e., the Mo and Ru concentrations were higher on the external surface of the catalysts. Also. they found that surface segregation was higher with catalysts prepared by co-impregnation technique than with sequential impregnation technique. Their TEM results corroborated their XRD results. Based on reaction studies. XRD results. CO chemisorption results and XPS results. Inoue et al. proposed that the active site for oxygenates are the interfacial sites[89,90].

Tatsumi et al.[59] have performed an extensive investigation of Nickel promoted molybdena/SiO_2 catalysts. They find that the catalytic performance for alcohol synthesis is improved on nickel addition. The rate enhancement is ascribed to an alloy formation.

Recently, Walther et al.[91] have synthesized $RhMo_2cp_3(CO)_6$. They report that the alumina supported catalysts dervied from the above precursor is more active than the conventional catalysts. However the differences in the reactivity are marginal.

2.3 Catalysts Preparation: Effect of pH

It is important to recognize the effect of pH on the aggregation of metals used in catalyst preparation because these artifacts during preparation can lead to misleading conclusions. The theory of impregnation of salts on oxide support is well developed[92-94]. Al_2O_3 is a diprotic acid in solution. The charge on the Al_2O_3 surface is observed to change with pH of the solution. In the case of alumina particles in a solution we have the following equilibria:

$$Al - OH_2^- = Al - OH + H^+$$

$$Al - OH = Al - O^- + H^+$$

where

$$K_1 = \frac{[Al - OH][H^-]}{[AlOH_2^-]}$$

and

$$K_2 = \frac{[Al - O^-][H^+]}{[Al - OH]}$$

Rearranging these equations we have

$$[Al - OH_2^-] = \frac{[Al - OH][H^-]}{K_1}$$

and

$$[Al - O^-] = \frac{K_2[Al - OH]}{[H^-]}$$

thus the number of positive and negatively charged species on the surface would depend on $[H^+]$ i.e. the pH of the solution.

The pH_{PZC} (also known as pzpc) is the pH at which the surface in equilibrium with the solution has no net charge.

i.e., $[Al-O^-]_{pzc} = [Al-OH_2^+]_{pzc}$

Substituting the above equations

$$[H^+]^2_{pzc} = K_1 K_2$$

or

$$pH_{pzc} = \frac{1}{2}(pK_1 + pK_2).$$

The pzpc for various oxides is tabulated below

Al_2O_3 : pzpc= 8-9

TiO_2: pzpc= 5-6

SiO_2: pzpc= 1-2

If a solution in contact with a solid has a pH less the pzpc of the solid, then

$$[H^-] \gg [H^-]_{pzc}$$

hence

$$[Al-OH_2^+] \gg [Al-OH_2^+]_{pzc}$$

therefore

$$[Al-O^-] \ll [Al-O^-]_{pzc}$$

Thus the surface is positively charged. If the surface is positively charged adsorption of anions from the solution is facilitated. Conversely, if the pH of the

solution is higher than the pzpc, then the surface is negatively charged. Hence the adsorption of cations is facilitated.

Coloumbic forces are not the only forces responsible for adsorption of ions from solution. Chemical interactions are also possible i.e. it is possible to adsorb anions on a surface which is negatively charged. It is important to note that the above considerations are based only on the thermodynamics of the solution, kinetic and steric factors are not taken into account.

The major molybdenum species is always in an anionic form. However the exact nature of this species is a complex function of the pH of the solution and the molarity of molybdenum in the solution. A phase diagram of various molybdenum anions is given by Baes and Messner[95]. Hall[96] has simplified this phase diagram.

2.4 Characterization

2.4.1 Ion-Scattering Spectroscopy(ISS)

Ion scattering spectroscopy or low energy ion scattering spectroscopy is used to find surface elemental compositions[97-104]. Coupling of ISS with sputter etching gives elemental depth profiles. Ions with energy 0.5-1 keV are used. If an ion beam strikes a surface several processes occur: reflection of the primary ions as ions, metastables or neutrals, or trapping of the ions. Momentum is usually transferred to target atoms causing movement within the solid (also known as radiation damage) and sputtering. The intensity of the primary ions is measured as a function of energy.

There is also release of secondary electrons and photons due to ion bombardment. An ion impinging on a solid interacts with atoms and electrons by means of

Coloumb force. The relative magnitude of these interactions is energy dependent. The electronic interactions, while not imparting sufficient momentum to deflect the ion in their totality causes overall energy loss. The ion therefore moves essentially on an undeviated trajectory through the solid, losing energy until it undergoes a large scale scattering collision with an atomic core. Atomic scattering is elastic while electronic interaction is inelastic. The mass of the target atom in an elastic scattering event can be known by measuring the energy of incident and outgoing ions. For low energy ions in the $\leq$ 2keV, atomic scattering cross-sections are much larger than the cross-sections for electronic interactions. This implies that the ion will traverse a few lattice spacing before it undergoes a violent collision.

As an ion approaches an atom within a distance of a bond length, the electrons on the solid start interacting with the ion. Usually the empty level of the ion is lower than the filled levels in the solid, this makes it energetically possible to neutralize the ion. The energy thus gained is emitted as an Auger electron. The release of the Auger electron causes extra charge accumulation on the non-conducting sample.

The principal mode of electron transport between the ion and solid is quantum mechanical tunnelling. The longer the ion stays near the atom, the higher is the probability of electron tunnelling, and therefore neutralization. The neutralization probability falls rapidly with increasing kinetic energy of the ions because the contact time between the ion and the atom is inversely proportional to the velocity of the ion, e.g., a 1keV Helium ion will be neutralized in passing through one layer of atom while 1MeV ions can penetrate 1μm . This is the reason for the extreme surface sensitivity of LEISS. Usually 1-10 % of ions survive collisions, and the ions that survive collisions form the ISS signal. Also, the lateral spatial resolution in ISS is of the order of micrometers.

Since the ion energy (in all ion scattering experiments) is order of magnitude higher than the bond strength of the chemical bond, the interactions between an atom on the surface and the ion is essentially an atom-ion collision rather than an ion-surface collision. Thus a simple billiard ball collision model is appropriate for describing ISS dynamics.

Depth profiles of atoms inside the catalysts can be determined by sputtering. Because of the gaussian density profile of the ion beam, the so called 'crater effect' is usually observed on sputtering. Even though the 'crater effect' causes non-uniform surfaces, it does present a formidable problem.

2.4.1.1 Problems with ISS on Particulates

Samples of real catalyst are usually prepared as pressed wafers or by vaporization of a suspension of catalysts in an inert volatile solvent. The geometric surface of a catalysts consists of irregularly formed porous particles with a wide distribution of crystallites sizes. Also, the catalyst may also have external surface segregation of the modifier or the metal. Since the catalysts is a polycrystalline powder, different parts of the catalysts surface are at different angles to the surface normal. Sputtering rates are well-known to depend markedly on the angle of incidence with a maximum near 10 to 30 relative to the surface normal. Hence homogenous erosion cannot be expected for real catalysts. Nevertheless the intensity ratios at zero bombardment time provide surface concentration ratios.

The probability that the primary ion survives its ionic state during the collision process is around 1-10% in the energy range below 2keV. It has been shown that the neutralization probability is only dependent on the of scattering atom . and not dependent on the chemical environment around the scattering atom as long as the incidence and scattering angles are within 30 to the surface normal.

However with real catalysts, the above condition of incidence and scattering angles cannot be satisfied. A convenient way of getting around the problem of unknown neutralization probability is to use intensity ratios. The only assumption made in this way of analysis is that the neutralization probability for a given element does not change during sputtering time and at a different area of the sample.

The spectra recorded within the average time for erosion of a monolayer should give significant qualitative information of the changes of the concentration ratios between the topmost and the next few atomic layers. A well defined sputtering depth cannot be attributed to a single sputtering time for powdered samples, because of the above mentioned reasons.

Many times the surface composition can be altered after sputtering, by the differences in sputtering yields for different surface atoms (also known as differential sputtering). This effect depends on the surface binding energy of the atom E_B and on the atomic mass.

2.4.1.2 Previous Work on Catalysts

This review discusses previous ISS work on either Mo/Al_2O_3 or $M\text{-}Mo/Al_2O_3$ where M is a transition metal. There is *no* reported ISS study of Rh/Al_2O_3 or any modified Rh/Al_2O_3. Almost all of the ISS studies in catalysis have been on hydorodesulfurization catalysts i.e. $Co\text{-}Mo/Al_2O_3$ and $Ni\text{-}Mo/Al_2O_3$. For the sake of completion, ISS investigation of CoO/Al_2O_3 and NiO/Al_2O_3 are dealt briefly.

The effect of coordination environment around a transition metal ion in an aluminate spinel on the shielding of other ions in ISS was investigated by Shelef et al.[105]. The first simultaneous application of ISS and XPS to catalysis was

the study of NiO/Al_2O_3 by Wu et al.[106]. The plot of (intensity of Ni/intensity of Al)$_{ISS}$ against the bulk Ni loading shows two distinct lines. The first line has lower slope and is present at lower nickel loading. The line at higher loading has a higher slope. The two regions are related to distribution of nickel in tetrahedral and octahedral sites of alumina.

ISS coupled with XPS and Secondary Ion Mass Spectrometry has been applied to NiO/Al_2O_3 and CoO/Al_2O_3 to study the effect of loading of the metal on the chemical and physical state of the metal[107,108]. The structural characteristics of $Co/Mo/Al_2O_3$ were investigated using ESCA, ISS and Photoacoustic spectroscopy[109]. At higher Mo loading a new phase of Co and Mo is formed. ISS results showed that Co ions were situated beneath the Mo ions. This spatial distribution of Co was named as bilayer formation. Delannay et al. have studied the surface structure of oxidic precursor of $CoMo/Al_2O_3$ hydrodesulfurization catalysts[110]. Sputtering profiles for each element were found. The sputter profiles show the absence of Co on the surface and the presence of large amounts of Mo atoms on the surface. The absence of Co on the surface is very striking because these catalysts were prepared by first impregnating Mo, followed by impregnation of Co. A model in which MoO_3 monolayer covers up the Co-oxide surface area is proposed. confirming the bilayer formation.

Jesiorowski et al. have studied the effect of calcination temperature on the elemental distribution in $Ni\text{-}Mo/Al_2O_3$ [111]. At calcination temperature less than 770K. the surface consisted of molybdate patches and uncovered Al_2O_3 surface. even though the loading corresponds to the theoretical monolayer loading. In contrast. calcination at 870K lead to the spreading of molybdena over Al_2O_3 surface and the formation of 2-D monolayer. The $(I_{Ni}/I_{Mo})_{ISS}$ decreases monotonically with depth after 570K and 770K calcination. In contrast. the intensity ratio goes through a maximum after 870K calcination. This result indicates that NiO is on the top of MoO_3 after 570K and 770K calcination while it forms a bilayer at 870K.

This is in contradiction with the results obtained for $CoMo/Al_2O_3$ by Delanney et al.[110] and Chin et al.[109] who find a bilayer formation at 500C.

Brinen et al. have also studied the effect of catalysts preparation techniques on CoO/MoO_3 $/Al_2O_3$ catalysts[102]. Kasztelan et al. have studied the influence of the method of preparation and the spectrometer operating conditions on the surface structure of the catalysts[103]. Drastic changes in the sputter profile were observed on the same sample at two different incident ion energy. Abart et al.[104] observed using ISS, XPS and magnetic measurements that the reduction of molybdena was significantly facilitated by incoporation of Ni^{2+} ions in Ni-Mo/Al_2O_3 catalysts. Kaztelan et al.[105] have observed a strong shielding effect of Mo by Ni in Ni-Mo/Al_2O_3 catalysts.

The normalization of the intensity of Mo with respect to Al (or the ion scattering response of Al) has a different significance than in XPS. Since the amount of Al atoms in the mean free path of the photoelectrons is high compared to Mo atoms, one can consider Al peak intensity to be good normalizing factor for instrumental correction. However the high sensitivity of ISS technique should preclude consideration of the Al intensity as a constant parameter when Mo loading is changed. The intensity of Al peak forms a good normalizing factor only when the surface area occupied by Mo is a small fraction of the total surface area.

2.4.2 Transmission Electron Microscopy

Transmission electron microscopy(TEM) is a characterization tool to find surface topography, the size and the shape of particles, the different phases present, particle-support interaction, and the spatial distribution of various components on the surface[106-121]. It can also be used in an analytical mode to find the composition and the spatial distribution of various elements on the surface using scanning transmission electron microscopy and energy dispersive x-ray analysis.

The application of TEM in catalysis is done in three stages

(A) Sample preparation

(B) Operation of the microscope

(C) Analysis and interpretation of images

2.4.2.1 Sample Preparation

In TEM, the specimen should be thin enough so that a substantial portion of electrons can penetrate the substrate or the support. Usually in catalysts a thickness of less than 5μm is needed for electron transmission. The first method of sample preparation is microtoming the catalyst powder after it is put in a plastic or epoxy matrix. The disadvantage of this method is that we do not know the extent of permanent changes in metal crystallite.

The second and the more popular method involves grinding the support particles either in a suspended solution or on a glass slide. The fine powder thus obtained is dispersed in water or an inert solvent preferably by use of an ultrasonic vibrator. The resultant slurry is deposited on a plain or "holey" carbon film. The advantages of this method are its simplicity and minimization of damage. The choice of solvent is very critical for preventing irreversible damage to the specimen. A simple modification of the second method is to rub the grid over the powder instead of suspending it in a solution.

Sprys et al.[122] have compared various sample preparation methods. Controlled atmosphere and in-situ electron microscopy experiments need modification of the microscope hardware. Unless the microscope is dedicated, these modifications are not feasible[123,124].

2.4.2.2 Operation of the Microscope

The operation of TEM and other accessories is well illustrated in excellent texts and monographs[125,126]. The operating modes of Conventional-TEM(CTEM) and Scanning-TEM(STEM) are summarized in table 2.11 [117].

2.4.2.3 Analysis and Interpretation of Images

It is very important to understand microscope physics in order to interpret the microscope pictures. Too often wrong conclusions are reached by drawing analogy between optical physics and electron microscope physics. The role of diffraction and image formation process should always be considered in image analysis. Proper application of all microscope capabilities can greatly enhance the quality of information obtained from the electron microscope. Howie et al.[127].. Sanders[128] and Schmidt et al.[129]. discuss some of the available methods in electron microscopy.

The analysis of transmission electron micrographs can be divided into two categories[130]

(a)Analysis of catalysts comprised of amorphous supports

(b)Analysis of catalysts comprised of crystalline supports.

Amorphous supports

In this case the contrast is controlled by the mass-density of metal. The catalysts particle will diffract part of the electron beam. Part of this diffracted bean will be diffusely scattered by the amorphous support. Because the largest contribution to diffuse scattering is near the transmitted beam, the use of bright

Table 2.11: Opertaing modes of CTEM and STEM

Mode	Use
CTEM	
Bright field	amplitude contrast:particle shape
	phase contrast:particle shape
Selected area diffraction	Identify different components
	phases in mixture:
	crystal orientation
Dark field	Identify diffraction features
	Separate components in image
Speciment tilt	Zone axis diffraction
	identify defects, lattice images
Grazing incidence	observe surface features
STEM	
Bright field	Image enhancement
Dark field	high contrast
	atomic number contrast
Electon diffraction	crystallography
	identification of small particles
Convergent beam	crystal symmetry determination
X-ray analyzer	detection of elements

field images is not recommended. In a very general case, there are five types of electron beams that produce the image. They are

(i) Transmitted by particle and support.

(ii) Transmitted by particle and diffracted by support. in the case of amorphous supports this beam is absorbed by the support

(iii) Diffracted by the particle and transmitted by the support

(iv) Transmitted by the support

(v) Diffracted by the support. in the case of crystalline support this beam is absorbed by the support.

Crystalline support

In most catalysts the support is crystalline. such as graphite, Al_2O_3 , MgO or TiO_2. The crystalline support produces diffraction by itself, that many times leads to invisibility of the particles. Supports such as Al_2O_3 or graphite tend to have a polycrystalline structure with crystallite size down to a few tens of nanometers. Supports such as TiO_2 or MgO have larger single crystal regions. Hence better contrast is obtained in supports such as MgO and TiO_2. In principle, for supports with reasonably large size support particles one should see two series of diffraction spots. one corresponding to the support and the other corresponding to the metal or metal oxide particles. In most real catalysts the interplanar spacings of the support and the metal particle are very close and therefore in reciprocal space . the spots also appear close.

If a metal particle supported on a locally crystalline substrate such as Pt · alumina or Pt · graphite is taken. The visibility of the particle in a transmission electron microscopy image will depend strongly on the orientation of both particle and the substrate with respect to the incoming electron beam. The interaction of electrons with a crystalline specimen can be understood within the framework of the kinematical and the dynamical theory of diffraction. Excellent reviews and texts are available on this subject[115. 119. 131-133]. Even though it is necessary

to understand the theories of diffraction in order to explain many characteristics of images in transmission electron microscopy, they will not be elaborated. Gomez, Romeu and Yacaman[134] have developed dynamical diffraction theory for bicrystals and applied to particle contrast problems. They find that the thicker particles (50Å) are always visible in a bright field image but their contrast is reduced with increasing deviation from the Bragg angle. On the other hand, the dark field image has an oscillatory character and particles will not be visible in many orientations. On the other hand for a thin particles (10Å), the bright field image always has a very low contrast and the particles are almost invisible. But the dark field image characteristics are very different. When the tilt angle is less than 1 degree, the particles show no contrast. However when the tilt angle is greater than 1 degree, the contrast becomes high. The intensity of the image is very low and problems similar to those in weak beam images arise. The problem stems from low intensity of image. This can be compensated by longer count times. The longer count times can seriously impair the resolution if there is substantial sample drift.

2.4.2.4 Techniques for Bimetallic Catalysts

Schmidt et al.[135]. have studied the effect of oxidizing and reducing atmosphere on the structure and surface compositions of Pt. Pd. Rh and Ir and their alloys supported on silica using TEM. STEM and XPS. Yacaman et al.[136.137]. have used high resolution weak beam images and the Heinemann method to show that an alloy of Pt and Ir is not formed in Pt-Ir/Al_2O_3 catalysts. The Heinemann method[138.139] uses the change in the observed image dimension with the amount of defocus to find the lattice constants. Freund and Dexpert[140] have investigated alloy formation in Pt-Pd/Al_2O_3 using EDX. Yacaman et al.[141. 142] have described a specialized technique based on dynamical diffraction theory to give the shape of a small metal particle.

There have been many moderately successful attempts at finding particle size distribution using transmission electron microscopy[143, 144]. However this method is not straightforward. Flynn et al.[145] have pointed out that the measurement of a reliable particle size distribution from electron images is based on the three assumptions:

1. The size measured on the image is equal to the true size of the particle

2. All particles have the same probability of being observed on the image, irrespective of their size.

3. Contrast arising from the support cannot be confused with that arising from the particle.

The above assumptions are very stringent especially for particle size less than 30Å. The limiting size depends on the support, the particle and the type of microscope used. Dark field images are more accurate than bright field images because the contrast is much better. In conclusion for particles less than 30Å, TEM can only be used in a qualitative manner.

EDX is often used in qualitative mode to identify the elements present in a given region of an electron microscope specimen. The theory, operating procedure and the limitations of EDX are well-known and are discussed elsewhere[146-151].

2.4.3 Nuclear Magnetic Resonance Spectroscopy

Fundamental investigations in catalysis on solid surfaces are carried out on two fronts. The first front is the study of single crystals, while the second front is the study of small particles supported on high-surface-area supports. As a rule of thumb, NMR studies of sample containing 10^{18} to 10^{20} NMR active nuclei are possible. Almost all the NMR work in catalysis is done on supported catalysts[152].

NMR investigations of metal particles through probe molecules is very popular. Until recently very few attempts have been made to look at NMR of transition metal nuclei on the catalysts. The possible parameters that can be found from a NMR experiment are Larmor frequency, chemical shift, Knight shift, coupling constants , signal intensities and relaxation times[153-155]. The problems with application of NMR to solids are broadening due to dipolar interaction, low sensitivity, chemical shift anisotropy and extremely fast relaxations due to paramagnetic interactions. Since NMR spectroscopy is a bulk technique, special techniques must be used to enhance the signal from the surface metal atoms when metal NMR is done. Some ways of partially overcoming the sensitivity problems are, increasing sample size, increasing magnetic field strength, cross-polarization, signal averaging and isotope enrichment. Techniques for line narrowing are magic angle spinning, homomuclear dipolar decoupling and heteronuclear dipolar decoupling. The relaxation times are shortened by the presence of paramagnetic species. Cross-polarization is used to enhance the signal.

The changes in the various adsorbed CO species on the surface of Rh/Al_2O_3 and modified Rh/Al_2O_3 can be monitored by infrared spectroscopy. However, there are many species where infrared spectroscopy is not useful because of low extinction coefficients. The nature of deposited carbon is one such type of species. In addition, the strong variation of scattering losses with particle size, the absence of narrow particle size distribution , the non-uniformity of optical properties of the pressed wafer and the absence of inert internal standard renders transmittance infrared spectroscopy a difficult quantitative tool. Furthermore interconversion of species cannot be monitored by infrared spectroscopy, because the time scale for diffusion inside pores is of the same order of magnitude of the time scale of interconversion of species (milliseconds) and because there is no good way of labelling species. NMR is an excellent technique to spin label a particular species within a couple of microseconds. Single pulse NMR is an inherently quantitative

tool; one can not only monitor the type of various species and their interconversion but also quantify them. A cross-polarization experiment can find the coupling between the protons and the NMR-active nuclei.

Anticipated problems with NMR are:

Difficulty in preparing sample

Large peak width due to inhomogeneity

Presence of paramagnetic species

2.4.3.1 Previous Work on Adsorbed ^{13}CO

This review deals with ^{13}C NMR spectroscopy of CO adsorbed on various transition metal particles on surfaces. Metal NMR spectroscopy of relevance to catalysis is also included. Proton NMR and NMR spectroscopy of supported organometallic clusters is not included here.

Duncan, Yates and Vaughan[156] have investigated the adsorbed carbon monoxide on Rh on alumina using ^{13}C NMR spectroscopy and IR spectroscopy. Their data showed that the relaxation of ^{13}C nuclei fit a sum of two mechanisms. The data were fitted to a model where there are two types of adsorbed carbon monoxide, each with different T_1. This is consistent with the IR results obtained. The model assumes that $N(T_1)$ is the sum of two delta function at T_{1a} and T_{1b} with relative areas α_a and α_b, which represent relative populations. The isotropic chemical shift of carbon monoxide bonded as a terminal group on various rhodium complexes ranges from -176ppm to -192ppm. The bridged bonded state of carbon monoxide has the largest chemical shift ranging from -212ppm to -236ppm. The isotropic chemical shift of the species with longer relaxation time (64ms) was -199ppm. This lies in the range of values for combination of linear

and bridged species. The isotropic shift for species with lower relaxation times (5.6ms) is -177ppm , which is closer to the value reported for gem-dicarbonyl species. Furthermore they used this assignment of peaks to calculate the extinction coefficients of the species for infrared absorption .

The reported relaxation times are very short, when compared with the relaxation times for diamagnetic rhodium complexes. They postulated that the higher relaxation rates were due to Fe^{+2} impurity in the support. Homonuclear ^{13}C -^{13}C flips are too slow to account for rapid dissemination of relaxation through the sample because of the large internuclear distances between various carbonyl sites.

When a NMR-active nucleus is relaxed by a fixed paramagnetic species, the relaxation rate is given by[157]

$$\frac{1}{T_1} = \frac{3\gamma_S^2\gamma_I^2(h/2\pi)^2 Sin^2\theta Cos^2\theta S(S+1)\tau}{r^6(1+\omega_I^2\tau^2)}$$

where

γ_S is the gyromagnetic ratio for the unpaired electron

γ_I is the gyromagnetic ratio for the nucleus under consideration

S is the spin state of the unpaired electron

θ is the angle between the magnetic field vector and the vector connecting the nucleus and the unpaired electron site

r is the distance between the NMR active nucleus and the unpaired electron site

τ is the longitudinal electron relaxation time

Abragam has discussed the theory of relaxation of NMR active nuclei by fixed paramagnetic species. In many, but not all systems, the strong dipole-dipole coupling maintains communication between all spins so that all spins can relax together. This is why only one spin lattice relaxation time is seen when nuclei are relaxed by randomly distributed paramagnetic species. The magnetization diffuses among the spins, and this polarization diffusion is called spin polarization.

Duncan,Winslow and Bell[158-160] have found three different kinds of carbon as intermediates in carbon monoxide hydrogenation reactions on Ru/SiO_2. They have shown that C_β would not exist as a two-dimensional overlayer of carbon (as graphite) since the T_2 of the peaks indicates a C-C bond distance of 2.0 Å. This C_β phase is bonded to silica, since the shift of C in SiC is -21ppm, while the shift of a binary transition metal carbide is -600ppm to -400ppm . and that of non-hydrogenated carbon in metal clusters is -450ppm to -300ppm. The broad peak at -350ppm is assigned to C_α and was in the range of transition metal carbides The helium treatment is known from reaction studies to give unreactive carbon deposits. In the NMR experiments the third peak is formed after helium treatment, which indicates that the third carbon peak is due to unreactive carbon deposits.

Table 2.12: Chemical shifts and relaxation time of different forms of carbon on Ru on silica

Type of Carbon	Fraction	Shift(δ in ppm)	T_1	T_2
C_β	35 %	-157	4.7s	0.8ms
$C_{unreactive}$	35 %	-100	1.7s	0.2ms
C_α	30 %	-350	1.0s	1.1ms

In bulk samples, the conduction electron spin polarization is uniform. This electron spin polarization exerts a magnetic field on the nuclei through the Fermi contact interaction giving rise to the Knight shift.

Rhodes et al.[161] have studied the ^{195}Pt NMR line shape as a function of size of the metal crystallites. Platinum samples with dispersion of 4 % gave a strong resonance at $H/\nu = 1.14$ kG/MHz, which is the position of the resonance for Pt metal. Platinum samples with 56% dispersion had a resonance peak at H/ν of 1.085 kG/MHz, which is in the range of dimagnetic platinum compounds. These studies clearly showed that the Knight shift is reduced in the surface region of the metal particle.

The resonance lines of the 26% dispersion sample did not show the clear position of the resonance of the surface atoms. Makowka et al.[162] used spin echo double resonance (SEDOR) to resolve the NMR spectra of surface of platinum. SEDOR is a pulse technique involving simultaneous excitation of of two NMR-active nuclei, in this case ^{195}Pt and ^{13}C . The resonance of ^{13}C affects the resonance of ^{195}Pt . The resonance of ^{13}C affects the resonance of ^{195}Pt either through the nuclear dipolar interaction, or indirectly through the electrons. The strength of ^{195}Pt -^{13}C spin-spin coupling as found from SEDOR is similar to the values obtained from diamagnetic platinum carbonyl compounds.

At 77K the spin-lattice relaxation times are similar for all metals investigated. At 300K the relaxation time is 150ms, which is much faster than ^{13}C relaxation times in diamagnetic compounds. They concluded that this rapid relaxation arises from the coupling of conduction electrons with the NMR active nucleus. The electrons in the tail of the fermi distribution are able to relax the NMR active nucleus. The observed linear dependence of relaxation rates on temperature is the hallmark of this mechanism.

Furthermore they have showed that conduction electrons have to overlap partially on the carbon atom to explain the observed results. Hence there is a mixing of molecular wave functions with metallic wave functions. The data on relaxation rate at different temperatures are used to calculate mixing coefficients.

Rudaz et al.[163] have investigated the causes of shifts in the NMR spectra of carbon monoxide adsorbed on Pt/alumina. The ^{13}C resonance of carbon monoxide adsorbed on platinum is shifted to higher frequency than its resonance in the gas or in the platinum carbonyl compounds by about 200ppm. This shift is nearly as large as the entire range of ^{13}C shifts in diamagnetic compounds (240ppm).

The large ^{13}C shift on platinum was postulated to be due to polarization of electron spins such as occurs to produce Knight shifts in metals. An isolated carbon monoxide molecule has no unpaired electron spins, hence cannot give Knight shift. However when carbon monoxide is adsorbed on the surface, the molecular orbitals of carbon monoxide mix with the conduction band wave function of the metal. Thus there is a finite contribution of the metal density of states to the carbon monoxide. The functional dependence of the Knight shift on various parameters is as follows:

$$K = \frac{4}{3}\gamma_e \hbar \, |\psi(R_c)|^2 \rho_c(E_f)$$

where

K is the Knight shift

γ_e is the gyromagnetic ratio of the electron

$\hbar$ is h/2π

$\psi(R_c)$ is the wave function of the bonding orbital on carbon

$\rho_c(E_f)$ is the density of states of the bonding orbital for single spin orientation

The spin-lattice relaxation time and the temperature are related by Korringa's equation

$$T_1 = \frac{1}{TK^2}\frac{\hbar}{4\pi k_B}(\frac{\gamma_e}{\gamma_n})^2$$

where

T_1 is the spin-lattice relaxation time

T is the absolute temperature

k_B is the Boltzman constant

γ_n is the gyromagnetic ratio of the nucleus

This hypothesis was proved from the following results

(i) The spin lattice relaxation time was independent of the field strength, H_0.

(ii) Spin lattice relaxation time was proportional to 1/T.

(iii) The value of Knight shift calculated from known value of spin-lattice relaxation time was the same as the observed Knight shift.

The relaxation was exponential only above 290K. The nonexponential character of relaxation below 290K was explained as a distribution of relaxation rates

from a distribution of sites. At temperatures greater than 290K, the diffusion rate is high, which leads to a single relaxation time.

Slichter[164] has reported spin lattice relaxation times of adsorbed carbon monoxide on Pt, Ru, Pd, Rh, Os and Ir metal particles. At 77K the relaxation of the ^{13}C nucleus consists of a sum of exponentials, which were shown to be due to different bonding sites. At 300K, the data indicated that the relaxation could be explained by a single exponential. This is because the time scale of NMR is greater than the time scale for interconversion of the species.

Robbins[165] has investigated Rh gem-dicarbonyl species on the alumina surface by using ^{13}C NMR spectroscopy, low temperature ESR, IR and TEM. $Rh(CO)_4Cl_2$ was deposited on alumina using an organic solvent. His NMR data show that a doublet with a peak centered at δ of 180.9. The 60Hz splitting is due to scalar coupling between ^{13}C and ^{101} Rh. The spin lattice relaxation time was 900ms. This relaxation time is high compared to the data by Duncan et al. and Slichter et al. No bands were observed with ESR at 20K. He concluded that Rh dicarbonyl sites are not directly bonded to one another. This is consistent with the well known observation that the infrared frequency of the gem-dicarbonyl bands does not change with the partial pressure of carbon monoxide in the gas phase. The Rh g-dicarbonyl sites contain dimagnetic $4d^8$ Rh^{-1} centers probably in square-planar coordination environment. The Rh gem dicarbonyl sites on reduced catalyst were clustered near the paramagnetic species in the system.

Huizinga[166] has observed a paramagnetic signal at 20K on reduced rhodium on alumina. The ESR signal intensities declined rapidly with increasing temperature. This indicates that the paramagnetic species has very fast relaxation times at higher temperatures. The number of spins corresponded to less than 5% of the rhodium in the sample. These broad resonances were assigned to Rh^{-2} centers interacting with larger metallic rhodium. An increase in signal intensity was ob-

served with particle size. Huizinga postulated that Rh^{+2} helps anchor Rh clusters on oxide surfaces. The temperature dependence of relaxation times due to fixed paramagnetic species is not known.

In summary the lower relaxation times observed for ^{13}C nuclei on Rh are attributed to different mechanisms:

(i) Duncan, Yates and Vaughan attributed the lower relaxation times to the presence of Fe^{+2} paramagnetic impurities on the support. However, no explanation was given for the lack of distribution in relaxation times due to the r^6 dependence of the relaxation times.

(ii) Robbins attributes it to the presence of small amounts of $4d^7$ Rh^{2+} The presence of small amounts of Rh^{+2} near the rhodium particle on the reduced catalyst is responsible for the lower relaxation times.

(iii) Slichter et al. have postulated that the lower relaxation times of adsorbed CO is due to coupling of conduction electrons with the molecular wave functions. They cite the linear dependence of relaxation rate on absolute temperature as a proof for their hypothesis. The changes in the relaxation rates are used to evaluate mixing coefficients.

The net magnetization is related to the gyromagnetic ratio by the expression $I(I-1)\gamma^{5/2}$. If the data collection time for ^{13}C nucleus is one day, then for the same S/N ratio, same acquisition time and for the same amount of NMR active nuclei the data collection time for Rh nucleus is about 300 days. This is because of the very low gyromagnetic ratio of rhodium nucleus.

Yermakov et al. [167, 168] have studied the interactions of carbon monoxide and hydrogen on Rh/La_2O_3 and Rh/SiO_2. They find that on Rh/La_2O_3 carbonyl groups transform to either alcohols and ethers or acids and esters depending on

CO/H_2 ratio. The catalysts were dosed with either CO or a mixture of CO and hydrogen at room temperature. After various sample treatments, the cell was cooled and spectra were collected. Below 473K, CO adsorbed on Rh/La_2O_3 showed a peak at 190ppm. Treatment at higher temperature broadens the above band. Peaks corresponding to hydrocarbons were seen when the sample was heated above 473K. Similar experiments on Rh/SiO_2 yielded ethylene and CO_2 (δ =123 and 125ppm). The source of hydrogen in the above experiment was surface hydroxyl groups. The formation of different products was explained to be due to higher basicity of hydroxyl groups on La_2O_3 than on SiO_2.

When a Rh/La_2O_3 sample was heated to 473K under a CO and hydrogen mixture with excess of hydrogen, particles having groups like CH_2-O (40-70ppm) were found. Under the same treatment, but at low hydrogen contents a shoulder at 150-170ppm corresponding to carboxylates and esters was found.

Shoemaker and Apple[169] have studied carbon monoxide adsorption on Ru-exchanged zeolite Y. The catalysts were prepared by impregnation of $RuCl_3$ followed by air calcination at 725K and reduction under hydrogen at 570K. Two different treatments were carried out. In the first treatment, the reduced catalyst was dosed with 700 torr of ^{13}CO at room temperature and subsequently the catalyst was evacuated. In the second treatment the ^{13}CO dosed catalysts were heated to 500K under ^{13}CO. The catalysts were cooled to room temperature after treatment. Unlike the results of Duncan et al. [5], Shoemaker and Apple could separate the linear and bridged species separately at room temperature. From previous infrared studies of CO adsorbed on various supported transition metals, the bridged and linear species are assigned to CO adsorbed on metal particles, while the gem-dicarbonyl is assigned to mononuclear dicarbonyl species attached directly to the support. The higher line widths observed only for linear species, were explained as a change in the electronic structure as the carbon monoxide site is moved from the edge of the metal particle to the center. It is interesting

to note that the band assigned to bridged species was narrow. They also found carbon dioxide impurity adsorbed on zeolite. The absence of deposited carbon peaks ruled out the Boudouard reaction. Their results are summarized below.

Table 2.13: NMR ^{13}C chemical shifts of adsorbed CO on Ru catalysts

species	shift ppm wrt TMS	line width fwhh	relative % 298K	relative % 500K
linear	$\sigma_{iso} = 180$	40	92	74
	$\sigma_{11} = -89$			
	$\sigma_{22} = 310$			
	$\sigma_{33} = 320$			
dicarbonyl	$\sigma_{iso} = 203$	7	8	18
bridged	$\sigma_{iso} = 168$	10		8

The salient features of the theory of relaxation and its relevance in estimation of distances between species is discussed in appendix B.

2.4.4 X-Ray Photoelectron Spectroscopy

2.4.4.1 Charge Correction with Insulating Materials

X-ray Photoelectron Spectroscopy is a powerful tool to investigate the chemical species on the surface[171, 172]. It is sensitive to almost all elements of the periodic table, their oxidation state and local environment. However there are problems with precise physical and chemical interpretation of the spectra particularly for insulators and heterogeneous samples. Because of the insulating nature

of the oxide support, they charge upon photoelectron emission. The major limitation with XPS for porous samples is that the area accessible for getting the photoelectron signal may not represent the entire catalyst surface.

Since the inelastic mean free path of the photoelectrons is of the order of a 10 Å, the surface of the catalyst deep inside the pores is not accessible for analysis. This can be partially solved by grinding the catalyst so that some of the internal area is exposed. One major assumptions with XPS is the transfer of deductions from observations made under ultra-high vacuum conditions to the conditions under which the catalyst works. In the analysis chamber most of the volatile component on the catalyst would be lost at the same time extraneous carbonaceous layers would be formed on the catalyst. The former problem can be minimized by exposing the catalyst to vacuum conditions only at temperatures below 75C.

Because of the insulating nature of the supported catalyst, there is a problem of the choice of binding energy reference. Siegbahn et al. first cited C(1s) from the hydrocarbon contamination originating from the vacuum pump oil as an internal reference[173]. Several authors reported wide range of C(1s) binding energy from 284.6eV to 285.4eV[174-178]. However C(1s) line is difficult to use as a reference due to its weak intensity and poor resolution. More ever it can exist in different chemical and electrical forms. Some investigators have mixed catalyst samples with Au and have used Au($4f_{7/2}$) as a reference line. However there is no guarantee that good electrical contact is maintained between gold and catalyst particles. One can also coat the surface with a gold monolayer. The effect of coating and the uniformity of thickness is not known. This method generally broadens and attenuates the sample signal. The use of flood gun to reduce charging is an option. However there are many cases, especially with heterogeneous samples where differential charging is observed when the flood gun is used. Another popular

method for supported catalyst is the use of support element peak as a reference line. The support is refractory in nature and the chemical nature of the support does not change during various treatment. Hence the support peak (in our case Al(2p)) forms a good standard. The data should be periodically referred with C(1s) peak for internal consistency.

The mean free path of X-rays is order of magnitude higher than the mean free path of the ejected photoelectrons. Hence the X-rays are not attenuated over the range of surface thickness from which photoelectrons reach the detector. In porous γ-Al_2O_3 (surface area $\approx 200 m^2/gm$), the average wall thickness is $\approx$ 100 Å, while the escape depth of the photoelectron is of the order of 10Å.

2.4.4.2 Oxidation State of Molybdenum

Molybdenum in air calcined Mo/Al_2O_3 exists as several Mo(VI) species depending upon, Mo loading, preparation method, calcination conditions and the nature of alumina[179-181]. Molybdena forms a monolayer on γ Al_2O_3 (surface area $\approx 200 m^2/gm$) at 17 wt% Mo loading. On reduction at 500C under hydrogen Mo(VI) is partly reduced to Mo(V) and Mo(IV). Mo(V) exist predominantly in the tetrahedral sites while Mo(IV) is in the octahedral site . Cumino et al.[182] have shown that Mo/SiO_2 can be completely reduced to metallic Mo under hydrogen at 400C, while Mo/Al_2O_3 was not reduced below Mo(IV). The greater reducibility of Mo in Mo/SiO_2 is due to weaker interaction between MoO_3 and SiO_2 compared to MoO_3 and Al_2O_3 . Jaganathan et al.[183] have studied the effect of sample treatments for a single Mo loading on Mo/Al_2O_3 . Their peak deconvolution is based on the assumption that the peaks are gaussian with full width at half height of 2.1eV. The fine structure in their Mo peaks on Mo/Al_2O_3 has not been seen on similar system. The existence of fine structure may be due to different method of preparation of Al_2O_3 . They report the presence of Mo(V) in $10\%MoAl_2O_3$ on evacuation after air calcination at 670C. On cooling Mo(V) disproportionates to

Mo(VI) and Mo(IV). They reported the presence of Mo(V) after reduction under hydrogen at and after dehydrogenation of cyclohexane on the above sample.

Holl et al.[184] have done a detailed XPS study of Mo/Al_2O_3 catalysts. They studied the reduction of Mo on Mo/Al_2O_3 at a variety of Mo loading (6.12.18 and 30 wt% Mo). A shift to higher binding energy of Mo(VI) on Mo/Al_2O_3 as compared to MoO_3 is reported. This shift is interpreted as a charge transfer from molybdenum to alumina. The supported oxide Mo/Al_2O_3 also shows a decrease in resolution of Mo(VI) 3d doublet. This is either due heterogeneity on alumina surface or due to existence of Mo ions in both tetrahedral and octahedral sites. After reduction under hydrogen at 550C, the 6%Mo/Al_2O_3 catalysts is close to oxide form. Further reduction at 750C shows the existence of both metallic and oxide forms. Reduction of the same catalysts at 950C shows aggregation of Mo particles at the surface. Further oxygen treatment at 550C completely redisperses molybdenum. Al(2s) was used as a reference peak. Zingg[185] has reported that the peak broadening on reduced Mo/Al_2O_3 is due to differential charging.

Nag[186] has reported the interaction and stability of MoO_3 on Al_2O_3 , SiO_2 ,ZrO_2 and TiO_2 supports. Based on the XPS data it was concluded that the Mo-support interaction is the strongest for Al_2O_3 and the least(none) for Silica, while it is intermediate for TiO_2 and ZrO_2 The catalyst was prepared by impregnation with a solution at a pH $\approx$1 . The effect of method of preparation on Mo dispersion is also investigated. Mo/ZrO_2 and Mo/TiO_2 show appreciable shift from MoO_3. Mo was found to be more dispersed on $CoMo/Al_2O_3$ than on Mo/Al_2O_3 .

2.4.4.3 Quantitative XPS on Supported Catalysts

Problems

Until recently there were few attempts at quantitative analysis of XPS data on supported catalyst . There are many complications that can obscure the results with supported catalysts. Some of them are listed below.

A. Surface segregation

The modifier may segregate on the external surface of the porous catalyst. This will give very high values of modifier concentration. This can be checked by grinding particles and observing if the modifier surface concentration decreases.

B. Signal attenuation due to hydrocarbon contamination

The XPS signal of the support element and modifier is attenuated by the presence of hydrocarbon contamination on the catalyst surface. The pressure in the UHV chamber during XPS analysis is $\approx 10^{-8}$ - 10^{-9} torr. At this working pressure substantial amount of hydrocarbon is expected on the catalyst surface at 30C. If the hydrocarbon layer is drastically different in two separate runs, the signal intensity can be attenuated to different extent. This can produce artifacts in the interpretation of the data. This can be avoided by operating close to a certain pressure (in our case 4X 10^{-8} torr).

C. Statistically representative area of analysis

The main assumption in the analysis of XPS data is that the area for analysis is a statistically representative area of the entire sample.

Models

Fung[187] has studied variation of XPS intensity ratio (or photoelectronic response or relative photoelectronic response) of modifier or noble metal as a function of size of particle for spherical, hemispherical and cubical particles. This model was applied to study sintering behavior of monoatomic Platinum

film on silica substrate under hydrogen atmosphere. Surface segregation was not considered.

Kerkhof[188] has presented a simple model for quantitative XPS study of supported catalysts. The model assumes that catalyst support is made of stacked layers with modifier(or noble metal) dispersed uniformly over the surface area either as a monolayer or as crystallites. The crystallites are cubic and the incoming X-rays and outgoing photoelectrons are perpendicular to the surface. This model can estimate particle size of the modifier provided mean free path of the photoelectron is known. This model has been successfully applied to Re/Al_2O_3 and F/Al_2O_3 . The model does not take into account concentration gradients and surface segregation.

Kerkhof's model has been refined by Kaliaguine et al.[189], in which the promoter is distributed among two population of crystallites having sizes C_1 and C_2. The microcrystallites of size C_1 are distributed over the entire surface while the segregated particles of size C_2 are formed only on the external surface area.

Rodrigo et al.[190] have studied Mo dispersion and surface segregation on Mo/SiO_2 and Mo/Al_2O_3 using low temperature oxygen chemisorption, quantitative XPS, laser raman spectroscopy and ion scattering spectroscopy. The catalyst were prepared by (1) aqueous impregnation (AI) method and (2) reaction of $Mo(\eta^3\text{-}C_3H_5)_4$ with surface -OH groups(SI). The Mo loadings were varied from 0 to 8 wt. %. They observed surface segregation for Mo/SiO_2 prepared form aqueous impregnation method while there is no surface segregation with Mo/SiO_2 prepared by SI. The effect of reduction and oxidation on dispersion is not considered. The surface segregation of Mo on the SiO_2 particles is checked by observing the decrease in Mo photoelectronic response of ground catalyst as compared to its original form. However, surface segregation was not observed for Mo/Al_2O_3 prepared by AI and SI. SiO_2 had a narrow pore size distribution at 19Å while

Al_2O_3 had a broad pore size distribution around 44Å. The pore size distribution was cross-checked with scanning electron microscopy.

Grimblot et al.[192] have studied Mo/Al_2O_3 and $Ni\text{-}Mo/Al_2O_3$ and $Co\text{-}Mo/Al_2O_3$ at various stages of treatment and at various Co.Ni and Mo loading. At monolayer coverage each Mo atom was found to occupy $20Å^2$. The Mo loading corresponding to monolayer coverage can be found from the point of intersection of the two asymptotes of the plot of photoelectronic response of Mo against the Mo loading. Two different aluminas were used: Al_2O_3 (1), surface area=100 m^2/gm and Al_2O_3 (2), surface area=$230m^2$/gm. Samples were impregnated using ammonium heptamolybdate. Mo photoelectronic response for both the Al_2O_3 is shown below

The photoelectronic curve for Ni/Al_2O_3 saturates at Ni/Al molar ratio of ≈ 0.06. The photoelectronic response for Ni in $Ni\text{-}Mo/Al_2O_3$ is 20% lower than that on Ni/Al_2O_3 . In comparison Co photoelectronic response gets saturated at Co/Al molar ratio of ≈ 0.02 for Co/Al_2O_3 . Table 2.14 shows area occupied by one molybdenum atom at monolayer coverage

2.4.5 Infrared Spectroscopy

The infrared spectra of CO adsorbed on supported transition metal catalysts is summarized in many reviews[196-202]. Hollin and Pritchard have discussed the various factors that affect the shifts in infrared spectrum[203]. The frequencies and the characteristics of the adsorbed carbonyl species seen on Rh/Al_2O_3 catalysts are summarized in table 2.15. For e.g., the gem-dicarbonyl species is known to occur on the single isolated rhodium sites with the rhodium in an oxidation state of 1. In contrast, the linear and bridged carbonyl species occur on the metal crystallite where the rhodium has an oxidation state of zero. The reasons for the absence of gem-dicarbonyl species with rhodium oxidation state of zero are elaborated by

Table 2.14: Mo occupation area

Area occupied by each Mo atom $Å^2$	Support and technique	Reference
20	Al_2O_3 -XPS	191
25	Al_2O_3 -XPS	192
250	SiO_2	193
17-25	Al_2O_3 -gas phase or solution impregnation	194
40	Al_2O_3 -CO and NO chemisorption	195

Worley et al.[204, 205]. The factors that prevent quantification of IR results are discussed by Hlavay and Inczedy[206].

In this section, only the recent reports on the role of surface -OH groups on the presence of different carbonyl species will be summarized. Recent EXAFS results of van't Blink et al.[207] have shown that the adsorption of CO leads to disruption of Rh-Rh bonds and to the formation of Rh(I) isolated species. This was observed in the IR spectrum by Solymosi and Paztor[208]. This was explained by the oxidative addition by the surface -OH groups given by reaction (2.2).

$$2Al-OH-2Rh-CO-CO=Al-O-Rh(CO)_2-H_2 \qquad (2.2)$$

Thus the surface -OH groups can convert the metal crystallite into the gem-dicarbonyl species. The mechanism is similar to "peeling of an onion". where the metal crystallites slowly breaks up due to oxidative addition of surface -OH groups. This is consistent with the EXAFS observations of van't Blink[207]. This process

takes place at room temperature and on Rh/Al_2O_3 the entire bridged and linear carbonyl species can be converted to gem-dicarbonyl species. At temperatures above 150C, and under the presence of hydrogen the reverse process of formation of rhodium crystallite at the expense of gem-dicarbonyl species takes place[209, 210]. These effects have also been used to explain the effect of promoters on the infrared spectrum[211, 212]. Zaki et al.[213] have stopped reaction (2.2) by reacting the surface -OH groups with hexamethyl disilazane as given in reaction (2.3).

$$2Al - OH + (CH_3)_3SiNHSi(CH_3)_3 \longrightarrow 2Al - O - Si(CH_3)_3 + NH_3 \quad (2.3)$$

2.4.6 Electron Spin Resonance Spectroscopy

The application of ESR spectroscopy to catalysis has been limited. Many a times, the results are used to corroborate information obtained from other techniques. The use of ESR in catalysis has been recently reviewed by Vedrine[214]. ESR spectroscopy has been extensively used in investigating supported molybdena catalysts, notable among them are the recent papers from Kevan's group[215]. In short, different environments around Mo(−5) have been investigated. In contrast, there have been very few investigations of supported rhodium catalysts. Using ESR spectroscopy, Wilson et al.[216] showed that Mn is concentrated on the surface of Rh crystallite as a surface mixed oxide which then stabilizes Rh(+) on the metal surface. Also, Huizinga[166] has detected the presence of Rh(2+) at the metal crystallite-support interface at 20K.

Table 2.15: Frequencies and characteristics of adsorbed CO species on Rh/Al_2O_3

Frequency range cm^{-1}	Variation with coverage	Site Distribution	Oxidation state	Structure
2136	No	Atomic	III	$RhCl_3(CO)2H_2O$
2116-2120	No	Atomic	II	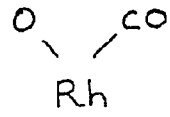
2096-2102 2022-2032	No	Atomic	I	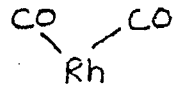
2082-2100	?	?	I	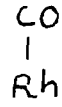
2042-2076	Yes	Cluster	0	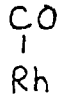
2000-2020	?	Cluster	I	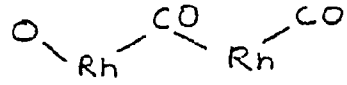
1900-1920	Yes	Cluster	0	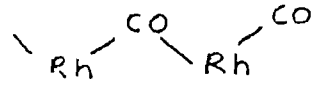
1845-1875	Yes	Cluster	0	

REFERENCES

1. G.A. Mills, "Catalysts for Fuels from Syngas: New Research Directions", IEA Coal Research, London, 1988.

2. W.O. Haag, J.C. Kuo and I. Wender, "Coal Gasification: Direct Application to Synthesis of Chemicals and Fuels", ed. S.S. Penner, U.S. Department of Energy, Washington D.C., 1987.

3. "Alcohols and Alcohol Blends as Motor Fuels" by Swedish Motor Fuel Company, International Energy Agency, Stockholm, 1986.

4. G.A. Mills and E.E. Eckland, Ann. Rev. Energy. 1987, 12, 47.

5. H.H. Storch, N. Golumbic and R.B. Anderson. "The Fisher-Tropsch and Related Synthesis", Wiley, 1951, New York.

6. M.E. Dry in "Catalysis: Science and Technology", eds. M. Boudart and J.R. Anderson, Vol. I, 1981.

7. P.J. Denny and D.A. Whan, in "Catalysis: Specialist Periodical Reports", Vol. 2. The Chemical Society, London, 1978.

8. G.A. Mills and F.W. Steffgen, Adv. Catal. 1973, 8, 159.

9. R.B. Anderson, "The Fisher-Tropsch Synthesis", Academic Press, 1984, New York.

10. P. Bileon and W.M.H. Sachtler, Adv. Catalysis, vol. 30, 1981, Academic Press, New York.

11. A.T. Bell, Cat. Rev. Sci. Eng. 1981, 23, 203.

12. G. Henrici-Olive and S. Olive, "The Chemistry of the Catalyzed Hydrogenation of Carbon Monoxide", Springer-Verlag, 1984, Berlin.

13. E.K. Poels and V. Ponec, in "Catalysis: Specialist Periodical Reports", Vol. 2. The Chemical Society, 1983.

14. F.G.A. van den Berg, Ph.D. thesis, University of Leiden, 1984.

15. A.T. Bell, in "Catalyst Design: Progress and Perspectives", ed. L.L. Hegedus, Wiley, New York, 1987.

16. "C_1-based Chemicals from Hydrogen and Carbon Monoxide", Ed. M.T. Gilles, Noyes Data Corp., Park Ridge, New Jersey, 1982.

17. M. Ichikawa, Bull. Chem. Soc. Japan. 1978, 51, 2268.

18. M. Ichikawa, JCS Chem. Commun. 1978. 566.

19. J.R. Katzer, A.W. Sleight, P. Gajardo, J.B. Mitchel, E.F. Gleason and S. McMillan, Far. Disc. Chem. Soc. 1981, 72, 121.

20. R.P. Underwood and A.T. Bell, Appl. Catal. 1986, 21, 157.

21. T. Iizuka, Y. Tanaka and K. Tanabe, J. Molec. Catal. 1982, 17, 381.

22. F. Solymosi, I. Tombacz and M. Kocsis, J. Catal. 1982, 75, 78.

23. H. Orita, S. Naito and K. Tamaru, JCS Chem. Commun. 1983, 993.

24. G.L. Haller, V.E. Henrich, M. McMilland, D.E. Resasco, H.R. Sadeghi and S. Sakellson. Proc. 8th Intl. Congr. Catal. Berlin, 1984, V, 135.

25. S.D. Jackson, B.J. Brandreth and D. Winstanley, Appl. Catal. 1986, 27, 325.

26. M. Ichikawa, , T. Fukushima and K. Shikakura, Proc. 8th Intl. Congr. Catal. Berlin. 69, 1984.

27. B.J. Kip, Ph.D. thesis, Eindhoven University of Technology, The Netherlands, 1987.

28. H. Arakawa, T. Fukshima, M. Ichikawa, S. Natsushita, K. Takeuchi, T. Maatsuzaki and Y. Sugi, Chem. Lett. Japan. 1985, 881.

29. S.C. Chuang, T. Tian, J.G. Goodwin Jr., and I. Wender, J. Catal. 1985, 95, 435.

30. A. Carimati, A. Girelli, S. Marengo, S. Martinengo, L. Zanderighi and T. Zerlia, Proc. 9th Intl. Congr. catal., II, 706.

31. P.C. Ellgen, W.J. Bartley, M.M. Bhasin and T.P. Wilson, Adv. Chem. Ser. 178, 147, ACS. Washington D.C., 1978.

32. M.M. Bhasin, W.J. Bartley, P.C. Ellgen and T.P. Wilson, J. Catal. 1978, 54, 120.

33. T.P. Wilson, W.J. Bartley and P.C. Ellgen, "Advances in Catalytic Chemistry", Proc. Conf. in Salt Lake City, Utah, 1982.

34. H. Arakawa, T. Hanaoka, K. Takeuchi, T. Matsuzaki and Y. Sugi, in Proc. 8th Intl. Congr. Catal. 1988, p 602, Chemical Institute of Canda, Ottawa.

35. K. Gilhooley, S.D. Jackson and S. Rigby, Appl. Catal. 1986, 21, 349.

36. S.D. Jackson, B.J. Brandreth and D. Winstanley, J. Chem. Soc., Farad. Trans. 1. 1988, 84, 1741.

37. S.D. Jackson, J. Chem. Soc., Farad. Trans. 1. 1988, 81, 2225.

38. S.D. Jackson, B.J. Brandreth and D. Winstanley, J. Chem. Soc., Farad. Trans. 1. 1987, 83, 1835.

39. K. Gilhooley, S.D. Jackson and S. Rigby, J. Chem. Soc., Farad. Trans. 1. 1986, 82, 431.

40. S.D. Worley, C.A. Rice, G.A. Matson, C.W. Curtis, J.A. Guin, A.R. Tarrer, J. Chem. Phys. 1982, 76, 20.

41. B.J. Kip, E.G.F. Hermans and R. Prins, Proc. 9th Intl. Congr. Catal. 1988, p821, Chemical Institute of Canada, Ottawa.

42. M. Araki and V. Ponec, J. Catal. 1976, 44, 439.

43. L.J.M. Luyten, M. van Eck, J. van Grondelle and J.H.C. van Hooff, J. Phys. Chem. 1978, 82, 2000.

44. G.C. Bond and B.D. Turnham, J. Catal. 1976, 45, 128.

45. E.K. Poels, E.M. van Broekhoven, W.A.A. van Barneveld and V. Ponec, React. Kinet. Catal. Lett. 1981, 18, 223.

46. J. M. Driessen, E.K. Poels, J.P. Hindermann and V. Ponec, J. Catal. 1983, 82, 20.

47. J.P. Hindermann, A. Kiennemann, A. Chakor-Alami and R. Kieffer, Proc. 8th Intl. Congr. Catal., Verlag-Chemie, 1984.

48. B.J. Kip. F.W.A. Dirne. J.van Grondelle, R. Prins. Appl. Catal. 1986, 25, 32.

49. C.P. Huang and J.T. Richardson, J. Catal. 1978, 51, 1.

50. D.G. Blackmond. J.A. Williams. S. Kesraoui and D.S. Blazewick, J. Catal. 1986, 10, 496.

51. G. van der Lee. B. Schuller, H. Post, T.L.F. Favre. and V. Ponec. J. Catal. 1986, 98, 522.

52. T. Mori, A. Miyamoto, N. Takahashi, H. Niisuma, T. Hattori and Y. Murakami, J. Catal. 1986, 102. 199.

53. T. Mori. A. Miyamoto. N. Takahashi. M. Fukagaya, T. Hattori, and Y. Murakami, J. Phys. Chem. 1986, 90, 5197.

54. J. Blyholder, J. Phys. Chem. 1964, 68. 2772.

55. T:G. Richmond. F. Basolo and D.F. Shriver, Inorg. Chem. 1982. 24, 1272.

56. J.P. Collman, R.G. Finke, J.N. Cawse and J.I. Brauman. J. Am. Chem. Soc. 1978, 100, 4766.

57. C. Sudhakar. N.A. Bhore, K.B. Bischoff. W.H. Manogue and G.A. Mills. Catalysis 1987, edited J.O. Ward, Elselvier. New York.

58. N.A. Bhore. S. Chakka. K.B. Bischoff, W.H. Manogue and G.A. Mills, Proc. 9th Intl. Congr. Catal., Chemical Institute of Canda. Ottawa. 1988.

59. T. Tatsumi. A. Maramatsu. T. Fukunaga and H. Tominaga. Proc. 9th Intl. Congr. Catal.. Chemical Institute of Canada. Ottawa. 1988.

60. T. Fukushima. Y. Ishii. Y. Onda. and M. Ichikawa. JCS Chem. Commun. 1985. 1752.

61. B.J. Kip. P.A.T. Smeets. J. van Grondelle and R. Prins. Appl. Catal. 1987. 33. 181.

62. W.D. Mross. Catal. Rev. Sci. Eng. 1983. 25, 591.

63. D. Kitselmann. W. Vielstich and T. Dittrich. Chem.Ing.Tech.1077. 49. 463.

64. R.B. Anderson. in Catalysis. Vol. IV, ed. P.H. Emmett. Reinhold. New York. 1956.

65. British Gas, DAS 2,634,541, 1985.

66. M.E. Dry, J.Catal. 1969, 15, 190.

67. M.E. Dry, T. Shingler, C.S. van Botha, J. Catal. 1970, 16, 341.

68. H. Praliaud, M. Primet and G.A. Martin, Appl. Surf. Sci. 1983,17, 107.

69. T. Mori, A. Miyamoto, H. Nizuma, T. Hattori and Y. Murakami, React. Kinet. Catal. Lett. 1984, 26, 335.

70. W. J. Bartley, Eur. Pat. 0053 386, assigned to Union Carbide, 1984.

71. C.T. Campbell and D.W. Goodman, Surf. Sci. 1982, 123, 413.

72. D.W. Goodman, "Heterogeneous Catalysis", Ed. B.L. Shapiro, Texas A & M University Press, College Station, Texas, 1984.

73. M.M. McClory and R.D. Gonzalez, J. Catal. 1984,89, 392.

74. H. Miura and R.D. Gonzalez, J. Catal. 1982, 77, 338.

75. M.E. Dry, T. Shinglees, L.J. Boschoff and G.J. Oosthuizen, J. Catal. 1969, 15, 190.

76. W.J. Bartley, T.P. Wilson and P.C. Ellgen, USP 4,235.798, to Union Carbide, 1980.

77. S. Kagami, S. Naito, Y. Kikuzono and K. Tamaru, J. Chem. Soc. Chem. Comm. 1983, 256.

78. H. Orita, S. Naito and K. Tamaru, Chem. Letts. 1983, 1161.

79. G. Ertl, M. Weiss and S. B. Lee, Chem. Phys. Lett. 1979, 60, 391.

80. J.E. Crowell, E.L. Garfunkel and G.A. Somorjai, Surf. Sci. 1982, 121, 303.

81. M. Inoue, T. Miyake, Y. Takegami and T. Inui, Appl. Catal. 1983, 11, 103.

82. P.C. Ellgen and M.M. Bhasin U.S. Patent 4,096,164; June 20, 1978; assigned to Union Carbide Corporation.

83. Y.Y. Huang, U.S. Patent 4,328,129; May 4, 1982; assigned to Ethyl Corporation.

84. S.D. Jackson. UK Patent Appl. 2.151.616A; July 24, 1985; assigned to Imperial Chemical Industries.

85. (a) H.C. Foley and M.P. O'Toole, U.S. Patent 4,684,618; August 4, 1987; assigned to American Cynamid. (b) H.C. Foley and M.P. O'Toole, U.S. Patent 4,687,784; August 18, 1987; assigned to American Cynamid.

86. (a) N.A. Bhore, S. Chakka, K.B. Bischoff, W.H. Manogue and G.A. Mills, Proc. 9th Intl. Congr. Catal. 1988, p594, Chemical Institute of Canada. Ottawa. (b) S. Chakka, N.A. Bhore, K.B. Bischoff, W.H. Manogue and G.A. Mills. in "Catalysis 1987", ed. J.O. Ward, Elselvier, 1988, Amsterdam..

87. M. Inoue, T. Miyake. T. Inui and Y. Takegami, J. Chem. Soc., Chem. Commun. 1983, 70.

88. M. Inoue, T. Miyake, Y. Takegami and T. Inui, Appl. Catal. 1984, 11, 103.

89. M. Inoue, T. Miyake, Y. Takegami and T. Inui, Appl. Catal. 1987, 29, 285.

90. M. Inoue, T. Miyake, S. Yonezawa, D. Medhanavyn, Y. Takegame and T. Inui, J. Mol. Catal. 1988, 45, 111.

91. B. Walther, M. Scheer, J.C. Buttcher, A. Trunschke, H. Ewald, D. Gutshick, H. Meissner, M. Skupin and G. Vorbeck, accepted, Inorg. Chim. Acta.

92. P.C. Heimenz. "Principles of Colloid and Surface Chemistry", Marcel Dekker Inc., 1976, New York.

93. G.D. Parfitt, Pure & Appl. Chem. 1986, 48,415.

94. C.P. Huang, Y.S. Hwieh. S.W. Park, M. Ozden Corapcioglu, A.R. Boweres and H.S. Elliot in, "Metal Speciation. Separation and Recovery", Eds. J.W. Patterson, R. Passino, Lewis Publishers Inc..Chelsa, Michigan. 1987.

95. C.F. Baes and R.E. Messmer. "The Hydrolysis of Cations, John Wiley and Sons. New York.

96. W.K. Hall. "Proceedings of the 4th International Conference on the Chemistry and Uses of Molybdenum". Climax Molybdenum Company. Ann Arbor. Michigan.

97. S.H.A. Begemann and A.L. Boers. Surf. Sci. 1972. 30. 134.

98. E.P.Th.M. Suurmeijer and A.L. Boers, Surf. Sci. 1973, 43, 309.

99. H. Niehus and E. Bauer, Surf. Sci. 1975, 47, 222.

100. E. Taglauer and W. Heiland, Appl. Phys. 1976, 9, 261.

101. (a) J.M. Poate and T.M. Buck in "Experimental Methods in Catalysis Research" ed. R.B. Anderson and P.T. Dawson, Vol.III, Academic Press, 1976. (b) B.A. Horell and D.L. Cocke, Cat. Rev. Sci. Eng. 1987, 29, 447.

102. T.M. Buck in "Methods of Surface Analysis", ed. A.W. Czanderna, Elselvier, Amsterdam, 1975.

103. M.J. Kelley, Chemtech. 1987, 294.

104. D.G. Swartzfager, Anal. Chem. 1984, 56, 55.

105. M. Shelef, M.A.Z. Wheeler and H.C. Yao, Surf. Sci. 1975, 47, 697.

106. M. Wu, R.L. Chin and D. M. Hercules, Spect. Lett. 1978, 11, 615.

107. M. Wu and D.M. Hercules, J. Phys. Chem. 1979, 83, 2003.

108. R.L.Chin and D.M. Hercules, J. Phys. Chem. 1982, 86, 360.

109. R.L.Chin and D.M. Hercules, J. Phys. Chem. 1982, 86, 3079.

110. F. Delannay, E. Haeussler, B. Delmon, J. Catal. 1980, 66, 469.

111. H. Jeziorowski, H. Knozinger, E. Taglauer and C. Vogdt, J. Catal. 1983, 80, 286.

112. J. Abart, E. Delgado, G. Ertl, H. Jeziorowski, H. Knozinger, N. Thiele, X. Zh. Wang and E. Taglauer, Appl. Catal. 1982, 2, 155.

113. J.S.Brinen, D.A. D'Avignon, E.A. Meyers, P.T.Deng and D.W. Behnken, Surf. & Int. Analysis, 1984, 6, 295.

114. S. Kasztelan, J. Grimblot and J.P. Bonnelle, J. Chim. Phys. 1983, 80, 793.

115. S. Kasztelan, J. Grimblot and J.P. Bonnelle, J. Phys. Chem. 1987, 91, 1503.

116. L. Reimer, "Transmission Electron Microscopy", Springer-Verlag, New York, 1984.

117. J.V. Sanders, in "Catalysis: Science and Technology", Ed. J.R. Anderson and M. Boudart, Volume 7, Springer-Verlag, 1985.

118. F. Delannay, in "Characterization of Heterogeneous Catalysts", ed. F. Delannay, Marcel Dekker, New York. 1984.

119. M.H. Loretto, "Electron Beam Analysis of Materials", Chapman and Hall, New York, 1984.

120. V.A. Drits, "Electron Diffraction and High-Resolution Electron Microscopy of Mineral Structures", Springer Verlag, New York, 1987.

121. G.R. Millward and J.M. Thomas, in "Surface Properties and Catalysis by Non-Metals", ed. J.P. Bonelle, B. Delmon and E. Derouane, D. Reidel Publishing Co., Boston. 1982.

122. J.W. Sprys, L. Bartosiewicz, R. McCune and H.K. Plummer, J. Catal. 1975, 39, 91.

123. I. Chan, J. Elect. Micr. Tech. 1981, 5, 181.

124. I. Chan, J. Elect. Micr. Tech. 1985, 2, 525.

125. J.W. Edington, "The Operation and Calibration of Electron Microscope", McMillan Press Ltd., London, 1974.

126. Phillips EM300 handbook, Eindhoven, Netherlands.

127. A. Howie, L.D. Marks and S.J. Pennycook, Ultramicroscopy. 1982, 8, 163.

128. J.V. Sanders, J. Elect. Micr. Tech. 1986, 3, 67.

129. L.D. Schmidt, T. Wang and A. Vacquez, Ultramicroscopy. 1982, 8. 175.

130. M.J. Yacaman, Appl. Catal. 1984. 13, 1.

131. P.B. Hirsch, A. Howie, R.B. Nicholson, D.W. Pashley and M.J. Whelan, "Electron Microscopy of Thin Crystals", Butterworths, Washington D.C., 1965.

132. R. Gevers, in "Diffraction and Imaging Techniques in Materials Science, eds. S. Amelinckx, R. Gevers and J. van Landuyt, North-Holland Publishing Company, New York, 1978.

133. M.J. Whelan, in "Diffraction and Imaging Techniques in Materials Science", eds. S. Amelinckx, R. Gevers and J. van Landuyt, North-Holland Publishing Company, New York, 1978.

134. M. Jose Yacaman and J.M. Dominiguez, J. Catal. 1981, 67, 475.

135. L.D. Schmidt and T. Wang, J. Vac. Sci. Technol. 1981, 18, 520.

136. M.J. Yacaman, J. Zenith and J.L. Contreras, Appl. Surf. Sci. 1980, 6, 71.

137. M.J. Yacaman, in "Catalytic Materials: Relationships Between Structure and Reactivity", ACS Symposium Series 248, American Chemical Society, Washington D.C., 1984.

138. D.J.H. Cockayne, in "Diffraction and Imaging Techniques in Materials Science", Eds. Amelinckx, R. Geevers and J. Van Landuyt, North-Holland Publishing Company, New York, 1978.

139. K. Heinemann, Optik. 1971, 34, 113.

140. E. Freund and H. Dexpert, in "Surface Properties and Catalysis by Non-Metals", ed. J.P. Bonelle, B. Delmon and E. Derouane, D. Reidel Publishing Co., Boston, 1982.

141. J.M. Dominguez and M.J. Yacaman, in "Growth and Properties of Metal Clusters", Ed. J. Bourdon, Elselvier, Amsterdam, 1980.

142. M.J. Yacaman, in "Growth and Properties of Metal Clusters", Ed. J. Bourdon, Elselvier, Amsterdam, 1980.

143. R.J. Matyi, L.H. Schwartz and J.B. Butt, Cat. Rev. Sci. Eng. 1987, 29, 41.

144. J.L. Maitre, P.G. Menon and F. Delannay, "Characterization of Heterogeneous Catalysts", ed. F. Delannay, Marcel Dekker Inc., New York, 1984.

145. P.C. Flynn, S.E. Wanke and P.S. Turner, J. Catal. 1974, 33, 233.

146. C.E. Lyman, in "Catalytic Materials: Relationships Between Structure and Reactivity", ACS Symposium Series 248, American Chemical Society, Washington D.C., 1984.

147. J.M. Cowley, in "Catalytic Materials: Relationships Between Structure and Reactivity", ACS Symposium Series 248, American Chemical Society, Washington D.C., 1984.

148. M.M.J. Treacy, in "Catalytic Materials: Relationships Between Structure and Reactivity", ACS Symposium Series 248, American Chemical Society, Washington D.C., 1984.

149. S.J.B. Reed, "Electron Microprobe Analysis", Cambridge University Press, London, 1975.

150. J.C. Russ, "Fundamentals of Energy Dispersive X-ray Analysis", Butterworths, London, 1984.

151. S.J.B. Reed, in "Quantitative Electron-Probe Microanalysis, ed. V.D. Scott and G. Love, Ellis Horwood Limited, Chichester, West Sussex, England, 1983.

152. P.K. Wang, J.P. Ansermet, S.L. Rudaz, Z. Wang, S. Shore, C.P. Slichter and J.H. Sinfelt, Science, 1986, 244, 35.

153. T.M. Duncan and C.R. Dybowski, Surf. Sci. Reptorts. 1981, 1, 571.

154. C.R. Dybowski, Chemtech. 1985, 186.

155. A.D.H. Claque in "Catalysis : Vol 7" , A specialist periodical report, The royal Society of Chemistry, London.

156. T.M. Duncan, J.T. Yates Jr. and R.W. Vaughan, J. Chem. Phys. 1980, 73, 975.

157. A. Abragam, "Principles of Nuclear Magnetism", Oxford University Press, 1961, London.

158. T.M. Duncan, P. Winslow and A.T. Bell, Chem. Phys. Letts. 1983, 102, 163.

159. T.M. Duncan, P. Winslow and A.T. Bell, J. Catal. 1985, 93, 1.

160. T.M. Duncan, J.A. Reimer, P. Winslow and A.T. Bell, J. Catal. 1985, 95, 305.

161. H.T.Rhodes, in 'Catalytic Materials: Relationship Between Structure and Reactivity', ed. T.E. White.Jr., R.A. Dalla Betta, E.G. Derouane and R.T.K. Baker, ACS Symposium Series 248, 1984, Washington D.C.

162. C.D.Makowka, C.P.Slichter and J.H.Sinfelt, Phys. Rev. Letts. 1982, 49, 379.

163. S.L. Rudaz, J.P. Ansermet, P.K.Wang, C.P.Slichter, and J.H.Sinfelt, Phys. Rev. Letts. 1985, 54, 71.

164. C.P. Slichter, Ann. Rev. Phys. Chem., Vol.37, 1986.

165. J.L.Robbins, J. Phys. Chem. 1986, 90, 3381.

166. T. Huizinga, Ph.D. thesis. Eindhoven University of Technology, 1983, Netherlands.

167. V.L.Kuznetov, I.L. Mudrakovskii, A.V. Romanenko, V.M. Mastikhin and Yu. I.Yermakov, React. Kinet. Catal. Letts. 1984, 25, 147.

168. V.L.Kuznetov, A.V.Romanenko, I.L. Mudrakowski, V.M. Matikhin, V.A. Shmachkov and Yu. I. Yermakov, 8th Intl. Congr. Catal, 5-3, 1984, Springer Verlag.

169. R.K. Shoemaker and T.M. Apple, J. Phys. Chem. 1985, 89, 3185.

170. B.C. Gerstein and C.R. Dybowski, "Transient Techniques in NMR of Solids", Academic Press, New York, 1985.

171. C.D. Wagner, W.N. Riggs, L.E. Davis, J.F. Moulder and G.E. Mullenberg, "Hanbook of Photoelectron Spectroscopy", Perkin-Elmer Co., Eden Prarie, Minnesota, 1979.

172. J.C.Vedrine , in "Surface properties and catalysis by non-metals", ed. J.P. Bonnelle, B. Delmon and Derouane E., D. Reidel, Boston, 1983.

173. K. Seigbahn , C. Nording , A. Fahlman, K. Nordberg, K. Hamrin, J. Hedmen, G. Johansson, T. Bergmark, S. Karlsson, I. Lindgreen and B. Lindberg, ESCA, Nova Acta Regiae Soc. Ups, Ser IV,20(1967).

174. H. Windawi, J. Elect. Spect. & Rel. Phen. 1981, 22, 373.

175. J.P. Contour and G. Mouver.. J. Electr. Spect & Rel. Phen. 1975, 7, 85.

176. C.D. Wagner, J. Elect.Spect. & Rel. Phen. 1980, 18, 345.

177. P. Swift, Surf. & Int. Analysis. 1982, 4, 47.

178. T.E. Madey, C.D. Wagner and A. Joshi, J. Elect. Spect. & Rel. Phen. 1977, 10, 359.

179. C.S. Grove, "Transformations in Molybdenum catalyst morphology and surface chemistry", Ph.D. thesis. University of Minnesota, 1985.

180. P. Ratnaswamy, J. Catal. 1975, 40, 137.

181. T.L. Barr in "Practical Surface Analysis by Auger and X-Ray Photoelectron Spectroscopy" ed. D. Briggs and M.P. Seah.. John Wiley, New York, 1983.

182. A. Cumino and B.A. DeAngelis, J. Catal. 1975, 36, 11.

183. N. Jagganathan, A. Srinivasan and C.N.R. Rao, J. Catal. 1981, 60, 418.

184. Y. Holl, R. Tourounde, G. Maire, A. Muller, P.A. Engelhard and J. Grosmangin, J. Catal. 1987, 104, 202.

185. D.S. Zingg, L.E. Makovsky, R.E.Tisher, F.R. Browm and D.M. Hercules, J. Phys. Chem. 1980, 84, 2898.

186. N.K. Nag, J. Phys. Chem. 1987, 91, 2324.

187. S.C. Fung, J. Catal. 1979, 58, 454.

188. F.P.J.M. Kerkhof and J.A. Moulijn, J. Phys. Chem. 1979, 83, 1612.

189. S. Kaliaguine, A. Adnot and G. Lemay, J. Phys. Chem. 1987, 91, 2886.

190. L. Rodrigo, K. Marcinkowska, A. Adnot, P.C. Robergo, S. Kaliaguinne, J.M. Stencel, L.E. Makovsky and J.P. Diehl, J. Phys. Chem. 1986, 90, 2690.

191. P. Dufresne, E. Payen , J. Grimblot and J.P. Bonnelle, J. Phys. Chem. 1981, 85, 2344.

192. J.G. Grimblot, and E. Payen in 'Surface properties and catalysis by non-metals' ed. J.P. Bonelle, B. Delmon and E. Derouane., D. Reidel, Boston, 1982.

193. Y. Okamato, H.Tomika, Y. Katoh, T. Imanaka and S. Teranishi, J. Phys. Chem. 1980, 84, 1833.

194. Y. Okamato, T. Imanaka and S. Teranishi . J. Phys. Chem. 1981, 85, 3798.

195. J. Sonneman and P. Mars, J. Catal. 1973, 31, 1309.

196. L.H. Little, "Infrared Spectra of Adsorbed Species", Academic Press, 1966, New York.

197. J. Pritchard and T. Catterick, "Experimental Methods in Catalysis Research", eds. R.B. Anderson and P.T. Dawson, Vol. III, Academic Press, New York, 1976.

198. N. Sheppard and T.T. Nguyen, Adv. in IR and Raman Spect. 1978, 5, 67.

199. W.N. Delgass, G.L. Haller, R. Kellerman and J.H. Lunsford, "Spectroscopy in Heterogeneous Catalysis", Academic Press. New York, 1979.

200. M.L. Hair, in "Vibrational Spectroscopy for Adsorbed Species", eds. A.T. Bell and M.L. Hair, American Chemical Society, 1980, Washington D.C.

201. A. Zecchina, S. Coluccia and C. Morterra, Appl. Spect. Rev. 1985, 21, 259.

202. J.B. Peri, in "Catalysis: Science and Technology", ed. J.R. Anderson and M. Boudart, Springer-Verlag, New York, 1984.

203. P. Hollin and J. Pritchard, in "Vibrational Spectroscopy for Adsorbed Species", eds. A.T. Bell and M.L. Hair, American Chemical Society, 1980, Washington D.C.

204. M.L. McKee, C.H. Dai and S.D. Worley, J. Phys. Chem. 1988, 92, 1056.

205. M.L. McKee and S.D. Worley, J. Phys. Chem. 1988, 92, 3699.

206. J. Hlavay and J. Inczedy, Spectrochimica Acta. 1985, 41, 783.

207. H.F.J. van't Blink, J.B.A. van Zon, T. Huizinga, J.C. Vis, D.C. Koningsberger and R. Prins, J. Am. Chem. Soc. 1985, 107, 3139.

208. F. Solymosi and M. Pasztor, J.Phys. Chem. 1985, 89, 4789.

209. F. Solymosi and M. Pasztor, J. Phys. Chem. 1986, 90, 5312.

210. P. Basu, D. Panayotov and J.T. Yates, Jr., J.Phys. Chem. 1987, 91, 3133.

211. C.H. Dai and S.D. Worley, J. Phys. Chem. 1986, 90, 4219.

212. F. Solymosi, M. Pasztor and G. Rakhely, J. Catal. 1988. 110. 413.

213. M.I. Zaki, G. Kunzmann, B.C. Gates and H. Knozinger, J. Phys. Chem. 1987, 91, 1486.

214. J.C. Vedrine, in "Characterization of Heterogeneous Catalysts", ed. F. Delanney, Marcel Dekker. 1984.

215. R.Y. Zhan, M. Narayana and L. Kevan, JCS Far. Trans. 1. 1985. 81, 2083.

216. T.P. Wilson, P.H. Kasai and P.C. Ellgen, J. Catal. 1981, 69, 193.

CHAPTER 3
THE DELPLOT TECHNIQUE: A NEW AND SIMPLE METHOD FOR REACTION PATHWAY ANALYSIS

3.1 Introduction

Quantitative kinetic analysis of complex reaction systems involves discrimination between not only rival models for rate expressions, but also rival models for the network of reaction pathways. The use of quantitative statistical methods provides important information that usually narrows the spectrum of possible models. but fails to provide unequivocal discrimination. The problem is especially severe when many candidate rate models are considered within several candidate network models. Clearly a complementary procedure aimed at deduction of reaction network would be useful.

The methods discussed here apply to batch reactors and plug flow reactors, and hence the batch time and the space time will be used interchangeably. Since the perfectly mixed reactor gives rate versus concentration data. this method may not directly useful to perfectly mixed reactors. Non-ideal reactors, non-isothermal reactors and diffusion limited reactors are not considered. Hence the transport limitations on the data have to be evaluated by well-known methods discussed elsewhere[1]. The method developed here is a general kinetic method. and can be applied to catalytic and non-catalytic systems. and in catalytic systems to heterogeneous and homogeneous systems. The delplot (Delaware Plot) method is a modified initial rate method.

Herein, a simple but useful method for the discernment of the rank (i.e., primary, secondary, etc..) of the reaction product is developed, which is the first step in the deduction of reaction network. A primary product has a rank of one, a secondary product has a rank of two, and so on. In the first stage primary and non-primary products are separated by plotting [molefraction(y)/ conversion(x)] versus x. A finite intercept of the above plot denotes a primary product, while a zero intercept denotes a non-primary product (secondary, tertiary, etc.,). The advantage of the proposed method is in its simplicity and the ease of application. Detailed computation and parameter fitting is not needed. For a network of first order reactions, the method can be successively applied to separate products according to their rank. By discerning the rank of the product, we establish the sequential hierarchy of the products. The literature provides seminal, related treatments that are frequently limited by the allowable reaction order or by the ease of application or by their precision[1-7].

The first step in synthesizing a network is separating the products according to their rank. After the products have been separated three different types of reaction steps have to be identified. First, the reaction steps between products of lower rank to the products of next higher rank have to be identified. Secondly reaction steps between the products of same rank have to be identified. Thirdly steps from products of higher rank to species of lower rank need to be identified. The synthesis of consistent reaction network is complete once all the steps have been identified. The next step is to find the functionality of the rate expressions in each reaction step. The last step in kinetic modeling is to find the parameters in the rate function. Usually the above steps cannot be decoupled and the problem has to be solved in its entirety.

This method is especially useful when many products are formed. The complications in application of this method to heterogeneous catalytic systems are elaborated at the end of of this paragraph. The method gives network detail

of the system that may or may not be of any significance to the mechanistic details of the system. For example, in a hydrotreating reaction, this method can uses the product distribution to find the hierarchy of hydrogenation sites. The hierarchy of hydrogenation sites is an example of mechanistic information. So, in this example, the network information leads to mechanistic information.

Since the delplot method uses initial rates, some of the inherent limitations of the initial rate approach exists in this method and hence it is important to realize the pitfalls in the synthesis of reaction networks from initial rate data. Mathur and Thodos[8] have synthesized reaction networks for oxidation of sulfur dioxide on vanadium oxide catalysts using the initial rate approach. The problem with the initial rate approach occurs when a product inhibits the reaction. Boudart[9] has pointed out that the initial rate approach would give inconsistent results for sulfur dioxide oxidation since the reaction is inhibited by the product sulfur trioxide. Peterson[10] has analyzed some of the less known problems of initial rate studies when product inhibition is operative. Diffusional limitations due to the inhibiting product can be severe even though the ordinary Thiele criterion does not show any appreciable gradient of the reactant concentration in the catalyst pores.

The dependence of rate constants on the process parameters can be obtained by using the intercepts at various process conditions. Furthermore, this method was developed for separating regimes of space time (or percent conversion) where a product can be primary and secondary. Frequently, the reaction steps between products of lower rank to products of higher rank can be identified. The higher rank delplot method is proved for first order reactions. Furthermore, a general method is shown whereby the higher rank delplot method can be worked for any given kinetics.

3.1.1 Existing Methods

The separation of primary products from non-primary products can be done by two existing methods[1-5]. The first method is the initial rate method. Here the rate of formation of a given species is plotted against the space time. A finite initial slope suggests a primary product, while a zero slope suggests a non-primary product. The second method consists of collecting rate data for each species at various flow rates. If the rates of formation of species are finite at large flow rates; then that species is a primary product otherwise the species is a non-primary product. Both the methods are general and can be applied only to differential data. Furthermore, very little information can be obtained on identifying reaction steps. In addition, the functionality of the reaction steps cannot be obtained.

The classic work of Wei and Prater provides a matrix method for finding kinetic structure in a network[11]. This method can be applied only to first order reactions. The method is iterative unless all the rate constants are known. Even though the selectivity (amount of product P formed/ amount of reactant A converted) versus conversion plots are used often, their use in investigating reaction network structure is scarce. Furthermore, their application to-date is only qualitative. Klein and Virk have used selectivity plots to infer the reaction network[12]. Hofmann has discussed the various types of plots (yield vs. conv, yield vs. temp, etc..) to characterize the activity and selectivity of heterogeneous catalytic reactions[13]. He concludes that the selectivity versus conversion plots (differential and integral) are very useful in process evaluation. Lee et al. have proposed a method for synthesis of kinetic structure for many irreversible first order steps[14-16]. In Lee's method the products are separated into initial products and terminating products, then the products in between are found by a series of Laplace transforms. Since Lee's method uses Laplace transforms, it can be applied only to first order reactions.

3.1.2 Rank of a Product

In the delplot method the products are separated by the minimum number of slow steps on the process time scale leading to that product. The first step in kinetic analysis of products is to build a reaction pathway. A primary product has one slow step on the time scale of the process in the steps leading to its formation. Similarly a secondary product has two slow steps in the reaction network leading to its formation. The rank of the product is defined as the number of slow steps leading to its formation. Hence the rank of a primary product is one, while the rank of the secondary product is two. Lee et al.[17] define the rank of the product as the number of exponential terms in their rate expression. They called the rank of the product as the order of the product. To avoid confusion in the terminology, the hierarchy of the product is called rank, while the order is used exclusively for the functional form of the rate expression.

The concept of the rank of a product in a reaction network is implicitly determined by the reactants used and is best explained by an example. For example, for the network given in figure 3.1 on page 100, the rank of various products are given in the second column of table 3.1 on page 101, when A is the reactant.

Here B is a primary product since there is only one step leading to its formation. Even though there are many different routes for the formation of G, the route with the lowest rank always dominates in delplot analysis. Thus the step

$$A \text{ — } B \text{ — } C \text{ — } G$$

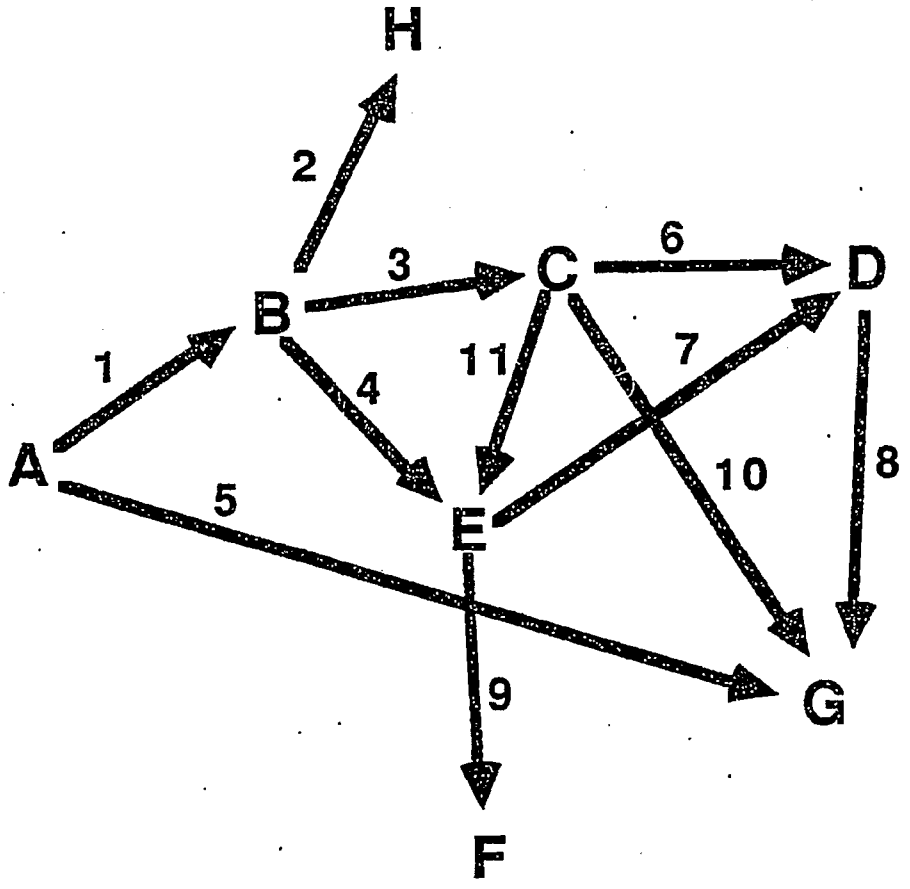

Figure 3.1: Rank of a product in a complex reaction pathway

Table 3.1: Rank of products for various reactants

Product	Rank A-reactant	Rank B-reactant	Rank A and B reactants
A	0	∞	0
B	1	0	0
C	2	1	1
D	3	2	2
E	2	1	1
F	3	2	2
G	1	2	1
H	2	1	1

does not affect the rank of G as long as there is another step with less than three slow steps (in the example, this step is $A \longrightarrow G$). Similarly, products C, E and H can be shown to be secondary products, while, products D and F can be shown to be tertiary products. The rank of a product depends on the reactant used. For example, in the network shown in figure 3.1 on page 100, the rank of a product depends on the reactants used. Table 3.1 shows the ranks of the products when A, B, and (A,B) are used as reactants. Note the changes in rank with changes in the reactants used. Here again, the lowest rank corresponding to any product dominates. Thus the rank of a product obtained from delplot analysis is a reactant-dependent information.

3.1.3 Time Scales

Whatever the method of its deduction, a reaction network implicitly defines a relevant time scale. This makes careful definition of times more than a semantic issue. A network comprises serial and parallel reaction pathways that connect only observable species in a reaction mixture. Pathways can be a single elementary step but will more generally consist of serial and parallel elementary reaction steps that combine to form the overall reaction path. For example, the Rice-Herzfeld pyrolysis of ethane to ethylene and hydrogen might appear as a pathway in a reaction network, although the reaction is well known to proceed through initiation, hydrogen transfer, β-scission and termination steps involving free-radicals. These are frequently unobservables in the context of reaction network analysis.

Thus the rank of a product is also implicitly determined by the time scale of data collection, i.e., the lowest reaction time at which data can be collected. It might be argued that in the Rice-Herzfeld example, only the initiation and chain transfer products(including radicals) are truly of primary rank, although it is common to accept ethylene and hydrogen as primary products. In principle, if it were possible to collect data at very small times, then, only the products formed

from the elementary reactions would be primary products. However, usually it is not possible or convenient to collect data on a very small time scale and hence the first set of observable species formed from the reactions are taken as primary products. Thus the rank of a product is inextricably connected to the number of rate determining steps.

3.1.4 Rate-Limiting Steps

According to Laidler[18], the concept of rate-limiting step even though well-used, is poorly understood on a quantitative basis. Usually, rate limiting step is referred to that elementary reaction that has a very strong influence on the overall reaction rate. The concept of rate limiting step is not a necessary one and many kinetics problems can be solved without it. However the concept not only simplifies the problem but also gives an additional insight into the problem. Gold[19] has defined a rate-determining step for a sequence of elementary reactions in a homogeneous system. If for a given reaction

$$A + B \overset{K_1}{=} C + D \overset{K_2}{=} \cdots \overset{K_g}{=} G \xrightarrow{k_j+(X)} P \xrightarrow{k_m} Q \cdots \tag{3.1}$$

the rate of reaction (r) is given by

$$r = F([A], [B], [C], [D], \cdots, [G], K_1, K_2, \cdots, K_g) \times k_j[X] \tag{3.2}$$

where F is a function only of the concentrations and of the equilibrium constants K for the pre-equilibria that precede the step j, then step j is called the rate limiting step. Gold further points out that in such a sequence, step j is the earliest step for which the chemical flux (corrected appropriately for the stoichiometric coefficients) does not greatly exceed the rate of formation of the final reaction product (again appropriately corrected for the stoichiometric coefficients), if the overall process is irreversible. Murdoch[20] has used transition state theory to

analyze the critical issues in the definition of the rate-determining step. Kost and Pross[21] have pointed out that the rate-limiting step may depend on the concentrations terms as well as the specific rate constants. Few attempts have been made to give a quantitative treatment of a rate-controlling step. Ray[22] defines Control Function (CF_i) as

$$CF_i = \left(\frac{\partial r}{\partial k_i}\right)_{K_j, k_j}$$

where r is the overall reaction rate . The control function for a reaction step i is the change in rate with respect to the rate constant k_i keeping all other rate constants and equilibrium constant the same. The elementary reaction with the highest control function, exerts the maximum control on the reaction and hence is the rate-determining step. However this method is not useful for real systems since the rate constants and equilibrium constants for each elementary step are not known. Thus there is no easy way of identifying the number and the nature of the rate-determining step. The delplot method can find the number of rate-limiting steps in a reaction network.

3.1.5 Overview

The object of this chapter is to develop a simple but useful method for the delineation of products according to their rank, i.e., the hierarchy of appearance in a reaction network and to extend the quantitative foundations of reaction network analysis. The method is developed in two parts, the first dealing with primary products ($r = 1$) for any order of the reaction. Here we formalize and provide quantitative proof of the analysis used by Klein and Virk[1]. The second part deals with products of higher rank($r > 1$), and is subdivided into sections dealing with the first order ($n = 1$) reactions and reactions of general order ($n \neq 1$). Herein, the important concepts of coupling between product rank and reaction

order are discussed. Then this method is applied to Fisher-Tropsch synthesis and oxygenate synthesis reaction networks to find the number of slow steps for each product and their location. Extensions of the extended delplot method, such as non-integer rank delplot method and product-based delplot method are discussed in the next section. The use of delplot analysis in reaction step identification is the topic of the fifth section. Finally, the use of order of magnitude analysis and singular perturbation analysis in separation of regimes wherein the apparent product rank changes is shown.

3.2 Basic Delplot: Products of Primary Rank

3.2.1 Development

Our objective is to first separate reaction products according to their rank. The basic method is a plot of (molar yield/conversion) versus conversion. The information gained from this analysis is in its intercepts. Therefore the data may be less precise than that needed for numerical differentiation. Hereafter the method is called the delplot method. The method is best explained through an example. Consider the network composed of

$$A \xrightarrow{k_1} B \xrightarrow{k_3} C \tag{3.3}$$

$$A \xrightarrow{k_2} D \tag{3.4}$$

equations (3.3) and (3.4). The temporal variation of species concentrations

$$A = A_0\, e^{-(k_1+k_2)t} \tag{3.5}$$

$$B = \frac{k_1 \times A_0}{k_3 - k_1 - k_2} \times (e^{-(k_1+k_2)t} - e^{-k_3 t}) \tag{3.6}$$

$$C = \frac{k_1 k_3 A_0}{k_3 - k_1 - k_2} \times \left[\frac{1 - e^{-(k_1+k_2)t}}{k_1 - k_2} - \frac{1 - e^{-k_3 t}}{k_3}\right] \tag{3.7}$$

$$D = \frac{k_2 A_0}{k_1 + k_2} \times \left(1 - e^{-(k_1+k_2)t}\right) \tag{3.8}$$

given in equations (3.5)- (3.8) are used to prove this method. In short, the basic delplot method consist of plotting the molar yield of product($y = (P - P_0)/A_0$) divided by the reactant conversion (x) versus the conversion (x). The intercept for any product P in basic delplot is denoted by ${}^1P_A$. The intercept is defined as follows.

$${}^1P_A = \lim_{\tau \to 0} \frac{P - P_0}{A - A_0} \tag{3.9}$$

where

τ is the batch time or the space time,

P_0, A_0 are the initial or inlet concentrations.

A finite intercept denotes a primary product ($r = 1$) while a zero intercept denotes a product of rank greater than one ($r > 1$). For the example of equations (3.3) and (3.4), B and D would have finite intercepts while C will have zero intercepts. Substituting equations (3.5) to (3.8) in equation (3.9), the intercepts for B, C and D are given by the following equations.

$${}^1B_A = \frac{k_1}{k_1 + k_2}$$

$${}^1C_A = 0$$

and

$${}^1D_A = \frac{k_2}{k_1 + k_2}$$

For rank $r = 1$, the method is independent of the type of the kinetics of each step. A Taylor series expansion of equation (3.9) allows a kinetics-independent proof. Consider the intercept for product B:

$${}^1B_A = \lim_{\tau \to 0} \frac{B - B_0}{A_0 - A}$$

Expanding A and B as a Taylor series in τ, we get

$$ {}^{1}B_A = \lim_{\tau \to 0} \frac{(B_0 + (B')_{\tau=0}\tau + \cdots) - B_0}{A_0 - A_0 - (A')_{\tau=0}\tau - \cdots} \tag{3.10} $$

$$ {}^{1}B_A = \frac{(B')_{\tau=0}}{(-A')_{\tau=0}} \tag{3.11} $$

Since the initial rate of formation of primary product is finite, the delplot gives a finite intercept. For a non-primary product, the initial rate is zero and hence a zero intercept is found. It is important to note that this method does not specify the shape of the curve in the delplot method. For a general pathway where there are many reactions (i=1,n) where A is consumed, the intercepts are

$$ {}^{1}B_A = \frac{(B')_{\tau=0}}{\sum_i (-A')_{i,\tau=0}} \tag{3.12} $$

where $(-A')_{i,\tau=0}$ is the initial rate of consumption of reactant in the reaction step i.

If there is more than one reactant the delplot can be based on any one reactant. A mass balance of reactant can be expressed in terms of intercepts. If there is only one reactant then

$$ \sum_{j=1}^{n} \frac{{}^{1}P_A^j \times \nu_i^A}{\nu_i^P} = 1 \tag{3.13} $$

where

ν_i^k is the absolute value of the stoichiometric coefficient of the species k in the reaction i given by

$$ \nu_i^A A - \cdots \xrightarrow{i} \nu_i^P P - \cdots $$

3.2.2 Rules for Basic Delplot

Some rules for the use of basic delplot are stated below. The significance of these rules is also discussed .

Rule 1

If $P_A = 0$ then P is not a primary product i.e. rank of P is greater than 1. If $P_A \neq 0$ then P is a primary product as proved above.

Rule 2

If $P_A = \frac{\nu_P}{\nu_A}$ ($\frac{\nu_A}{\nu_P}$ is the stoichiometric coefficients and is often one) then P is formed only from A and A is consumed only in the formation of P.

Rule 3

If there is only one reactant then

$$\sum_{j=1}^{n} \frac{{}^{1}P_A^j \times \nu_i^A}{\nu_i^P} = 1 \tag{3.14}$$

where

ν_i^k is the absolute value of the stoichiometric coefficient of the species k in the reaction i given by

$$\nu_i^A A - \cdots \xrightarrow{i} \nu_i^P P + \cdots$$

Equation (3.14) is the limit of the mass balance of A. A proof of equation (3.14) follows. and illustrates the key concepts of delplot analysis. The reactant A can be consumed in three different type of reactions.

a) A reacts to form an observable primary product P^j as in equation (3.15).

$$\nu_A^j A \longrightarrow \nu_P^j P - \cdots \tag{3.15}$$

b) A reacts with a product Q^k as in equation (3.16).

$$\nu_Q^k Q^k + A \longrightarrow \nu_R^k R + \cdots \tag{3.16}$$

c) A reacts to form a non-observable(intermediate) primary product, U, as in equation (3.17). The second step leading to the formation of B is also slow.

$$A \longrightarrow U \longrightarrow B \tag{3.17}$$

Assume that the stoichiometric coefficients are unity and there is no volume change. A material balance of A yields

$$dA_{total} = dA_a + dA_b + dA_c \tag{3.18}$$

Dividing equation (3.18) by dA_{total} and taking the limit as $t \longrightarrow 0$ gives

$$\lim_{t\to 0} \frac{dA_a}{dA_{total}} + \lim_{t\to 0} \frac{dA_b}{dA_{total}} + \lim_{t\to 0} \frac{dA_c}{dA_{total}} = 1 \tag{3.19}$$

The second term in equation (3.19) does not contribute because $Q^k(0) = 0$. Since U is not an observable species, it is present in low concentrations i.e., $U \ll B, A$. However, the delplot method uses the initial rate and the rate of reaction of intermediate U cannot be neglected even though it is present in low concentrations.

At small time, no B is formed and since U is a non-observable species, we get

$$dA_a \gg dA_c \tag{3.20}$$

Inequality (3.20) holds in the limit $t \longrightarrow 0$. Thus

$$\lim_{t\to 0} \frac{dA_a}{dA_{total}} \gg \lim_{t\to 0} \frac{dA_c}{dA_{total}} \tag{3.21}$$

Combining equations (3.19) with inequality (3.21) we get

$$\lim_{t \to 0} \frac{dA_a}{dA_{total}} \approx 1 \tag{3.22}$$

Incorporating parallel steps 'j' and stoichiometric coefficients in (3.22) yields

$$\sum_{j=1}^{n} \frac{{}^{1}P_A^j \times \nu_i^A}{\nu_i^P} \approx 1 \tag{3.23}$$

This derivation shows that the presence of multiple rate determining steps would not appreciably affect the limit of mass balance of A, i.e., the sum of first rank delplot intercepts. In contrast, if the limit is not taken, the rate of consumption of A to form U is substantial and cannot be neglected. Thus the sum of all first rank delplot intercepts appropriately corrected for stoichiometric coefficients should be unity.

Rule 4

If B is a primary product and $B_A \neq f(\epsilon_j)$ then B is only formed from A. ϵ_j is the ratio of reactant j with a standard reactant.

The first rule is a statement of the basic delplot method. The second rule states that if a product P is formed only from reactant A and that the only primary reactions where A is consumed is the formation of P, then the initial rate of formation of P is the same as the initial rate of consumption of A corrected appropriately for stoichiometric coefficients. Equation (3.14) states that the rate of consumption of reactant A is the sum of rate of formation of each product corrected appropriately for stoichiometric coefficients. This provides an internal check of the data. The fourth rule can identify cross reactions where there is more than one reactant. The fourth rule does not apply when the rate of formation of the product P formed from reactant A is poisoned by another reactant B that strongly adsorbs on the catalyst. This rule is used to synthesize reaction networks.

The applications of this method to carbon monoxide hydrogenation is shown in chapters 6 and 8.

3.3 Extended Delplot

The extended delplot method is used to sort products of rank $r > 1$. This method is completely general for first order kinetics. As will be shown later the extended delplot method can be applied to many other type of kinetics. First the extended delplot method is developed for first order reactions. Then, this method is applied to non-integer order reactions. An example of series-consecutive reactions is then considered to show the application of delplot analysis to non-first order reactions. In the second subsection, the rules for extended delplot analysis are enumerated. Lastly the concept of effective rank is developed and its use explained.

3.3.1 Development

The delplot intercept ${}^{r}P_R$ is

$$ {}^{r}P_R = \lim_{\tau \to 0} \frac{\frac{P-P_0}{R_0}}{\left(\frac{R_0-R}{R_0}\right)^r} \tag{3.24} $$

where ${}^{r}P_R$ is the intercept of the rth rank delplot of product P based on reactant R. If the rank of the plot is 1 then there is no need to write the superscript 1. An intercept can be based on any reactants. For example, if there are two reactants A and B. then there can be three second rank intercepts ${}^{2}P_{AA}(={}^{2}P_A)$, ${}^{2}P_{AB}$ and ${}^{2}P_{BB}$ $(={}^{2}P_B)$.

Ideally, the method should sort products according to their rank while being independent of the order of reaction, so that the problem of identifying the hierarchy of products can be separately solved from the problem of identifying

the functional form of kinetics of each step. Often. there is coupling between the order of reaction and the rank of the product. The basic delplot holds for any kinetics and hence completely decouples the order of reaction and the rank of the product. The extent of decoupling of the order of reaction from the rank of the product is discussed below.

3.3.1.1 First Order Reactions

We consider n=1 first. Recall the network of equations (3.3) and (3.4), where B and D were shown to be primary products. The extended delplot will show that the non-primary product C is a secondary product. The first stage of the extended delplot method consists of plotting (y/x^2) versus x: the intercept will be finite for secondary products(r=2) and zero for higher-rank products $(r > 2)$.

$$^2C_A = \lim_{\tau \to 0} \frac{\frac{C-C_0}{A_0}}{\left[\frac{A_0-A}{A_0}\right]^2} \tag{3.25}$$

First this method will be shown to work for the network given in equations (3.3) and (3.4) using their analytical solutions given in equations (3.5) to (3.8). Substituting the analytical solutions in equation (3.25) and using series expansions for the exponential terms. gives

$$^2C_A = \frac{k_1 k_3}{k_3 - k_1 - k_2} \times \lim_{t \to 0} \frac{\left[\left(\frac{(k_1-k_2)t + \frac{(k_1-k_2)^2 t^2}{2} + \cdots}{k_1-k_2}\right) - \left(\frac{k_3 t - \frac{k_3^2 t^2}{2} + \cdots}{k_3}\right)\right]}{2!\Big((k_1-k_2)t + \cdots\Big)^2} \tag{3.26}$$

Equation (3.26) can be simplified to

$$^2C_A = \frac{k_1 k_3}{(k_3 - k_1 - k_2)k_3(k_1 - k_2)} \times \lim_{t \to 0} \frac{\left[k_3(k_1-k_2)(k_3-k_1-k_2)t^2 + O(t^3)\right]}{2!(k_1-k_2)^2 t^2 - O(t^3)}$$

$$^2C_A = \frac{k_1 k_3}{2!(k_1-k_2)^2} \tag{3.27}$$

Thus the second rank delplot intercept is finite, hence C is a secondary product. Now, a general proof will be shown. To evaluate the right hand of equation (3.25) which is a $\frac{0}{0}$ form, the numerator and the denominator can be expanded as a Taylor series.

$$ {}^2C_A = \lim_{\tau \to 0} \frac{\frac{C_0 - (C')_{\tau=0}\tau - \frac{1}{2}(C'')_{\tau=0}\tau^2 - \cdots - C_0}{A_0}}{\left[\frac{A_0 - A_0 - (A')_{\tau=0}\tau - \frac{1}{2}(A'')_{\tau=0}\tau^2 - \cdots}{A_0}\right]^2} \tag{3.28} $$

$$ {}^2C_A = \lim_{\tau \to 0} \frac{A_0 \times (C')_{\tau=0} \times \tau + O(\tau^2)}{(A')_{\tau=0}{}^2\tau^2 + O(\tau^3)} $$

$$ {}^2C_A = \frac{A_0}{(A')^2_{\tau=0}} \times \lim_{\tau \to 0} \frac{(C')_{\tau=0}}{\tau} \tag{3.29} $$

Continued expansions of the second term on the right hand side of equation (3.29) requires the rate expression of C. The above proof is an approximate one. A rigorous proof is cumbersome and it yields results similar to the results obtained from approximate method within a multiplicative constant. The rigorous general proof is shown later for the above example.

$$ A \xrightarrow{k_1} B \xrightarrow{k_2} C \xrightarrow{k_3} D \tag{3.30} $$

For the reaction scheme of (3.30), the kinetics of C are given by,

$$ (C') = k_2 B - k_3 C \tag{3.31} $$

and

$$ B_0 = C_0 = 0 $$

$$ {}^2C_A \sim \frac{A_0}{(A')^2_{\tau=0}} \times \lim_{\tau \to 0} \left[k_2 \times \frac{B_0 - (B')_{\tau=0} - \cdots}{\tau} - k_3 \times \frac{C_0 - (C')_{\tau=0} - \cdots}{\tau} \right] $$

$$ {}^2C_A \sim \frac{A_0\left(k_2 \times (B')_{\tau=0} - k_3 \times (C')_{\tau=0}\right)}{(A')^2_{\tau=0}} \tag{3.32} $$

Since the initial rate of reaction of C, $C' = 0$, the second term in equation (3.32) does not contribute to the intercept. If $(A')_{\tau=0} = (B')_{\tau=0} = k_1 A_0$ in the network (3.30), then

$$^2C_A \sim \frac{k_2}{k_1} \tag{3.33}$$

Also for the reaction network given in equation (3.5) to (3.8), $(A')_{\tau=0} = (k_1 + k_2)A_0$, $(B')_{\tau=0} = k_1 A_0$.

$$^2C_A \sim \frac{k_1 k_3}{(k_1 + k_2)^2} \tag{3.34}$$

Now, a rigorous general proof will be given. The second rank delplot intercept of C is given by equation (3.35).

$$^2C'_A = \lim_{\tau \to 0} \frac{\frac{C_0 + (C')_{\tau=0}\tau + \frac{1}{2}(C'')_{\tau=0}\tau^2 + \cdots - C_0}{A_0}}{\left[\frac{A_0 - A_0 - (A')_{\tau=0}\tau - \frac{1}{2}(A'')_{\tau=0}\tau^2 - \cdots}{A_0}\right]^2} \tag{3.35}$$

Consider the network of equation (3.30).

$$(C')_{\tau=0} = k_2 B(\tau = 0) = 0 \tag{3.36}$$

$$(C'')_{\tau=0} = ((C')')_{\tau=0} = (k_2 B)'_{\tau=0} = k_2 B'_{\tau=0} = k_2 k_1 A_0 \tag{3.37}$$

Also, $A'_{\tau=0} = k_1 A_0$. Substituting equations (3.36) and (3.37) in equation (3.35), and simplifying and taking limits we get equation (3.38).

$$^2C'_A = \frac{k_2}{2! k_1} \tag{3.38}$$

Products of successive rank are sorted in a similar fashion. For example, the series network of (3.30) includes D as a tertiary product(r=3), whose third rank intercepts $y_D, x^3(^3D_A)$ as $x \longrightarrow 0$.

$$^3D_A = \frac{k_2 k_3}{k_1^2 3!} \tag{3.39}$$

given in equation (3.39) is finite.

The above results can be generalized for an infinite chain of series reactions.

$$A \xrightarrow{k_1} B \xrightarrow{k_2} \cdots \xrightarrow{k_r} X$$

The rth rank delplot intercept for product X is

$${}^{r}X_A = \frac{k_1 k_2 \cdots k_r}{k_1^r r!} \tag{3.40}$$

The extended delplot ($r > 1$) method is thus general for first order (n=1) reactions.

3.3.1.2 Non-First Order Kinetics

For nth order kinetics for step 2 in equation (3.30), the expression for C' can be written as

$$(C') = k_2' B^n - k_3 C \tag{3.41}$$

Here again, using an analysis similar to equation (3.32), the second term on the right hand side of equation (3.41) does not contribute to the second rank delplot intercept. Substituting equation (3.41) in equation (3.29), and expanding B^n in a taylor series about $\tau = 0$ provide;

$${}^{2}C'_A = \frac{k_2' \times A_0}{(A')^2_{\tau=0}} \times \lim_{\tau \to 0} \frac{B_0^n + (\frac{d(B^n)}{d\tau})_{\tau=0} + \cdots}{\tau}$$

$${}^{2}C'_A = \frac{k_2' \times A_0}{(A')^2_{\tau=0}} \times \lim_{\tau \to 0} \frac{B_0^n - nB_0^{n-1}(\frac{d(B)}{d\tau})_{\tau=0} + \cdots}{\tau} \tag{3.42}$$

$${}^{2}C'_A = \frac{k_2' \times A_0}{(A')^2_{\tau=0}} \times nB_0^{n-1} \times \lim_{\tau \to 0} \frac{(\frac{d(B)}{d\tau})_{\tau=0}}{\tau} \tag{3.43}$$

Since $B_0 = 0$, the second term on the right hand side of equation (3.43), B_0^n, causes the second rank intercept to diverge for order, $n < 1$. If the order of the second step, $n > 1$, then the intercept ${}^{2}C'_A$ is zero.

3.3.1.3 Characteristics of Delplot Intercepts

A summary of delplot intercepts for various ranks and different order of reactions is given in table 3.2 on page 117.

Table 3.2 shows the characteristics of delplot intercepts for various reaction orders (first column) and for various product ranks (first row). To keep the intercepts simple, parallel steps are not yet included. However, it is simple to extend this analysis to parallel steps as done in equation (3.12). The second column shows that the first rank delplot intercept for a product of rank one is equal to its stoichiometric coefficient. This intercept is independent of the order of the reaction. In contrast, for $n = 1$ and $r > 1$, the rth rank delplot intercepts of products with rank r is finite. Here all the delplot intercepts with rank less than r are zero and the delplot intercepts with rank $> r$ diverge. The element in the third row and the third column corresponds to delplot intercepts of product of rank r greater than one and having only the order of the final reaction step less than one($r > 1$ and $n < 1$). All the other reaction steps are first order. In contrast to the previous elements, here the rth rank delplot intercepts diverge. The rth delplot intercept of product of rank $r > 1$ and $n > 1$ is zero. Thus it is clear from table 3.2 that the higher rank delplot can not only be used to sort products according to their rank, but also to find estimates of the order of the reaction steps.

3.3.1.4 Series-Parallel Reactions: Effective Order of Reaction

Another important set of reactions is given below

$$A - B \xrightarrow{k_1} C + D \tag{3.44}$$

$$C + B \xrightarrow{k_2} E + D \tag{3.45}$$

$$E - B \xrightarrow{k_1} F - C \tag{3.46}$$

Table 3.2: Summary of information from delplot intercepts

Order/Rank	$r = 1^*$	$r > 1$
$n = 1$	${}^1P_A = \frac{\nu_P}{\nu_A}$	${}^mP_A = 0$ for $m = 1,(r-1)$ ${}^rP_A$ finite
$n < 1^!$	${}^1P_A = \frac{\nu_P}{\nu_A}$	${}^mP_A = 0$ for $m = 1,(r-1)$ ${}^rP_A$ diverges
$n > 1^!$	${}^1P_A = \frac{\nu_P}{\nu_A}$	${}^mP_A = 0$ for $m = 1,r$

*- no parallel steps

!- only the last step has order $n \neq 1$

These set of reactions are important in many industrial reactions such as successive chlorinations and nitrations. All the reactions are second order. This examples illustrates the concept of effective order.

Here C and D are primary products and a basic delplot analysis shows,

$${}^1C_A = {}^1C_B = {}^1D_A = {}^1D_B = 1$$

and ${}^1E_A = {}^1E_B = {}^1F_A = {}^1F_B = 0$

The second rank delplot intercept for E is given by

$${}^2E_A = \lim_{\tau \to 0} \frac{\frac{E}{A_0}}{\left[\frac{A_0 - A}{A_0}\right]^2} \tag{3.47}$$

Expanding the numerator and the denominator of equation (3.47) as a Taylor series about zero we get,

$${}^2E_A = \frac{A_0}{(A')^2_{\tau=0}} \times \lim_{\tau \to 0} \frac{(E')_{\tau=0}}{\tau} \tag{3.48}$$

Continued expansions of the second term on the right hand side of equation (3.48) requires the rate expression of E.

For the case where,

$$(E') = k_2 C' B - k_3 E B \tag{3.49}$$

Here again the second term of equation (3.49) does not contribute to the second rank delintercepts and therefore neglected.

$${}^2E_A \sim \frac{A_0 B_0}{(A')^2_{\tau=0}} \times \lim_{\tau \to 0} \left[k_2 \times \frac{C_0 - (C')_{\tau=0} + \cdots}{\tau}\right]$$

$${}^2E_A \sim \frac{A_0 B_0 \left(k_2 \times (C')_{\tau=0}\right)}{(A')^2_{\tau=0}} \tag{3.50}$$

Also $(A')_{\tau=0} = (C')_{\tau=0} = k_1 A_0 B_0$, therefore

$$^2E_A \sim \frac{k_2}{k_1} \tag{3.51}$$

Similarly it is easy to show $^2F_A = 0$.

A third rank delplot analysis similar to the one presented above shows that

$$^3F_A \sim \frac{k_2 k_3}{k_1^2} \tag{3.52}$$

Thus this example shows that the delplot intercepts are not affected by the order of the reaction. The reaction network of equations (3.44) - (3.46) can be simplified to equation (3.53).

$$A \xrightarrow{k_1 B_0} R \xrightarrow{k_2 B_0} S \xrightarrow{k_3 B_0} T \tag{3.53}$$

Hence we can define an effective order with respect to product. The effective order for delplot analysis is the total order minus the order with respect to the reactants. In the network of equation (3.44), even though the reactions are of second order, their effective order is one and hence the same results are obtained as for an infinite series of sequential reactions.

3.3.2 Rules for Extended Delplot

Rule 1

For a set of first order reactions, if $^2P^j_A = 0$ and P^j is a non-primary product, then products P^j are secondary products. Similarly if for non-primary products, $^2P^j_A = 0$ then the rank of product P is greater than 2.

Rule 2

If for a given non-primary product P^j,

${}^{2}P_A^j \neq f(\epsilon_j)$, for all j,

then product P^i is formed from primary products C^k such that

$$C_A^k \neq f(\epsilon_j)$$

for all j

The first rule is a statement of second rank delplot method. As suggested earlier it holds for first order reactions. For any other type of kinetics the delplot intercepts have to be derived. The second rule is similar to the fourth rule of the basic delplot method. It is used to identify reaction steps in the synthesis of reaction networks.

3.3.3 Effective Rank of the Product

3.3.3.1 Definition

Effective rank of a species is the lowest integer r, for which the plot of y/x^r versus x gives a finite intercept. In contrast, the network rank is the minimum number of slow steps between the reactant and the product. Unless otherwise specified the rank of a product means the network rank. For reactants and primary products the network rank is same as the effective rank. However, as will be shown later, for higher rank products, the two ranks for the same species can be different. For non-integer reaction order, there may not be an integer effective rank. In this section only integer order reactions will be considered. The concept of effective rank is important to find the applicability of delplot analysis. Maximum amount of information of the network can be obtained when the effective rank is same as the network rank. $\hat{\mathbf{E}}$ and $\hat{\mathbf{N}}$ are the effective rank and the network rank operators, these operators when operated on a species yield their respective ranks.

3.3.3.2 Derivation of Effective Product Rank Equation(EPRE)

The difference between the network rank and the effective rank is best illustrated with an example.

Consider the network given in equations (3.54) to (3.56).

$$A + B \xrightarrow{1} C + D \tag{3.54}$$

$$C + D \xrightarrow{2} E + F \tag{3.55}$$

$$E + F \xrightarrow{3} G + H \tag{3.56}$$

The kinetics of each step are given by

$$r_1 = k_1 A^{m_1} B^{n_1} \tag{3.57}$$

$$r_2 = k_2 C^{m_2} D^{n_2} \tag{3.58}$$

$$r_3 = k_3 E^{m_3} F^{n_3} \tag{3.59}$$

Assume $m_1, n_1, m_2, n_2, m_3, n_3, \in$ N.Since a plot of y_C/x and y_D/x versus x yields a finite intercept, the effective rank of C and D is one. Also, there is only one slow step in the formation of C and D and hence their network rank is also one.

$$\hat{\mathbf{E}}(C) = \hat{\mathbf{E}}(D) = \hat{\mathbf{N}}(C) = \hat{\mathbf{N}}(D) = 1 \tag{3.60}$$

To find the effective rank of E, consider the zth rank delplot (z$\in$N).

$$E_A = \lim_{A \to 0} \frac{\frac{E}{A_0}}{\left(\frac{A_0 - A}{A_0}\right)^z} \tag{3.61}$$

$$^{z}E_A \sim \frac{A_0^{z-1}}{(A')^{z}_{\tau=0}} \times \lim_{\tau \to 0} \frac{(E')_{\tau=0}}{\tau^{z-1}}$$

Substituting $(E')_{\tau=0} = k_2 C^{m_2} D^{n_2}$ in the above equation

$$^{z}E_A \sim \frac{k_2 A_0^{z-1}}{(A')^{z}_{\tau=0}} \times \lim_{\tau \to 0} \frac{(C)^{m_2}_{\tau=0}}{\tau^{m_2}} \times \lim_{\tau \to 0} \frac{(D)^{n_2}_{\tau=0}}{\tau^{n_2}} \times \lim_{\tau \to 0} \frac{1}{\tau^{z-1-m_2-n_2}} \qquad (3.62)$$

Again, the second and the third term of equation (3.62) can be expanded as a Taylor series about zero, to give

$$^{z}E_A \sim \frac{k_2 A_0^{z-1} (C')^{m_2}_{\tau=0} (D')^{n_2}_{\tau=0}}{(A')^{z}_{\tau=0}} \times \lim_{\tau \to 0} \frac{1}{\tau^{z-1-m_2-n_2}} \qquad (3.63)$$

From equation (3.63),

$^{z}E_A$ is finite if $z = 1 + m_2 + n_2$,

$^{z}E_A$ is zero if $z < 1 + m_2 + n_2$,

$^{z}E_A$ diverges if $z > 1 + m_2 + n_2$,

Thus, here the effective rank of E and F is $(1 + m_2 + n_2)$, while the network rank of E and F is 2. It is important to note that for first order reactions, i.e., $m_2 = 0$ and $n_2 = 1$, or , $m_2 = 1$ and $n_2 = 0$, the effective rank and the network rank both have a value of 2. If the reaction given by equation (3.55) is second order, i.e. $m_2 = 1$ and $n_2 = 1$, then the effective rank of E and F is three while the network rank of E and F is 2.

To determine the effective rank of G and H consider the zth rank delplot intercept of G.

$$^{z}G_A \sim \frac{A_0^{z-1}}{(A')^{z}_{\tau=0}} \times \lim_{\tau \to 0} \frac{(G')_{\tau=0}}{\tau^{z-1}}$$

Substituting $(G')_{\tau=0} = k_3 E^{m_3} F^{n_3}$ in the above equation

$$^{z}G_A \sim \frac{k_3 A_0^{z-1}}{(A')_{\tau=0}^{z}} \times \lim_{\tau\to 0} \frac{(E)_{\tau=0}^{m_3}}{\tau^{m_3}} \times \lim_{\tau\to 0} \frac{(F)_{\tau=0}^{n_3}}{\tau^{n_3}} \times \lim_{\tau\to 0} \frac{1}{\tau^{z-1-m_3-n_3}} \tag{3.64}$$

Expanding the second and the third term of equation (3.64) as a Taylor series about zero,

$$^{z}G_A \sim \frac{k_3 A_0^{z-1}}{(A')_{\tau=0}^{z}} \times \lim_{\tau\to 0} \frac{(E')_{\tau=0}^{m_3}(F')_{\tau=0}^{n_3}}{\tau^{z-1-m_3-n_3}} \tag{3.65}$$

Substituting $(E')_{\tau=0} = (F')_{\tau=0} = k_2 C^{m_2} D^{n_2}$ in equation (3.65)

$$^{z}G_A \sim \frac{k_3 k_2^{m_3+n_3} A_0^{z-1}}{(A')_{\tau=0}^{z}} \times \lim_{\tau\to 0} \frac{(C)_{\tau=0}^{m_2m_3+m_2n_3}(D)_{\tau=0}^{n_2m_3+n_2n_3}}{\tau^{z-1-m_3-n_3}}$$

$$^{z}G_A \sim \frac{k_3 k_2^{m_3+n_3} A_0^{z-1}}{(A')_{\tau=0}^{z}} \times \lim_{\tau\to 0} \frac{(C)_{\tau=0}^{m_2m_3+m_2n_3}}{\tau^{m_2m_3+m_2n_3}} \times \lim_{\tau\to 0} \frac{(D)_{\tau=0}^{n_2m_3+n_2n_3}}{\tau^{n_2m_3+n_2n_3}} \times \lim_{\tau\to 0} \frac{1}{\tau^{\delta}} \tag{3.66}$$

where $\delta = z - 1 - m_3 - n_3 - m_2m_3 - m_2n_3 - n_2m_3 - n_2n_3$

Once again, expanding the second and the third term of equation (3.66) as a Taylor series about zero,

$$^{z}G_A \sim \frac{k_3 k_2^{m_3+n_3} A_0^{z-1}(C')_{\tau=0}^{m_2m_3+m_2n_3}(D')_{\tau=0}^{n_2m_3+n_2n_3}}{(A')_{\tau=0}^{z}} \times \lim_{\tau\to 0} \frac{1}{\tau^{\delta}}$$

Thus $^{z}G_A$ is finite if $\delta = 0$, zero if $\delta < 0$ and $^{z}G_A$ diverges if $\delta > 0$.

Here again, the effective rank of G and H is $z(\delta = 0)$, while the network rank of G and H is three. A pattern emerges from the given example for effective rank of a product in pathways containing integral order kinetics.

For example,

$$\hat{\mathrm{E}}(G) = z(\delta = 0) = 1 + m_3 + n_3 + m_2m_3 - m_2n_3 - n_2m_3 + n_2n_3$$

$$\hat{\mathrm{E}}(G) = 1 + m_3(1 + m_2 + n_2) - n_3(1 + m_2 + n_2)$$

but, $\hat{\mathbf{E}}(E) = \hat{\mathbf{E}}(F) = 1 + m_2 + n_2$

hence

$$\hat{\mathbf{E}}(G) = 1 + m_3\hat{\mathbf{E}}(E) + n_3\hat{\mathbf{E}}(F)$$

Also, $\hat{\mathbf{E}}(E) = 1 + m_2\hat{\mathbf{E}}(C) + n_2\hat{\mathbf{E}}(D)$

Thus for a general reaction given by equation (3.67) and with kinetics given by equation (3.68),

$$\nu_i^A A_i + \cdots \xrightarrow{j} \nu_i^P P_i + \cdots \tag{3.67}$$

$$r_j = k_j A_1^{n_1} \cdots \tag{3.68}$$

then

$$\hat{\mathbf{E}}(P) = 1 + \sum_i n_i\hat{\mathbf{E}}(A_i) \tag{3.69}$$

Equation (3.69) is called as the effective product rank equation(EPRE). EPRE is a recursive relation which gives the effective rank of the next product in the rank hierarchy provided the order of the reaction is known.

3.3.3.3 Application of EPRE

The application of Effective Product Rank Equation(EPRE) to various reaction schemes will now be considered. EPRE shows the coupling between effective rank of a product and the order of the reaction. For a series of reactions given by equation (3.30), $\hat{\mathbf{E}}(A) = 0$ and $\hat{\mathbf{E}}(B) = 1$. Applying EPRE, the effective rank of C can be obtained

$$\hat{\mathbf{E}}(C) = 1 + n_i\hat{\mathbf{E}}(B)$$

but $n_i = 1$, since all reactions are first order. Therefore, $\hat{\mathbf{E}}(C) = 2$. Because n_i is always one, each reaction step will increase the effective rank only by one, and hence the effective rank will always be equal to the network rank in a network of first order reactions.

For a scheme given by equation (3.44) to (3.46),

$$\hat{\mathbf{E}}(A) = \hat{\mathbf{E}}(B) = 0$$

and

$$\hat{\mathbf{E}}(C) = \hat{\mathbf{E}}(D) = 1$$

To find the effective rank of E, we apply EPRE. Here, $n_C = 1$ and $n_B = 1$.

$$\hat{\mathbf{E}}(E) = 1 + n_C\hat{\mathbf{E}}(C) + n_B\hat{\mathbf{E}}(B)$$

Hence $\hat{\mathbf{E}}(E) = 2$. Thus the effective rank and the network rank of E is two. It is important to note that the effective rank of E is not dependent on the order of the reaction with respect to B because the order is multiplied by the effective rank of B. which is zero. Thus using EPRE, we find that the network of equations (3.44) to (3.46) behave as first order reactions. This result was derived earlier from a more detailed analysis. Also using EPRE, the effective rank of F can be found to be three.

Thus for an integer order reaction pathway, a simple algebraic recursive equation EPRE can be used to find the effective rank of a product. The delplot analysis is most useful when the effective rank of the product is same as the network rank.

3.4 Application to Fisher-Tropsch Synthesis and Oxygenate Synthesis Reaction Networks

The reaction network for Fisher-Tropsch Synthesis(FTS) and oxygenate synthesis, shown in figure 3.2, was reported by Sachtler[23]. There four types of step identified by the subscript on the first order rate constant in figure 3.2. The first step is the formation of precursor A_1 from CO and hydrogen. The second